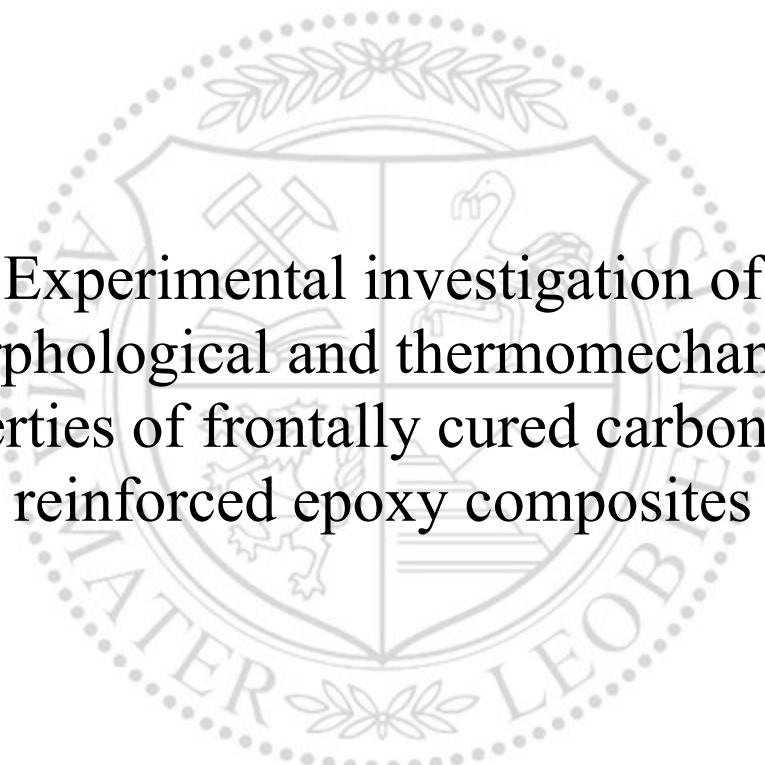




Chair of Materials Science and Testing of Polymers

Master's Thesis



Experimental investigation of
morphological and thermomechanical
properties of frontally cured carbon fibre
reinforced epoxy composites

Valerie Grasser, BSc

August 2021

EIDESSTATTLICHE ERKLÄRUNG

Ich erkläre an Eides statt, dass ich diese Arbeit selbstständig verfasst, andere als die angegebenen Quellen und Hilfsmittel nicht benutzt und mich auch sonst keiner unerlaubter Hilfsmittel bedient habe.

AFFIDAVIT

I declare in lieu of oath, that I wrote this thesis and performed the associated research myself, using only literature cited in this volume.

LEOBEN, August 2021


(Valerie Grasser)

ACKNOWLEDGEMENTS

The research work was performed within the COMET-project „Exploiting frontal polymerization techniques for the efficient and rapid curing of epoxy-based composites“ (project-no.: VII-1.02) at the Polymer Competence Center Leoben GmbH (PCCL, Austria) within the framework of the COMET-program of the Federal Ministry for Climate Action, Environment, Energy, Mobility, Innovation and Technology and the Federal Ministry for Digital and Economic Affairs with contributions by Montanuniversität Leoben (Department Polymer Engineering and Science, Chair of Chemistry of Polymeric Materials, Chair of Materials Science and Testing of Polymers) and Magna Energy Storage Systems GesmbH. The PCCL is funded by the Austrian Government and the State Governments of Styria, Lower Austria and Upper Austria.

To anyone who opened a door for me

– *thank you for letting me in.*

KURZFASSUNG

Das Thema Leichtbau mit duromeren Faserverbundwerkstoffen ist in Hinblick auf eine nachhaltige Mobilität von wesentlicher Bedeutung. Allerdings werden diese Werkstoffe in der Regel bei hohen Temperaturen und Drücken sowie langen Zykluszeiten gehärtet, weshalb die Herstellung von Bauteilen aus faserverstärkten Kunststoffen energie- und zeitaufwendig ist. Eine Möglichkeit zur kosteneffizienten Herstellung von Faserverbundbauteilen ist die Technologie der Frontalpolymerisation. Nach dem Start der Aushärtereaktion durch einen externen Energieeintrag (z. B. Wärme oder UV-Strahlung), generiert die bei der Härtungsreaktion freiwerdende Reaktionswärme eine selbsterhaltende Reaktionsfront und sorgt so für die Härtung des Harzes.

Im Rahmen dieser Masterarbeit wurden kohlenstofffaserverstärkte Epoxidharze mit einem Faservolumengehalt von mindestens 50 % mittels thermisch induzierter frontaler Polymerisation gehärtet. Anschließend wurden die thermo-mechanischen Eigenschaften in Hinblick auf einen Vergleich mit den entsprechenden Kennwerten des konventionell thermischen gehärteten Faserverbundes bestimmt. Als Faserverstärkung kamen ein unidirektionales Gelege (UD) und ein Gewebe in 2x2 Körperbindung zum Einsatz. Zwei kommerziell erhältliche Bisphenol A basierende Harzsysteme wurden als Matrixwerkstoff ausgewählt. Die Herstellung der für die Werkstoffprüfung benötigten Prüfkörper erfolgte mittels Nasslaminieren und eines vakuumunterstützten Harzinfusionsprozesses.

Im Zuge der dynamisch mechanischen Analyse konnten höhere Temperatureinsatzgrenzen für die frontal gehärteten Prüfkörper ermittelt werden. So wurden die Glasübergangstemperaturen, verglichen mit der konventionellen Härtung, um etwa 20 °C nach oben verschoben. Im Zugversuch wurden vergleichbare Modulwerte, jedoch geringere Festigkeiten und Dehnungen für die frontal polymerisierten Prüfkörper aller Fasertypen gemessen. Der Unterschied der Festigkeits- und Dehnungswerte war stark ausgeprägt. Die Druckmoduli und -festigkeiten der frontal polymerisierten Prüfkörpersets waren vergleichbar mit einem der konventionell gehärteten Materialien und höher als das zweite Vergleichsmaterial. Versuche zur interlaminaeren Scherfestigkeit zeigten nicht normkonformes Versagen, plastische Verformung, der konventionell gehärteten Prüfkörper. Trends bezüglich der Spannungswerte, bei denen das Versagen auftrat, konnten nicht festgestellt werden.

ABSTRACT

Lightweight coupled with high mechanical strength are the most important parameters of fibre reinforced thermosets in order to comply with the concept of sustainable mobility. However, the curing processes of those materials are usually linked with high temperatures and pressures, as well as prolonged cycle times. Therefore their manufacturing is costly and time-consuming. A possibility of reducing manufacturing costs of fibre reinforced composites is by following curing of composites via frontal polymerization. In this curing technique, the reaction is initiated by an external trigger (e. g. UV-radiation or heat), that releases high amount of energy in the course of the curing process, generating a self-sustaining reaction front and consequently curing the resin without further input of an external trigger.

In the course of this master's thesis, carbon fibre reinforced epoxy composites, with a fibre volume content of at least 50%, were cured via thermally initiated frontal polymerization. Subsequently, the thermomechanical properties were determined, in comparison to the corresponding conventionally cured composites. A unidirectional (UD) 50 k lamina and a 2×2 twill fabric were used as reinforcement material along with two commercially available bisphenol A based derivatives as matrix materials. These composites based on UD and carbon fibre fabric were manufactured via a wet lay-up (wlu) and a vacuum assisted resin infusion (VARI) process.

From the results of dynamic mechanical analysis (DMA), approximately 20 °C higher glass transition temperature (T_g) values were determined for the frontally cured specimens than the conventional anhydride/amine cured specimens. Tensile test results from frontally cured specimens of both fibre types showed comparable modulus values, yet lower maximum strength and strain values than the corresponding conventional cured specimens. The difference in tensile strength, comparing specimens with same manufacturing process, reinforcement and resin material, yet different curing method showed high deviations. The compression properties of the frontally cured specimens were comparable to one conventionally cured resin type and higher than the other resin material used. The analysis of the inter laminar shear strength (ILSS) on the one hand showed different failure modes for frontally (shear failure) and conventionally (plastic deformation) cured specimens. Yet on the other hand, the strength values at which the failure appeared show no distinct trends to higher values for neither curing nor resin type.

CONTENTS

1	Introduction and objectives	1
2	Theoretical background	4
2.1	Chemistry of epoxide monomers	4
2.2	Radical induced cationic frontal polymerization	6
2.3	Thermo mechanical properties of FRP	9
2.3.1	Macro vs. micro mechanics	9
2.3.2	Dynamic mechanical analysis	12
2.3.3	The effect of voids on mechanical properties	13
3	Experimental part	15
3.1	Materials	15
3.1.1	Reinforcement materials	15
3.1.2	Matrix Materials	15
3.2	Processing	17
3.2.1	Wet lay up	17
3.2.2	Vacuum assisted resin infusion	17
3.3	Characterization	18
3.3.1	Morphology	18
3.3.2	Neat resin characterization	19
3.3.3	Dynamic mechanical analysis	20
3.3.4	Tensile tests	21
3.3.5	Compression tests	22
3.3.6	Inter laminar shear stress tests	23
4	Results and discussion	24
4.1	Neat resin characterization	24
4.2	Morphological analysis	26
4.3	Dynamic mechanical analysis	30

4.4	Tensile tests	37
4.5	Compression tests	45
4.6	Inter laminar shear strength tests	50
4.7	Joint discussion	56
5	Summary and outlook	57
A	Appendix	67

ABBREVIATIONS AND SYMBOLS

α	degree of cure
BADGE	bisphenol A diglycidyl ether
CF	carbon fibre
CF-epoxy	carbon fibre reinforced epoxy composites
con	conventional
DIC	digital image correlation
DMA	dynamic mechanical analysis
DSC	differential scanning calorimetry
E'	storage modulus
E''	loss modulus
E_c	compression modulus
ϵ_c	compressive strain
ϵ_t	tensile strain
E_t	tensile modulus
$\epsilon_{t_{Max}}$	strain at break
eq	equation
FP	frontal polymerization
FRP	fibre reinforced plastic
FTIR	Fourier-transform infrared
HCCF	hydraulic composites compression fixture
ILSS	inter laminar shear strength
MMA	methyl methacrylate
PAG	photo acid generator
RICFP	radical induced cationic frontal polymerization
SBS	short beam shear
σ_c	compressive stress
$\sigma_{c_{MAX}}$	maximum compressive stress
σ_t	tensile stress
$\sigma_{t_{MAX}}$	maximum tensile stress

$\tan(\delta)$	lossfactor
T_g	glass transistion temperature
T_{gel}^{onset}	onset gelation temperature
TGA	thermogravimetric analysis
UD	unidirectional
VARI	vacuum assisted resin infusion
v_f	fibre volume content
v_v	void content
wlu	wet lay-up

 LIST OF FIGURES

1.1	Comparison of the advantages (+) and disadvantages (-) between frontal and conventional curing.	2
1.2	Overview on experimental part, divided in specimen manufacturing and characterization.	3
2.1	Overview on the application fields of epoxy in the U.S. from 2014 – 2024 [1].	4
2.2	Chemical structures of: (2.2a) epichlorhydrin and (2.2b) bisphenol A, the constituents of (2.2c) BADGE.	5
2.3	Examples for typical curing agents: (2.3a) phthalic anhydride and (2.3b) 4, 4'-Diaminodiphenyl methane.	6
2.4	Relation between RICFP, frontal and cationic polymerization.	7
2.5	Reaction scheme of the cationic polymerization of a epoxy monomer.	8
2.6	Stress-strain relationship of fibre/matrix and composite material after [2].	10
2.7	Test pyramid for composite materials, after [3].	11
2.8	Influence of the molecular weight i.e. crosslink density on E' and loss factor after [4].	13
2.9	Example of UD CF/epoxy composite with a high void content.	14
3.1	Chemical structures of the prepolymer components used as resins: ep1 (3.1a) the BADGE monomer, ep2 (3.1b) BADGE based oligomers and (3.1c) the aliphatic diluent.	16
3.2	Chemical structures of thermal radical initiator: tetraphenyl ethanediol (3.2a) and the photoinitiator: p-octyl oxyphenyl phenyliodonium hexafluoro antimonate (3.2b).	16
3.3	Set up of VARI process used for manufacturing plates.	18
3.4	Geometry of tensile test specimens, all values in mm.	21
3.5	Geometry of compression test specimens, all values in mm.	22
3.6	Detailed picture of: (3.6a) the HCCF, used for compression testing and (3.6b) the camera set-up.	23

4.1	Viscosity in Pa s against temperature in °C for all resin and curing types, with indicated onset gelation temperature (T_{gel}^{onset}).	24
4.2	IR spectra for the determination of the epoxy group conversion rate. . .	25
4.3	Micrographs of 2 mm ep1 plates for compression, DMA and ILSS tests: (4.3a) wlu-UD-ep1_con, (4.3b) VARI-UD-ep1_con, (4.3c) VARI-UD-ep1_FP and (4.3d) VARI-fb-ep1_FP.	27
4.4	TGA-graphs with estimated fibre volume content (v_f) for two plates, (4.4a) a UD-ep2_con manufactured via wlu and (4.4b) a UD-ep2_FP manufactured via VARI.	28
4.5	Micrograph of a wlu-UD sample with different morphological aspects. .	29
4.6	storage modulus (E') and lossfactor ($\tan(\delta)$) in dependence of temperature, derived from DMA, for: (4.6a) wlu-UD-ep1_con and (4.6b) VARI-UD-ep2_FP specimens, measured with different parameters, as indicated in the legend. Each measurement was performed with 1 Hz. .	31
4.7	Average T_{gpeak} values for all UD specimens compared with regard to manufacturing type.	33
4.8	Average E' values derived from DMA for all UD specimens compared with average tensile modulus (E_t) values, with indicated standard deviation, from tensile testing.	34
4.9	E' and $\tan(\delta)$ in dependence of temperature, derived from DMA, for wlu-UD specimens with (4.9a) ep1 and (4.9b) ep2 matrix, respectively. Each graph shows one con and one FP specimen. All measurements were performed with 1 Hz.	36
4.10	Example tensile stress (σ_t) vs tensile strain (ϵ_t) curves of tensile tests for (4.10a) UD and (4.10b) fb specimens produced via VARI.	38
4.11	Comparison of the average maximum tensile stress (σ_{tMAX}), including standard deviation.	39
4.12	Comparison of the average strain at break (ϵ_{tMax}), including standard deviation.	41
4.13	Comparison of the average E_t values, including standard deviation. . .	42
4.14	Picture of a typically failed fb specimen.	43

4.15	Typical fracture images of UD-ep1_FP specimens, manufactured in a (4.15a) wlu and (4.15b) VARI process, exhibiting rough fragmentation and little loss.	44
4.16	Typical fracture images of UD-ep2_FP specimens, manufactured in a (4.16a) wlu and (4.16b) VARI processes, exhibiting rough fragmentation and little loss.	44
4.17	Typical fracture images of UD-ep1_con specimens, manufactured in a (4.17a) wlu and (4.17b) VARI processes, exhibiting fine fragmentation and much loss.	44
4.18	Typical fracture images of UD-ep2_con specimens, manufactured in a (4.18a) wlu and (4.18b) VARI processes, exhibiting finest fragmentation and much loss.	45
4.19	Typical compressive stress (σ_c) vs compressive strain (ϵ_c) curves from compression tests, for (4.19a) UD and fb (4.19b) specimens, respectively.	46
4.20	Comparison of the average maximum compressive stress (σ_{cMAX}), including standard deviation.	47
4.21	Comparison of the average compression modulus (E_c) values, including standard deviation.	48
4.22	Example pictures of different failure types appeared during compression tests: (4.22a) showing complex failure in fabric specimen, (4.22a) showing through thickness shear in fabric specimen and (4.22c) showing a typically failed UD specimen.	50
4.23	Typical stress vs displacement curves for ILSS tests, of all types of specimens: (4.23a) showing curves for wlu-fb, (4.23b) VARI-fb, (4.23c) wlu-UD and (4.23d) VARI-UD specimens.	51
4.24	Comparison of the average ILSS values, including standard deviation.	53
4.25	Image of the (4.25a) bottom side and (4.25b) side view of a wlu-UD-ep1_con specimen after testing, showing plastic deformation.	54
4.26	Image of the (4.26a) bottom side and (4.26b) side view of a wlu-fb-ep1_con specimen after testing, showing plastic deformation.	54
4.27	Image of the (4.27a) bottom side and (4.27b) side view of a wlu-fb-ep1_FP specimen after testing, showing shear failure.	55
4.28	Image of the (4.28a) bottom side and (4.28b) side view of a wlu-UD-ep2_FP specimen after testing, showing shear failure.	55

A.1	Visualisation of the method for calculating T_{gel}^{onset} in viscosity measurements.	67
A.2	Micrographs of 2 mm plates for compression, DMA and ILSS tests: A.2a showing VARI-UD-ep2_con, A.2b showing VARI-UD-ep2_FP, A.2c showing wlu-UD-ep1_FP and A.2d showing VARI-UD-ep2_FP.	68
A.3	Visualisation of the two methods used for calculating T_g	70
A.4	E' and $\tan(\delta)$ in dependence of temperature, derived from DMA, for: (A.4a) VARI-UD-ep1 and (A.4b) VARI-UD-ep2 specimens, in each case con and FP cured as indicated in the legend. Each measurement was performed with 1 Hz and method 1.	71
A.5	Visualisation of the ratios expected to real thickness and wlu to VARI for $\sigma_{t_{MAX}}$ and E_t	72
A.6	Example σ_t vs ϵ_t curves of tensile tests for A.6a fb and A.6b UD specimens produced via wlu.	73

LIST OF TABLES

2.1	Examples for the network structure's influence on DMA curves.	13
3.1	Reinforcement properties	15
3.2	Matrix materials.	17
3.3	Number of plies.	18
3.4	TGA method.	19
3.5	Method adopted for the DSC.	20
4.1	Conversion rates derived from IR spectroscopy.	26
4.2	T_g mid-point values obtained by DSC measurements for the first and second heating run.	26
4.3	Average T_g values for all UD-specimens, derived from DMA, calculated via two different methods.	32
4.4	Average values for tensile moduli: E_t , derived from tensile tests and E' from DMA.	34
4.5	Average values and standard deviation of $\sigma_{t_{MAX}}$ in MPa.	40
4.6	Average values and standard deviation of ϵ_t values at $\sigma_{t_{MAX}}$ in %.	41
4.7	Average values and standard deviation of E_t in GPa.	43
4.8	Average values and standard deviation of $\sigma_{c_{MAX}}$ in MPa.	47
4.9	Average values and standard deviation of E_c in GPa.	49
4.10	Average values and standard deviation of ILSS in MPa.	53
A.1	Calculated v_f , void content (v_v) and thickness ratio.	69
A.2	Comparison of tensile properties.	70
A.3	Comparison of ILSS.	71

1 INTRODUCTION AND OBJECTIVES

The potential of carbon fibre reinforced epoxy composites (CF-epoxy) as high-performance and lightweight construction materials is being exploited in a broad range of industries, especially in the transport sector. The amount of CF-epoxy used in industry is increasing steadily as are the variety of application fields [6] [7]. However, the most common curing type, thermal curing, restricts the application fields due to some inherent drawbacks. Firstly, the part size is limited by the size of the oven, or autoclave. Secondly, due to the low heat conductivity of epoxy, and the need for uniform curing, the thickness of the part is restricted. Thirdly, manufacturing process is limited by the resin pot life. In the context of lightweight construction due to environmental aspects, another considerable inconvenience is the energy, time and cost required for curing. Consequently, further research is being conducted in the field of rapid curing methodologies that could cut down cycle time of composite manufacturing and at the same time, allow a uniform and high degree of cure [8] [9] [10]. One such potential curing technology is frontal polymerization (FP).

Frontal polymerization combines radical induced cationic ring opening reaction of epoxides with auto-accelerating fronts resulting from cleavage of radical thermal initiators continuing the ring opening reaction [11]. The curing of epoxide monomers relies strongly on the radical-cation exchange during polymerization and the exothermicity of the epoxide ring opening. Figure 1.1 summarizes the main distinctions between conventional curing (con) and FP [8] [12] [13] [14]. Frontal polymerization typically involves solvent-free formulations preventing the use of toxic solvents or curing agents as used in conventional amine/anhydride curing. Moreover, the manufacturing process via FP provides longer pot life, typically several months. Furthermore, energy and time can be saved by the rapid autocatalytic curing process. Additionally, FP provides more freedom in product design, such as the aforementioned possible higher wall thickness and bigger part size. The costs for long heating cycles and expensive equipment, such as autoclaves can be prevented by FP. However, rapid curing via FP comes also with some drawbacks such as high cost of photo/thermal initiators. Currently, there is no reported industrial-scale set-up for curing via FP while on the contrary, conventional (con) curing is already well studied and resins and hardeners, optimized for a wide variety of applications are available.

The goal of this master's thesis is to compare some thermomechanical properties of different CF-epoxies cured via two methods- conventionally cured and via radical induced cationic frontal polymerization (RICFP). The latter method has not yet been used for manufacturing carbon fibre reinforced composites on a large scale. Carbon fibre based epoxy composites are characterized by a high fibre volume fraction (>50 %)

that qualifies them for several engineering applications such as aerospace, transportation and construction. Therefore, the target of the current study was to compare the properties of composites with a fibre volume content greater than 50 %. Consequently, the results from the performed thermomechanical characterizations mark the first step towards applying frontal polymerization as a rapid and efficient curing alternative to conventionally cured composites employed in industry.

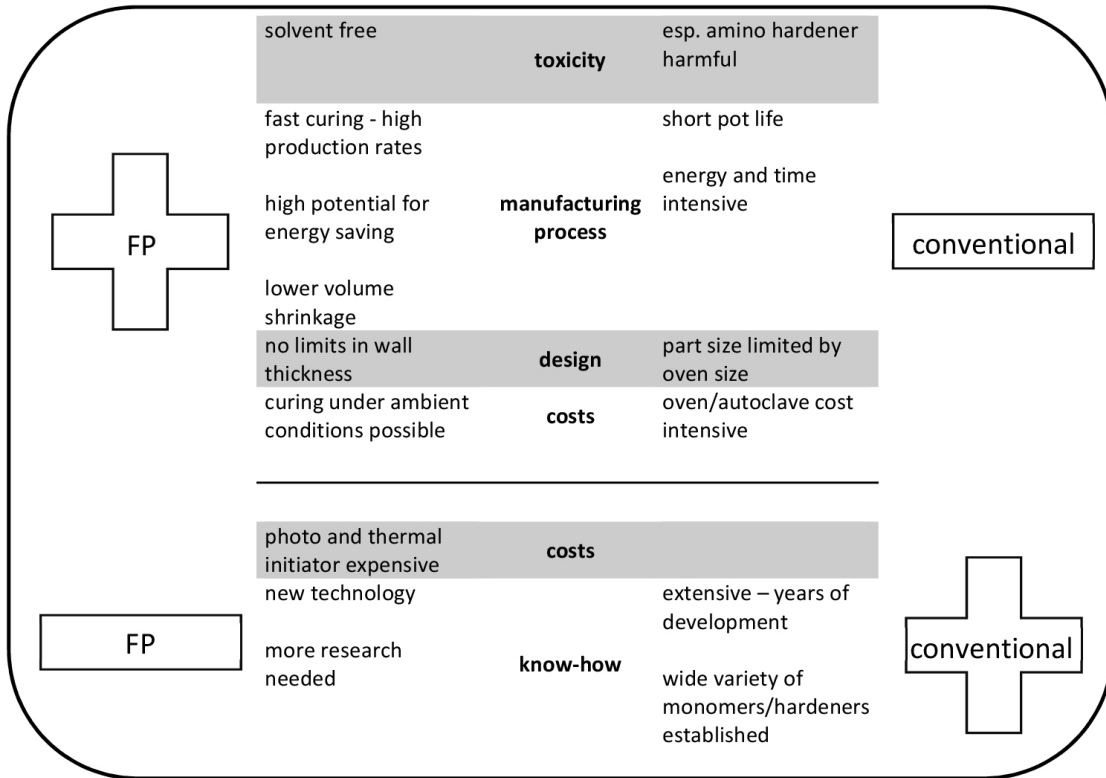


Figure 1.1: Comparison of the advantages (+) and disadvantages (-) between frontal and conventional curing.

The successful curing of epoxy resins with RICFP has already been reported by a variety of research groups [9] [10] [15] [13]. However, a detailed study on the thermal and mechanical properties of highly filled frontally cured carbon fibre (CF) reinforced composites is still missing in literature. Klikovits et al. studied RICFP on SiO₂ nanopowder composites [16], Mariani et al. used montmorillonite nano reinforcements [12], wherein the focus of these studies was directed on low fibre/filler content unsuitable for engineering composites. Tran et al. showed the effect of different diluents and performed tensile tests on woven fabric reinforced composites with a v_f of 35 % [17]. They reported no difference in tensile properties concerning the curing methods. Knaack et al. investigated the influence of different photoinitiators on composites with a v_f up to 22 % [9]. Additionally, they reported the possibility of underwater curing. Sangermano et al. reported a higher T_g and a lower $\sigma_{t_{MAX}}$ for a CF-epoxy cured via FP with approximately 43 vol% fibres [18].

The work of the present thesis can be divided into two parts. In the first part, composite test specimens were manufactured according to their corresponding standards via wlu process and VARI. Two different resin and reinforcement materials (unidirectional 50k fibre (UD) and twill weave fabric (fb)) were used and cured either via FP or conventionally (con), with a commercially available hardener. A total of 16 different types of plates were manufactured. Figure 1.2 provides an overview on the different manufacturing and curing methods and the used materials. More details can be found in chapter 3.

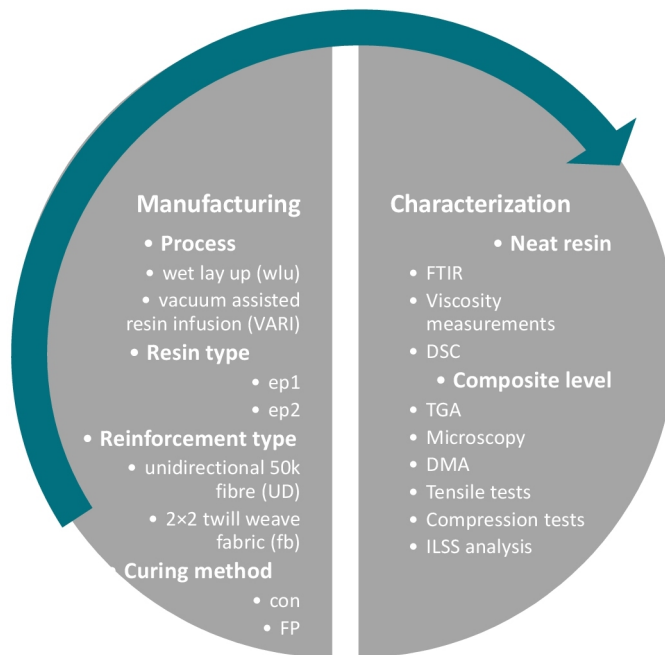


Figure 1.2: Overview on experimental part, divided in specimen manufacturing and characterization.

The second part of this thesis addresses the thermomechanical and morphological characterization of the produced specimens. To explore the feasibility of FP as curing method for CF reinforced composites, a test program, depicting the most vital properties for composites was created. It included DMA, tensile and compression tests and the analysis of the ILSS. Additionally, microscopy and thermogravimetric analysis (TGA) was performed to investigate the fibre distribution, specimen quality and fibre volume content. Furthermore, differential scanning calorimetry (DSC), Fourier-transform infrared (FTIR) spectroscopy and viscosity measurements were performed on neat resin to provide a deeper understanding on the materials and explanations on the material behaviour.

2 THEORETICAL BACKGROUND

2.1 Chemistry of epoxide monomers

In 1934 the Swiss chemist Pierre Castan started his work on epoxy resins, which led to a first important patent in this field and laid the foundation for the industrial use of epoxy resins. At the beginning, the major usage field were coatings, which is still an important application. However, over the last few years, the amount of epoxy used for electrical goods increased to about one third of the whole turnover. The composite market takes the third place. A detailed overview of the different usage fields is given in figure 2.1. In the composite sector itself glass fibre reinforcement types are the most common, followed by carbon fibre. Other fibres, such as natural fibres make up just a small share. Automotive and aerospace are the most important industries for epoxy based-composites. [19] [20] [7]



Figure 2.1: Overview on the application fields of epoxy in the U.S. from 2014 – 2024 [1].

From early days on, epoxy resins were produced by a reaction of bisphenol A and epichlorhydrin, the chemical structures of the mentioned substances are depicted in figure 2.2. Until today a wide variety of epoxy resins based on the diglycidylether of bisphenol A (BADGE or DGEBA) are used. The two-step reaction of bisphenol A and epichlorhydrin visible in figure 2.2c usually is used for creating BADGE. In addition to BADGE, a wide variety of other products (derivates of BADGE) of epichlorhydrin and bisphenol A are used. They resemble BADGE but can show a higher molecular weight, due to, for example, integrated linear ether- or altering bisphenol A- sections. Addi-

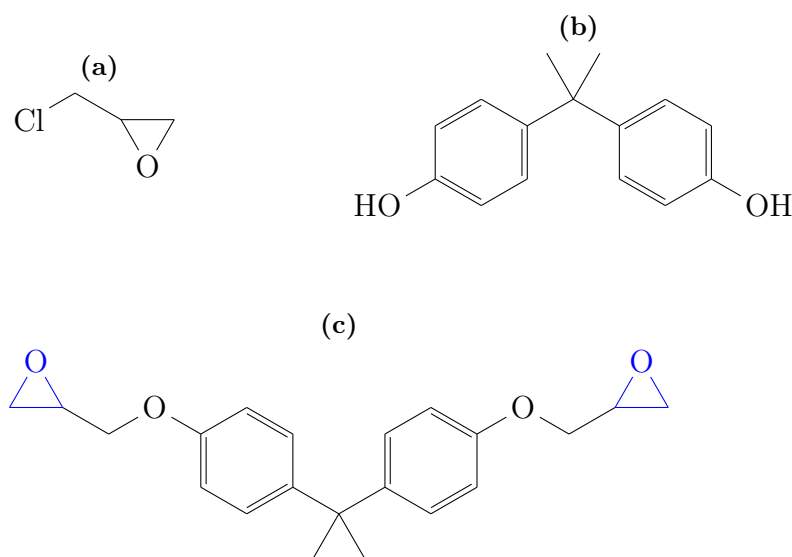


Figure 2.2: Chemical structures of: (2.2a) epichlorhydrin and (2.2b) bisphenol A, the constituents of (2.2c) BADGE.

tionally, a wide range of other epoxy monomers, such as novolac, has been established over the last decades [21].

The eponymous epoxy group, marked blue in figure 2.2c, is the reactive part of most of the available oligo- and monomers respectively. This ring formed of an oxygen and two hydrogen atoms, shows a significantly higher reactivity than other ethers. The main reason for this is the high strain of the ring [11] [22]. Like all thermosets, the material is characterized through irreversible crosslinks between the polymer chains. Prior to their formation, the epoxy resin is either a fluid or a meltable solid at room temperature and called uncured. The curing of epoxy monomers follows a polyaddition mechanism that involves ring opening of oxirane groups ultimately releasing large sum of energy (116 kJ/mol), owing to a high ring strain in oxirane groups.

In general, epoxide curing can be classified as either a two-component system where the hardener is integrated in the chemical network or catalytic curing. The latter, a cationic polymerization scheme, describes a mechanism where the epoxy groups of the oligo- or monomers interact to form a three-dimensional structure. To enable the formation of a three-dimensional network, the reactive substances or, –in a two-component curing system, the hardener needs to have at least two functional groups. Most commonly the energy for starting and supporting the network formation is derived from heat, which is supplied externally.

In the current master thesis, epoxy curing agents based on amines as well as anhydride derivatives have been employed as two component curing examples. Detailed

information about them and other hardener types, such as polymercaptanes are given in [23] [20] [24] [19].

The chemical structure of phthalic anhydride is shown in figure 2.3a as an example for a commonly used anhydride hardener. A drawback of this type of curing agent is their low reactivity compared to amino-hardeners. However, a lower reactivity results in a longer pot life, which is a favourable aspect while using anhydride curing agents. In addition, their significant electrical and physical properties qualifies for their usage in various commercial applications. In figure 2.3b a typical diamino hardener, 4-4'-diaminodiphenyl methane, is depicted. An amino hardener however does not necessarily contain cyclic structures [23] [25].

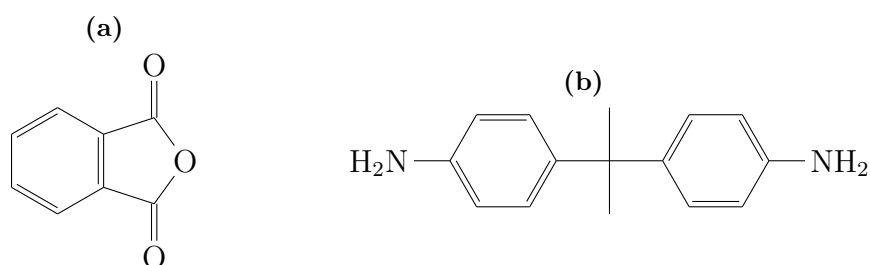


Figure 2.3: Examples for typical curing agents: (2.3a) phthalic anhydride and (2.3b) 4, 4'-Diaminodiphenyl methane.

2.2 Radical induced cationic frontal polymerization

In the following section and figure 2.4 a short overview on the relations and contrasts of different forms of frontal, cationic and photo polymerization is provided. Frontal Polymerization is divided into three types amongst which thermal FP is the most commonly investigated mechanism in literature. The other types – photofrontal and isothermal frontal polymerization, play just minor roles in research, since they are limited in usage. Therefore, the term FP usually is used equivalent with thermal FP. First studied in Russia on methyl methacrylate (MMA) in the 1970s by Chechilo [26] – frontal polymerization since then has been a subject of research in various publications [27] [28] [29] [30] [15] [31].

Thermal frontal polymerization is defined by a reactive, propagating front, which is driven by heat, generated via the ring opening of oxirane moiety. Therefore, it is a self-propagating reaction, which only needs a trigger such as radiation (e.g. heat or UV - light) for initiation.

UV-light also is used as source of energy for photo polymerization, which is already state of the art in a variety of application fields (e.g. coatings and adhesives). On

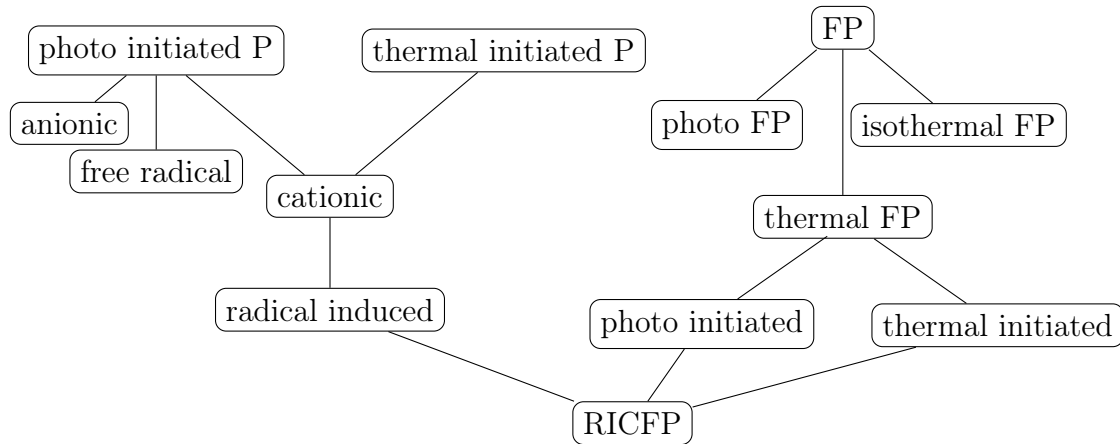


Figure 2.4: Relation between RICFP, frontal and cationic polymerization.

the contrary to FP, irradiation is required throughout the process for supporting the reaction, no propagating front is established. The radiation energy, most common in the UV spectrum, is transfigured into chemical energy, in form of ions, by photo initiators [32] [33] [34] [35] [36].

Epoxy ring opening frontal polymerization can follow either a cationic or a free radical-mediated curing route. The latter shows some distinct disadvantages compared to cationic polymerization, for instance pronounced shrinkage and inhibition by oxygen. Another vital difference between free radical and cationic polymerizations is the fact that radical polymerization are not "living". A living polymerization remains active after turning off the irradiation, which can be either an issue or an advantage, depending on the usage. The reason for this phenomenon, also called dark curing, is the durability of the super acid. Furthermore, a cationic polymerization is not necessarily initiated by light, also heat can start the reaction.

For photo polymerization of epoxide monomers cations initiate a ring-opening reaction, illustrated in figure 2.5. For such polymerization processes, a small amount of a super acid (HX) is needed. In photoinitiated reactions, the super acid typically is formed through hetero- and homolytic cleavage of a photo acid generator (PAG). Such UV triggered photo initiators often are onium salts, such as iodonium or sulfonium salts, see section 3.1.2. The reaction is started by addition of the super acid to a monomer, which furthermore interacts with the nucleophilic oxygen atom of the oxirane group. This nucleophilic attack leads to the formation of a secondary oxonium cation. This intermediate reacts with further monomers to form tertiary oxonium cations. The reaction continues by addition of more monomers, so a polymeric structure is formed. The velocity and rate of this polymerization are controlled by the exothermicity of the reaction and the stability of the secondary oxonium cation, which furthermore depends on the type of PAG used [37].

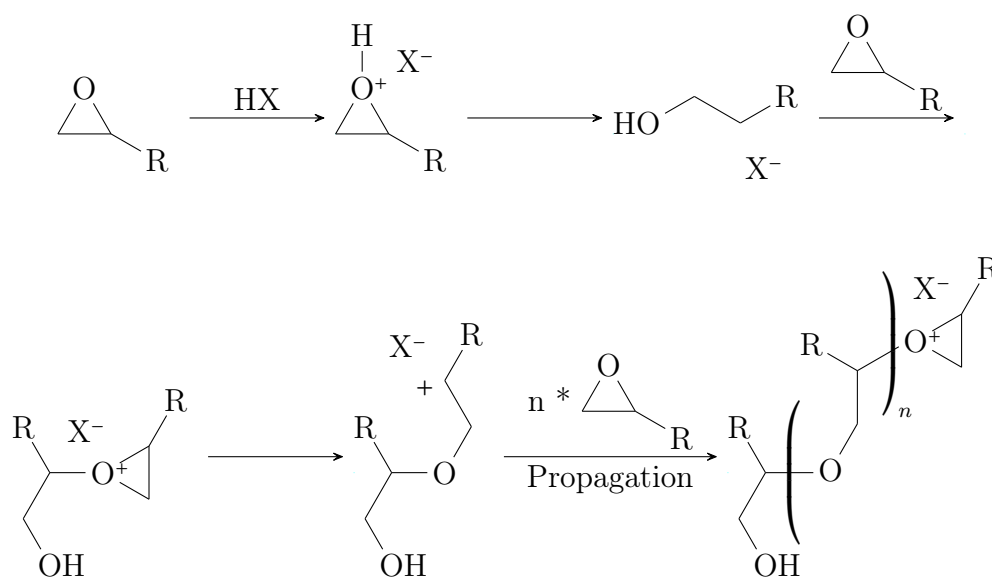


Figure 2.5: Reaction scheme of the cationic polymerization of an epoxy monomer.

Crivello et al. [38] were the first who described a combination of photo induced cationic polymerization and FP of epoxy monomers using a special class of PAGs based on iodonium salts. In their experiments they first exposed a thin film of 3-ethyl-3-phenyloxymethyl mixed with 1 mol% of an iodonium salt cationic photo initiator to UV irradiation, for about 1 min. After the irradiation was turned off the still liquid substance was slightly heated at one spot. The polymerization takes place in the form of a self-sustaining propagating front without further irradiation and cures the entire film while utilizing the exothermicity of the oxirane ring opening.

Further investigations in this field conducted by Mariani et al. [15] showed that the dissociation of an onium salt can be achieved with radicals instead of UV irradiation as well. The advantage of this reaction chain is, that the polymerization is not dependent on light. On the contrary, it can be started by a variety of chemicals, which generates free radicals for example a thermal radical initiator such as dibenzoyl peroxide. These findings lead to the establishment of RICFP, where the cleavage of a photo initiator starts a cationic polymerization, as explained earlier. The initiation can be stimulated by either UV - light or heat [30]. The heat, generated in the addition of the oxirane monomers, cleaves the thermal initiator. As a result of this cleavage reactive radicals are generated, that are capable of cleaving the photo initiator instead of prolonging UV irradiation time. It was demonstrated, that the highest amount of epoxy conversion can be reached by adding the same quantity of thermal and photo initiator [10] [11] [15] [32].

2.3 Thermo mechanical properties of FRP

2.3.1 Macro vs. micro mechanics

Generally, it can be summarized that in case of fibre reinforced plastic (FRP), macro mechanics treats the composite as a homogeneous material with properties representing an average of the apparent material properties. Whereas, micro mechanics divides the composite in matrix and reinforcement material and analyses their interactions. Moreover, it studies the behaviour of single parts of the heterogeneous material on a very small scale. The common feature they share is a single UD lamina, representing the smallest portion in macro mechanics and the largest constituent in micro mechanics, respectively.

Although micro mechanics theoretically provides the possibility to predict the properties of a composite, if the properties of the components are known, it is hardly used for engineering purposes. This is caused by, on the one hand the high amount of assumptions which have to be made, but are not valid for real materials. On the other hand a variety of parameters influenced by the manufacturing process and therefore nearly impossible to control for example: Curing behaviour, voids, misaligned or damaged fibres.

However, some basic rules concerning the influence of the component's material properties on the behaviour of the composite can be derived from macro mechanics such as:

- the fibre's E-Modulus significantly influences the composite's tensile modulus
- the matrix's E-Modulus significantly influences the composite's compression and shear modulus
- the fibre volume fraction slightly affects compression and shear modulus of the composite, however has little impact on its tensile modulus

The first rule, concerning the tensile modulus also is tackled in the attempt to predict the composite's e-modulus with the rule of mixture, depicted in equation (eq) 2.1

$$E = v_f \cdot E_f + v_m \cdot E_m \quad (2.1)$$

Where v_f and v_m are the volume fraction of the fibre and the matrix, respectively and E_f and E_m the corresponding E-moduli. This rule of mixture can be used in a similar way to calculate the maximum stress of a composite (see eq 2.2).

$$\sigma_{c_{MAX}} = \sigma_{f_{MAX}} \cdot v_f + (\sigma_m)_{\epsilon_{f_{MAX}}} \cdot v_m \quad (2.2)$$

Where $\sigma_{f_{MAX}}$ is the fibre's maximum tensile stress and $(\sigma_m)_{\epsilon_{f_{MAX}}}$ the matrix stress at a strain corresponding to the maximum fibre strain. Additionally, it has to be mentioned, that a minimum value for the fibre volume fraction, $v_{f_{MIN}}$, exists which has to be exceeded to ensure a reinforcing effect of the fibres. Otherwise, the fibres would appear to have zero material properties and therefore act like holes.

$$v_{f_{MIN}} = \frac{\sigma_{m_{MAX}} - (\sigma_m)_{\epsilon_{f_{MAX}}}}{\sigma_{f_{MAX}} + \sigma_{m_{MAX}} - (\sigma_m)_{\epsilon_{f_{MAX}}}} \quad (2.3)$$

Furthermore, figure 2.6 illustrates the relation between the maximum stress and strain of a fibre, a matrix and their composite. In summary, the maximum elongation of the fibre is substantially lower than that of the matrix and resembles to that of the composite. The relatively brittle behaviour of the fibres compared to the matrix leads to the fact that they cannot elongate as much as the matrix. Therefore, the composite's elongation depends on the elongation of the fibres.

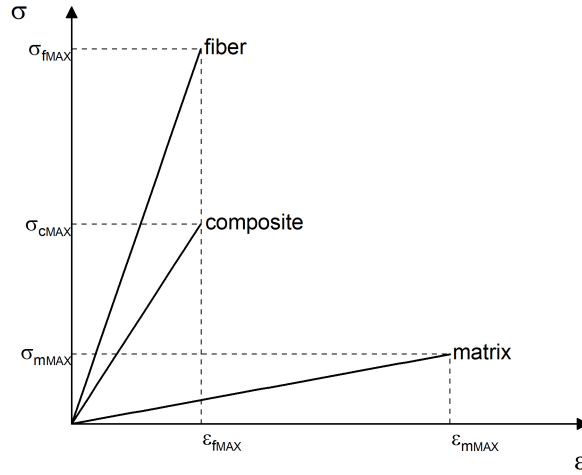


Figure 2.6: Stress-strain relationship of fibre/matrix and composite material after [2].

However, as explained earlier, the micromechanical approach is not generally used for construction purposes. Calculations concerning the design of a structural element are done via macro mechanics. Macro mechanics regards the composite rather as one material, than as a combination of matrix and reinforcement material and their interface. This combined material is mainly represented by a single ply with blurred material properties. Achieving these properties of a single ply and predicting its failure

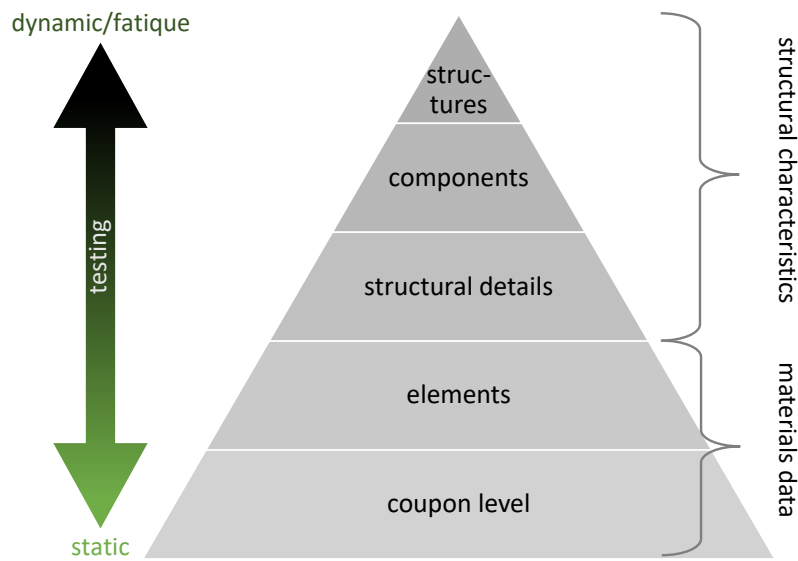


Figure 2.7: Test pyramid for composite materials, after [3].

has been a focus of many researchers [39] [40] [41]. It can be summarized that different damage processes, dependent on the direction of stress, leads to failure. Typical damage processes are fibre shearing, failure of the fibre-matrix interface (cohesive failure) or fibre failure through kinking due to insufficient support by the matrix. For predicting failure, different criteria has been developed, such as the Puck- [41] or Tsai-Wu criterion [42]. In addition to the criterion, knowledge of the material properties in the three main directions i.e, along the thickness axis, the fibre axis and perpendicular to it is essential.

Figure 2.7 illustrates the test pyramid where the broadness of a level represents the quantity of tests. The costs and complexity of the tests increase bottom-up. The tests at coupon level are done for the validation of a material model and for gaining material properties. Since the influence of the geometry and design is least at the lowest level. As mentioned earlier, the focus lies on characterising a material in the three main axes. The most vital mechanical test methods are:

- flexural tests e.g. three- or four- point bending
- shear tests e.g. lap shear or short beam shear (SBS)
- compression tests e.g. in 0° or 90° , open hole compression
- tension tests e.g. in 0° or 90° , under dynamic load

Furthermore, the behaviour under different temperatures, or at least the T_g are important to know. For this purpose, the DMA is a widespread method of performing

mechanical tests at different temperatures. Additionally, gaining knowledge on the material properties of single constituents is a vital tool for a better understanding of composite materials. This is achieved by performing mechanical tests on the single constituents. Furthermore, the mechanical behaviour of the interface is of interest, which can be investigated by special test methods, such as the fibre-pull out test [43] [44].

2.3.2 Dynamic mechanical analysis

For highly filled composite materials the evaluation of the T_g via DSC is often impossible, since the changes in heat capacity and heat flow, respectively are too low to detect. A common way to circumvent this issue is to use DMA instead. Since for highly crosslinked polymers the change in E' usually is pronounced covering a range of $10 - 10^3$ Pa. The micro mechanical background, the functionality, the broad range of usage, etc. of a DMA would go far beyond the scope of this thesis and are well explained in literature, such as: [4] [44] [45]

This chapter summarizes the most important material parameters which can be measured or defined in a DMA, with regard to thermosets. Additionally, it should be emphasized, that the common load application type for very stiff materials, such as composites, metals or ceramics, is three- or four-point bending. Three-point bending is on the one hand simpler to conduct, yet on the other hand inter laminar shear stresses can occur. This drawback of additional, undesired shear stresses within a plane, which usually is neutral, can be avoided by choosing specimens with a suitable length to thickness ratio [45].

As mentioned above, one main purpose of this measurements is to define the T_g . In addition to its mechanical properties, such as the E' and loss modulus (E'') can be specified. Hence also conclusions on the cure behaviour and network structure of the resin can be drawn.

An increasing crosslink density equals lower molecular weights between the crosslink points and therefore less room for molecular movements. Consequently, the loss factor curve- tangents δ , shifts to higher temperatures ultimately leading to broadening of the tangents δ curve. At the same time the loss in E' becomes less pronounced, which means less change in altitude over a wider temperature range. This trends also can be seen in figure 2.8 The more heterogeneous a network is, the more this behaviour is promoted.

It is recommended in literature to calculate the T_g for thermosets with a high degree of crosslinking or heterogeneity using the tangent method. For this the onset of the start of glass transition is determined by the intersection of two tangents, one applied

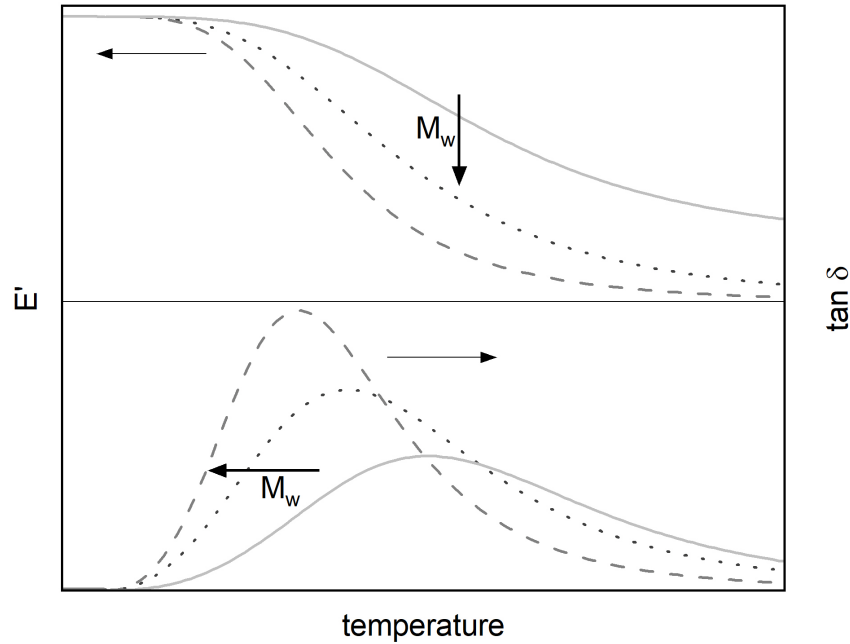


Figure 2.8: Influence of the molecular weight i.e. crosslink density on E' and loss factor after [4].

to the linear section of the E' curve before the transition region and the other one in the inflection point of the curve. In table 2.1 it is outlined which curve effect can be attributed to what characteristic of the material.

Table 2.1: Examples for the network structure's influence on DMA curves.

Additional peak in loss factor	Post curing
E' plateau above T_g rise in magnitude	Post curing
Broadness of loss factor	Network heterogeneity
Location and width of transition region	Crosslink density
Magnitude of E'	Crosslink density and reinforcements

2.3.3 The effect of voids on mechanical properties

Entrapped air, generally referred to as voids, is a common issue in all sectors of material science. Their major drawback is their strong influence on mechanical properties. They induce either defects or inhomogeneity in the material. On one hand they can act as micro notches or on the other hand lead to local fibre kinking. In FRP, the amount of voids vary depending on the used manufacturing process. Hand or wet lay-up is regarded as the process resulting in products with the highest void content. An

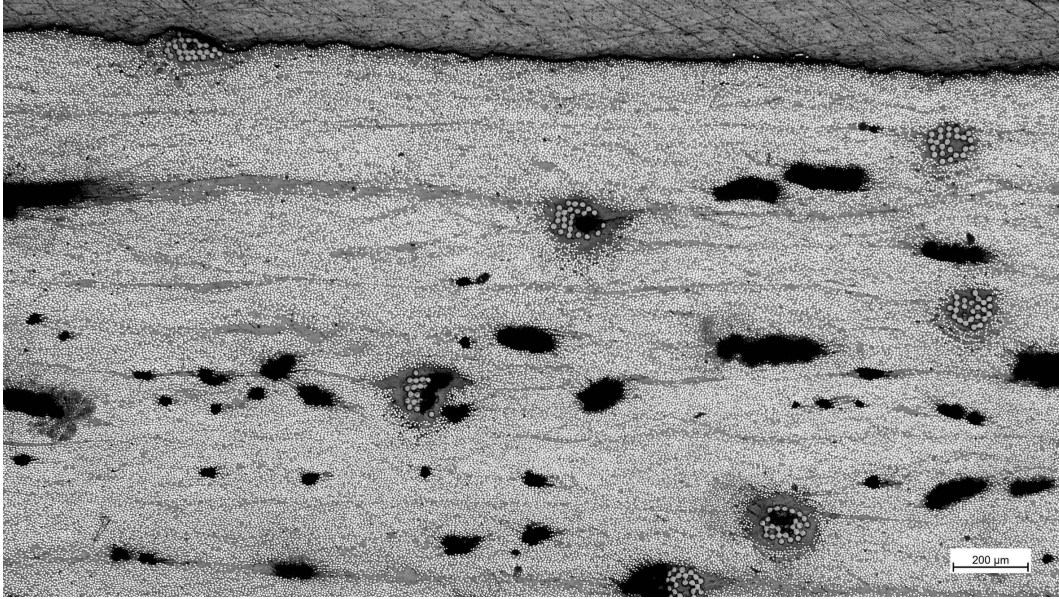


Figure 2.9: Example of UD CF/epoxy composite with a high void content.

example of a UD reinforced composite produced via wlu is depicted in figure 2.9. Voids of different size and shape are clearly visible. Applied vacuum and pressure, as well as elevated temperatures reduce the amount of entrapped air to a high degree [19] [46]. However, these voids do not affect every material property in the same way.

Generally, it can be stated that fibre dominated properties, such as tensile strength and toughness, are not essentially affected if the v_f exceeds the critical value. Whereas, matrix dominated properties, such as transverse and shear properties are influenced considerably by voids. However, the influence of voids varies in extent, depending on the type of deformation, it is reported that the ILSS is affected the most. Costa et al. for example showed, that an increase of void content from nearly no voids to 5 % can reduce the ILSS by almost one third. Another common observation of the influence of voids in ILSS-tests is, that, if the specimen fails in shear, either single or multiple, the origin of the crack usually is a void in the matrix [47] [48]. However, it has been documented, that the void content alone is not enough to characterize the influence. The relative size, shape and the location of voids have an effect on the material behaviour [49] [50].

In terms of compression testing, the influence of voids on the material properties are caused by fibre instabilities such as buckling or kinking. While flexural properties are affected in a way, which can be described as a combination of the mechanics prompting failure in ILSS and compression testing. Other properties such as the fatigue or impact behaviour, are influenced as well by voids however, since they are not object of this thesis they shall not be discussed here [46] [51] [52].

3 EXPERIMENTAL PART

In the following chapter the used materials and processing techniques are discussed in detail. Furthermore, the performance of the conducted material tests is explained. Additionally, all vital test parameters are listed. In the course of this thesis, a uniform nomenclature was used according to equation 3.1, using the abbreviations listed in figure 1.2.

$$\text{manufacturing method} - \text{fibre type} - \text{resin type_curing method} \quad (3.1)$$

3.1 Materials

3.1.1 Reinforcement materials

Two types of carbon fibres were chosen as reinforcement materials that were purchased from R & G Faserverbundwerkstoffe GmbH (*Germany*). One UD lamina and one 2×2 twill weave fabric was used. The most important material properties, derived from the data sheets are depicted in table 3.1.

Table 3.1: Reinforcement properties

	fb	UD
Type	unidirectional	2 by 2 twill fabric
Density / kg/m ³	1.78	1.81
Weight / g/m ²	245	200
Tensile Strength / MPa	3800	4137
Tensile Modulus / GPa	240	242
Elongation at Break / %	1.6	1.7

3.1.2 Matrix Materials

Two different resin materials named ep1 (OLIN CORPORATION, *United States*) and ep (DOW EUROPE GMBH, *Switzerland*), were used as matrix. These resins were provided by MAGNA Energy Storage Systems GmbH *Austria* and therefore only general properties can be named, as indicated in table 3.2. Both epoxy resins contain 75 % aromatic BADGE-based structures. The chemical structures of these prepolymers are depicted in figure 3.1, figure 3.1a for ep1 monomers and figure 3.1b for ep2 oligomers, respectively. 25 % aliphatic epoxide monomer (figure 3.1) was added to lower the viscosity and thereby simplify the processing.

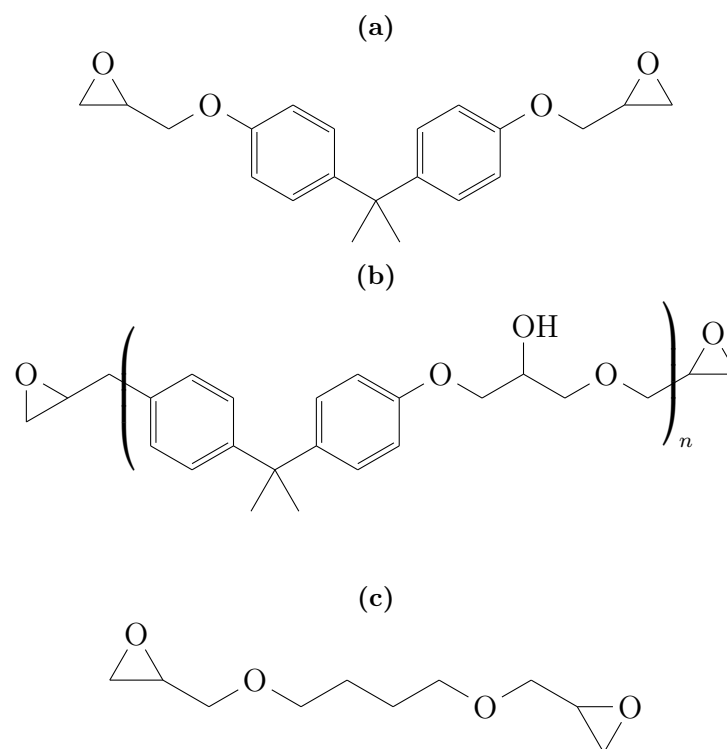


Figure 3.1: Chemical structures of the prepolymer components used as resins: ep1 (3.1a) the BADGE monomer, ep2 (3.1b) BADGE based oligomers and (3.1c) the aliphatic diluent.

In table 3.2 some important characteristics, given in the data sheets are depicted. In the lower part of the table mechanical properties of frontally cured epoxy specimens are listed. They were measured in former tensile tests according to ISO 527 under standardized laboratory conditions. For both resin types, 1.5 wt% of a photo- and a thermal initiator were used. Their chemical structures are depicted in figure 3.2. To ensure a good distribution of the initiators, a Vortex Mixer was used for mixing initiators.

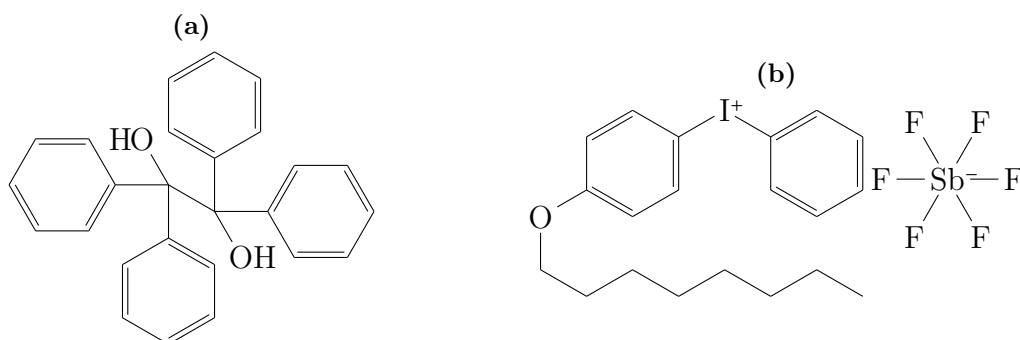


Figure 3.2: Chemical structures of thermal radical initiator: tetraphenyl ethanediol (3.2a) and the photoinitiator: p-octyl oxyphenyl phenyliodonium hexafluoro antimonate (3.2b).

Table 3.2: Matrix materials.

	ep1	ep2
Conventional curing (con)		
Density – resin @ 25 °C, g/m ³	1.2	1.1 – 1.2
Density – hardener @ 25 °C, g/m ³	1.2	0.9 – 1
Mixing ratio (per weight)	100:104–108	100:22
Hardener type	anhydride	amino
Typical curing cycle	3 – 4 h@ 105 °C	6 – 8 h @ 100 °C
T _g , DSC (10 K/min), °C	110 – 115	114
Tensile modulus / MPa	3100	3050 ±960
Tensile strength / MPa	75 – 80	66 ±5.3
Elongation at Break / %	3 – 5	3.2 ±1,11
Frontal curing (FP)		
Tensile modulus / MPa	3000 ±530	3200 ±210
Tensile strength / MPa	45± 7.5	53 ±5.5
Elongation at break / %	2 ±0.35	2.2 ±0.21

3.2 Processing

For the production of specimens, plates were manufactured in two different ways which are explained in the following discussions. Curing times and temperatures were the same with regard to manufacturing methods however, different for frontal and conventional curing. It should be mentioned here that the FP was initiated with heat, and therefore kept at 150 °C for 50 min per mm of plate thickness. The con plates were cured for 5 h at 120 °C. Cutting of specimens was performed with a diamond saw and great precision concerning the alignment of fibres.

3.2.1 Wet lay up

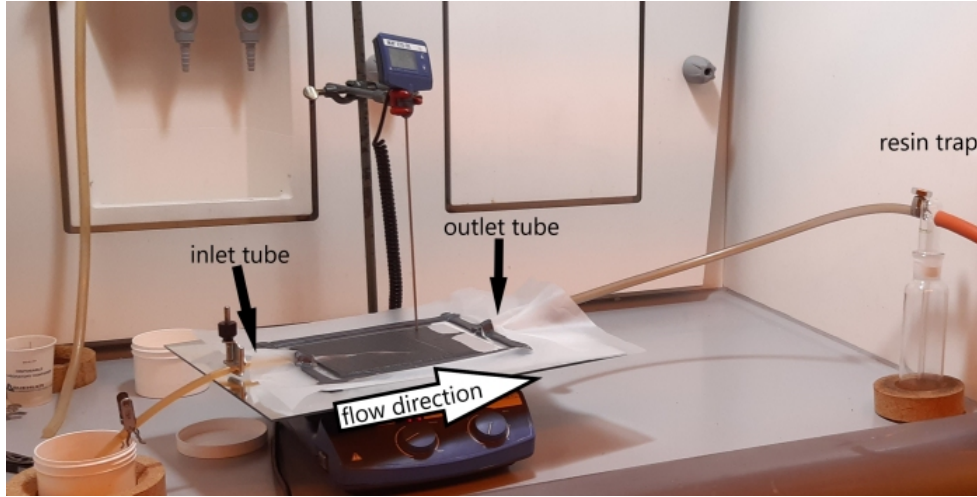
The number of plies, listed in table 3.3 and the amount of epoxy resin were calculated in advance for achieving an approximate thickness of 1 mm and 2 mm, respectively while maintaining a v_f of approximately 50 %. The plates were built up layer by layer into a silicon mould of the desired size. After each carbon fibre layer, a portion of the epoxy resin was added, distributed and compressed with a metal roller.

3.2.2 Vacuum assisted resin infusion

Figure 3.3 illustrates the set-up of the VARI process used in the current study. The same number of plies as used in the wlu process were also used in the VARI process. Since the infusion process is driven by vacuum and stopped when the resin reaches the outlet tube, the amount of epoxy cannot easily be controlled. Nevertheless, better

Table 3.3: Number of plies.

	Unidirectional		Fabric	
	Number of plies	Total thickness / mm	Number of plies	Total thickness / mm
Tensile specimens	5	1	8	2
Compression specimens	10	2	8	2
ILSS specimens	10	2	8	2
DMA specimens	10	2	8	2

**Figure 3.3:** Set up of VARI process used for manufacturing plates.

geometry for composite specimens were achieved. The calculation of the v_f showed that for the fabric plates, the content was slightly lower than those for the UD specimens. Due to impregnation problems, in first trials at room temperature, especially with the UD lamina and FP-resin formulations, the bottom plate and the resin vessel were heated up to 40 °C to reduce the viscosity.

3.3 Characterization

3.3.1 Morphology

The average v_f was calculated from the mass of the components by using the following equation:

$$v_f = \frac{\rho_m \cdot m_f}{\rho_f \cdot m_m + \rho_m \cdot m_f} \cdot 100 \quad (3.2)$$

Where $\rho_{m/f}$ is the density of the matrix/fibres and $m_{m/f}$ the corresponding weight. For the validation of this method TGA was performed on several different specimen types.

The measurements were done on a thermogravimetric analyser (METTLER TOLEDO, *United States*). Specimens of about 20 mg were taken out of the plate on different positions. The used method is described in table 3.4.

Table 3.4: TGA method.

Segment	Start Temperature °C	End Temperature °C	Heating rate °C/s	Gas Type mL/min
1	30	700	0.08	N ₂ , 50
2	700	200	-0.33	N ₂ , 50
3	200	800	0.08	O ₂

Since voids have a significant influence on mechanical testing such as ILSS, specific attention was laid on quantifying them. Microscopy pictures of cross sections were taken and the content of voids calculated using an image processing program (IMAGEJ, *United States*) for determining the percentage of black within a specific specimen area. However, the content of voids varied a lot throughout the plates. Therefore, the thickness measurements of the specimens were taken for evaluating a representative average thickness value t_{av} . Additionally, an expected thickness value, t_{ex} , was calculated using the actual v_f . Using these values, a ratio $t_{av}:t_{ex}$ can be used to quantify the amount of voids within a specimen.

For optical investigations a light microscope MAT 7 microscope (CARL ZEISS AG, *Germany*) was used. The samples were embedded in an epoxy matrix, grinded and polished.

3.3.2 Neat resin characterization

Rheological measurements were performed on a MCR501 rheometer (ANTON PAAR, *Austria*). Since the aim of the measurements was to determine the gelation temperature a temperature/time-sweep was performed. A shear rate of 100 s^{-1} within the temperature range 70 to 120 °C was chosen.

For calculating the degree of cure (α) via FTIR spectroscopy, a Bruker Vertex 70 Spectrometer (BRUKER, *United States*) with attenuated total reflectance was used. The spectral range covered 400 to 4000 cm^{-1} with 16 scans per sample and a resolution of 2 cm^{-1} was set. The calculation of α , in %, was done according to eq 3.3, where $A_{uncured}$ and A_{cured} correspond to the peak area determined for the uncured and cured epoxy resins, respectively, at the characteristic epoxy absorption band (915 cm^{-1}).

$$\alpha = 100 * \left(1 - \frac{A_{cured}}{A_{uncured}}\right) \quad (3.3)$$

Table 3.5: Method adopted for the DSC.

Segment	Start temperature °C	End temperature °C	Heating rate °C/min
1	20	160	20
2	160	20	
3	20	210	20

The DSC measurements were conducted on a DSC 4000 (PERKINELMER, INC, *United States*) for characterizing the exothermic heat and eventual post curing effects on uncured as well as cured neat resin specimens. The used method is described in table 3.5. Specimens of about 20 mg were weighed into aluminium pans and at least two specimens per type were investigated.

3.3.3 Dynamic mechanical analysis

The DMA was performed following DIN EN ISO 6721 [53] on a dynamic mechanical analyser, DMA/STDA 1+ (METTLER TOLEDO, *United States*). As recommended for very stiff materials like metals, ceramics and composites, three point-point bending was chosen as the force loading type. To circumvent the influence of additional shear stresses a support distance of 60 mm was chosen. Before measuring, the specimens were sanded on both sides to receive a smooth surface, and thereby, to circumvent load application issues. In the course of the process of defining the optimum measuring parameters, two methods were found as preferable for getting reliable and reproducible results. The main difference between those two methods is the offset control mode. The offset force is applied additionally to the amplitude to prevent times without contact between sample and clamping assembly. Method 1 uses a constant offset force throughout the experiment. For method 2 the autooffset control mode was chosen. In this mode the minimal force to keep contact to the sample is evaluated. This corresponds to 100 % autooffset. During the experiment the offset force adapts iteratively dependent on the set value and the current minimal force needed [54]. The following two methods were defined for DMA:

- Method 1
 - Heating rate = 2 K/min
 - Amplitude = 40 μm
 - Offset force = 10 N
- Method 2

- Heating rate = 2 K/min
- Amplitude = 10 μm
- Auto-offset = 400 %

The T_g was estimated with two different methods, described in [55] and shown in the appendix (A.3):

1. $T_{g(eig)}$: extrapolated onset temperature; the intersection of the extrapolated tangents below glass transition and inflection point in E' curve
2. $T_{g(peak)}$: peak of $\tan(\delta)$ curve

3.3.4 Tensile tests

The tensile tests were performed according to DIN EN ISO 527-4 [56], for fabric reinforcement, and DIN EN ISO 527-5 [57] for UD reinforced specimens. The geometry of specimens is illustrated in figure 3.4. The UD specimens were exclusively tested in fibre direction. As recommended in the standard, scarfed glass fibre reinforced tabs

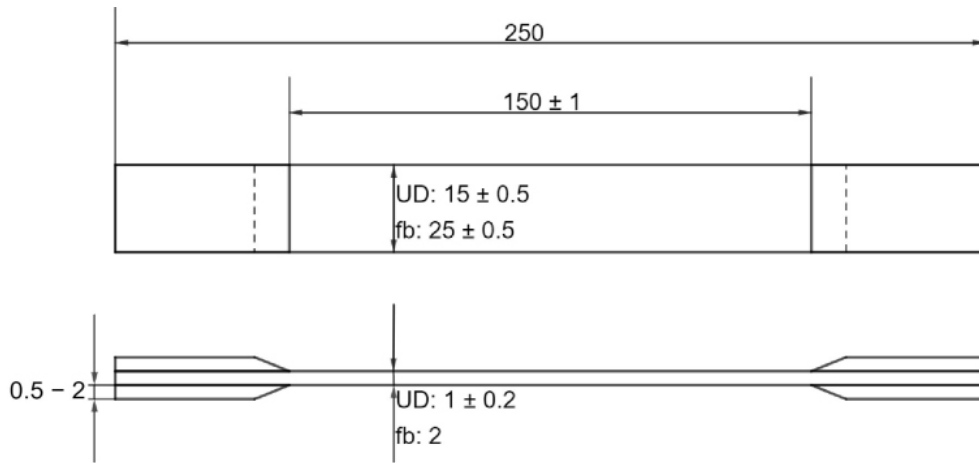


Figure 3.4: Geometry of tensile test specimens, all values in mm.

were applied to the specimens, to enhance gripping. Tensile tests were performed under standardised laboratory conditions (23 °C air temperature and 50 % relative humidity) on a Zwick Z250, (ZWICKROELL GMBH & CO. KG, *Germany*) with a 100 kN load cell. At least 5 specimens of each type were tested. The crosshead speed was set to 2 mm/min and the strain was measured with a mechanical extensometer, furthermore hydraulic grips were used. Due to non-conformal failure (in tab region) of the first tested fabric specimens mechanical gripping devices were tried. However, no change in failure behaviour was observed with the different gripping device. The same issue

had occurred in former tests and the experience had been made, that if replicable the results can be used. Hence, it was decided to conduct the tests with hydraulic grips. All the wet lay-up samples showed non-linearities in the region of small deformation ($\leq 0.015\%$), therefore the tensile modulus was calculated in the range of 0.15 to 0.25 % strain. The specimens produced via VARI showed no difference in tensile moduli using either values for 0.05 or 0.015 % strain.

3.3.5 Compression tests

The compression tests were performed according to DIN EN ISO 14126 [58]. The sample geometry is illustrated in figure 3.5. To improve the introduction of force glass fibre reinforced tabs were mounted on the specimens. The tests were performed under standardised laboratory conditions (23 °C air temperature and 50 % relative humidity) on a Zwick Z250, (ZWICKROELL GMBH & CO. KG, *Germany*) with a 100 kN load cell. At least 5 specimens of each type were tested.

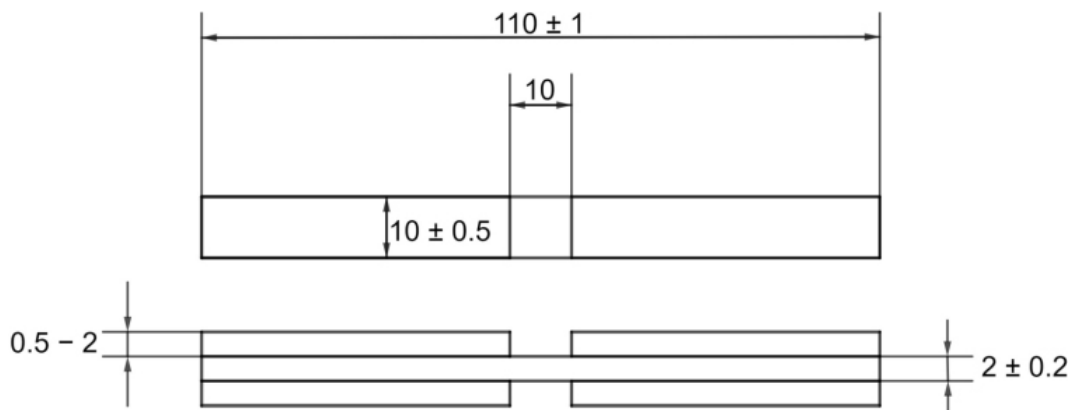


Figure 3.5: Geometry of compression test specimens, all values in mm.

Additionally, a hydraulic composites compression fixture (HCCF), depicted in figure 3.6a from ZwickRoell GmbH was used, since there were good results achieved from prior tests. The fixture couples end- and shear load application to the so-called combined load. For achieving good results, the insertion of the specimens in the HCCF and the parallelism of their edges is essential. After the specimen was placed inside, the lower grip was closed and then the machine was brought to contact manually. The last step was to close the upper grip. Both grips were closed with a pressure of 50 bar. The strain was measured by means of three-dimensional digital image correlation (DIC). For this purpose, a stochastic dot pattern was applied to the gauge length, by a white and a black spray paint (CRC INDUSTRIES EUROPE, *Belgium*). The used software was Mercury (SOBRIETY, *Czech Republic*). The camera system consisting of

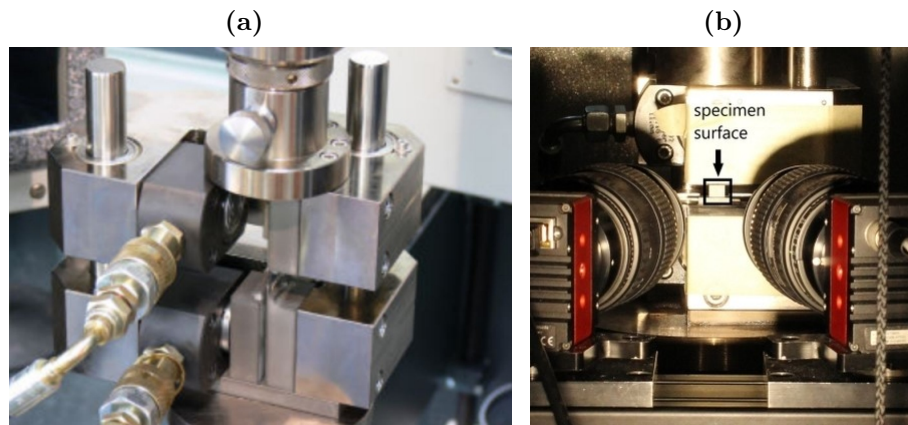


Figure 3.6: Detailed picture of: (3.6a) the HCCF, used for compression testing and (3.6b) the camera set-up.

two 4-megapixel cameras with macro lenses, was placed slightly diagonally in front of the specimen. The set-up can be seen in figure 3.6b. For the evaluations a fictive extensometer was placed in the middle of the specimen surface. The compression modulus was calculated in the range of 0.05 and 0.25 % strain.

3.3.6 Inter laminar shear stress tests

The ILSS tests were performed according to DIN EN ISO 14130 [59], which characterizes the apparent ILSS by the short beam method. Samples with a rectangular shape, $(20 \pm 1 \times 10 \pm 0.2 \times 2 \pm 0.2 \text{ mm})$ were used, as required by the standard. For each set of specimens the distance between the supports was set according to the standard and the mean thickness value. Specimens with an uneven surface were sanded to ensure a good load application. The deflection was measured by the crosshead travel. As suggested by the standard the ILSS was also calculated for specimens which did not fail due to shear, since the purpose of the test was a direct comparison to each other. However, the exact failure types are described for each set in the results chapter.

4 RESULTS AND DISCUSSION

The main focus of this thesis lies on characterizing the influence of different curing methods on material properties. Four sets of specimens with equal reinforcement materials and manufacturing methods were tested. The comparison of resin type and curing method mainly is done within one set. The data reduction was done with Origin (ORIGINLAB, *United States*). In the following section preferably one curve with typical behaviour is depicted instead of an average curve, since average curves often are blurred or show other artefacts.

4.1 Neat resin characterization

The graphs obtained from rheological measurements for all epoxy and curing types, are shown in figure 4.1. The temperature at which the viscosity starts to increase towards infinity, which can be referred to as T_{gel}^{onset} , is indicated below. For the calculation of T_{gel}^{onset} tangents were fitted to the curve and their intersection calculated, as shown in figure 4.1. Ep2_con shows the lowest T_{gel}^{onset} with 73.4°C, yet the broadest onset curve. The highest T_{gel}^{onset} can be found for ep2_FP with 98.3°C. This leads to the conclusion

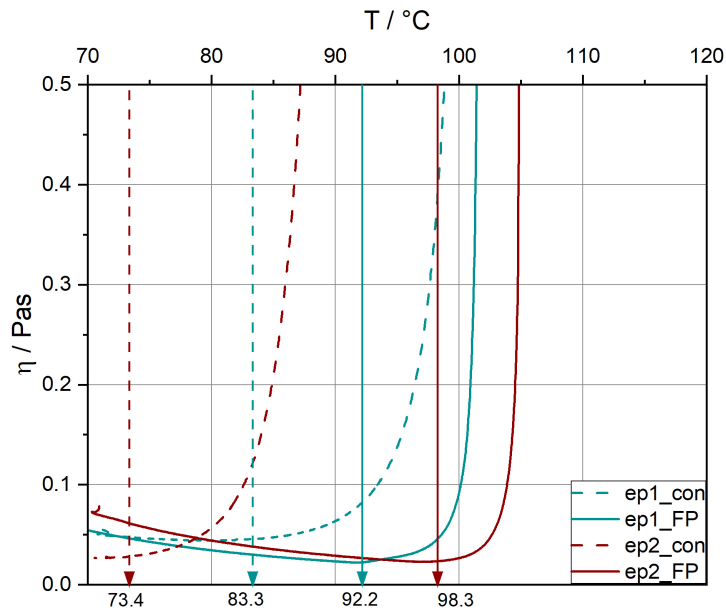


Figure 4.1: Viscosity in Pas against temperature in °C for all resin and curing types, with indicated T_{gel}^{onset} .

that the network formation is more dependent on the type of curing, than chemistry of the monomer. In equation 4.1 a ranking, in value, of the T_{gel}^{onset} can be found. Furthermore, it can be concluded that both conventional cured resin formulations already

have reached their minimum viscosity before 70 °C. The viscosity of the FP samples, on the contrary, is constantly decreasing from 70 °C until finally reaching T_{gel}^{onset} .

$$\text{ranking } T_{gel}^{on} : ep2_con < ep1_con < ep1_FP < ep2_FP \quad (4.1)$$

The formulations of both epoxy types contain 25 % of the same aliphatic diluent and 75 % of a BADGE-based prepolymer. Ep2 contains BADGE based oligomers whereas ep1 contains BADGE monomers. Hence for FP, the differences in material properties found within one set are strongly influenced by the network structure resulting from crosslinking density. For better understanding, FTIR spectroscopy was performed and the conversion rates of the epoxy groups were calculated. The spectra can be found in figure 4.2 and the monomer conversions in table 4.1.

The differences in conversions between the curing types are hardly interpretable, since the molecular structures are different. In the course of con curing, the hardener is integrated in the network resulting in a completely different type of crosslinked network in comparison to frontal cured resins. However, the conversion rates for FP provide insight in the network forming behaviour. The conversion rate for the FP specimens

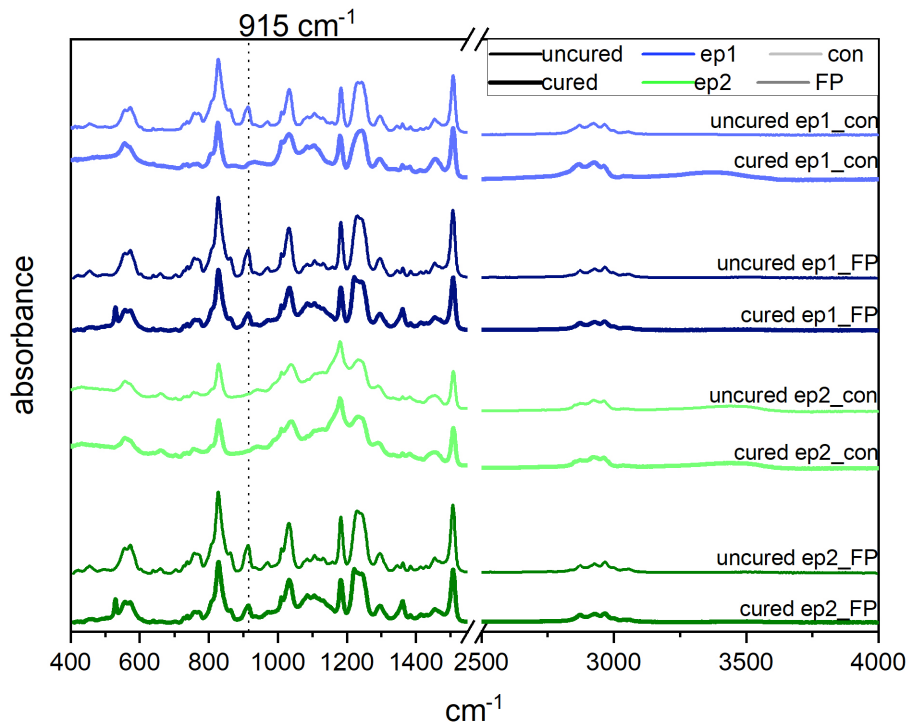


Figure 4.2: IR spectra for the determination of the epoxy group conversion rate.

out of BADGE monomers is 70 %, which is 15 % higher than for the BADGE oligomers. This could indicate that the formed network for both epoxy types is similar.

Table 4.1: Conversion rates derived from IR spectroscopy.

Conversion rate in %	
ep1_con	44
ep1_FP	70
ep2_con	55
ep2_FP	57

The results of interest from DSC measurements are the T_g (mid point) values. They were calculated for the first and second heating runs, depicted in table 4.2. Both FP resins show two glass transitions in the first heating run. It is assumed that two network formations take place and indicate one T_g at a time. Therefore, the lower T_g , at 74 °C, can be attributed to the crosslinking of the aliphatic diluent, which makes up 25 % of the resin [60]. This theory is additionally supported by the accordance of the first T_g values for both FP samples. The second T_g values and the ones determined in the second run differ 11 °C. It is assumed, that this mismatch is caused by differences in network structure due to the oligomers and monomers, respectively. For both con materials the T_g indicated in the data sheet lies between 110 °C and 115 °C. The values found in this experiments were lower for the ep1_con and higher for the ep2_con. However, the manufacturing processes and the heating rate during measurements were different, which could explain the mismatch. For all formulations, except ep2_con, the T_g of the second heating run are up to 4 °C higher whereas, for the ep2_con the T_g of the second heating run was 8 °C higher. A higher second T_g indicates post curing effects, increasing in extent with the deviation between the T_g values. Therefore, it can be summarized that more postcuring takes place for the ep2_con resin, indicating an insufficient curing time.

Table 4.2: T_g mid-point values obtained by DSC measurements for the first and second heating run.

T_g / °C		
ep1_con	100	103
ep1_FP	74 & 102	105
ep2_con	119	127
ep2_FP	74 & 112	116

4.2 Morphological analysis

At the beginning, it should be mentioned, that for both manufacturing methods the upper surfaces of the plates did vary depending on curing method. For most of the con plates, the surface was smooth and the resin appeared to be evenly distributed. The

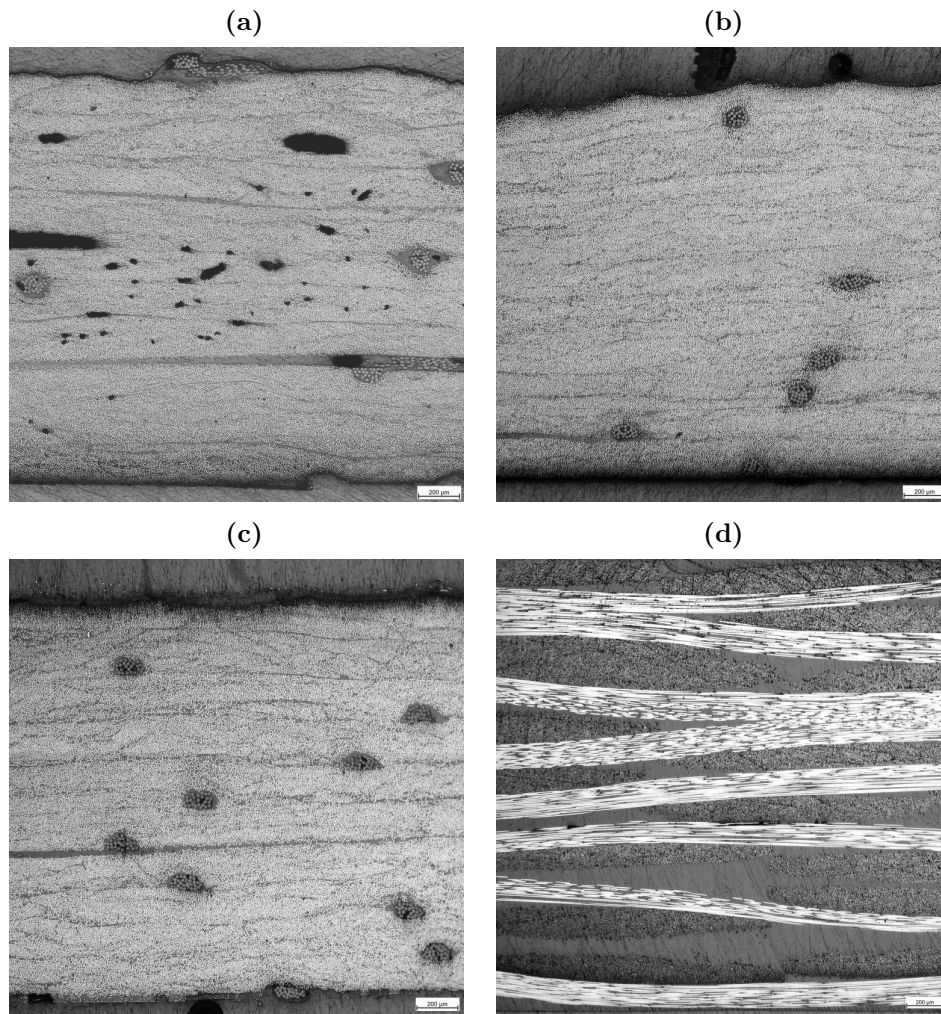


Figure 4.3: Micrographs of 2 mm ep1 plates for compression, DMA and ILSS tests: (4.3a) wlu-UD-ep1_con, (4.3b) VARI-UD-ep1_con, (4.3c) VARI-UD-ep1_FP and (4.3d) VARI-fb-ep1_FP.

FP plates however showed wave like resin bumps on the upper surfaces, even the ones produced via VARI, where a peel ply was used on the upper surface.

In the appendix (table A.1) the v_f calculated with the weights of the components, the ratio of average and expected thickness, $t_{av} : t_{ex}$, and for some specimens the v_v , gained via image processing are listed. The UD specimens produced via VARI show the highest v_f of around 57 %, whereas the lowest v_f were calculated for the fabric specimens produced via VARI i.e, between 41.6 and 46 %. It should be emphasised on this point, that different v_f do not mean a higher or lower amount of fibres. The number of plies were the same for every specimen type and only the amount of epoxy varied through out the manufacturing processes. The variations in v_f are caused by different infusion behaviours of the respective fibre types. For UD fibres, the vacuum caused a tight packing hence, there was little free space where the resin could distribute. The

tight fibre packing can be seen in figure 4.3b and figure 4.3c. For the twill fabric, due to their structure such tight packing was not possible to be achieved with the present devices and consequently, more space in between needed to be filled with resin.

Two TGA-graphs are illustrated in figure 4.4 in which the weight of the sample in percent of the initial weight is displayed against temperature. The horizontal plateau indicates the mass loss during heating under inert atmosphere, i.e. the mass fraction of the epoxy. Next to the plateau, the corresponding v_f is given. Figure 4.4a shows the TGA of a wlu-UD-ep2_con plate, where three specimens were taken from different regions. The v_f is about 3.2 % higher than expected (approximately 56 %). A possible explanation could be, that an exceptional high share of epoxy resin was located in the edge region and removed over the course of edge trimming. However, the v_f values determined via TGA show a total deviation of 0.9 %, which indicates a uniform distribution of the resin. The TGA of the plate used for tensile test specimens and

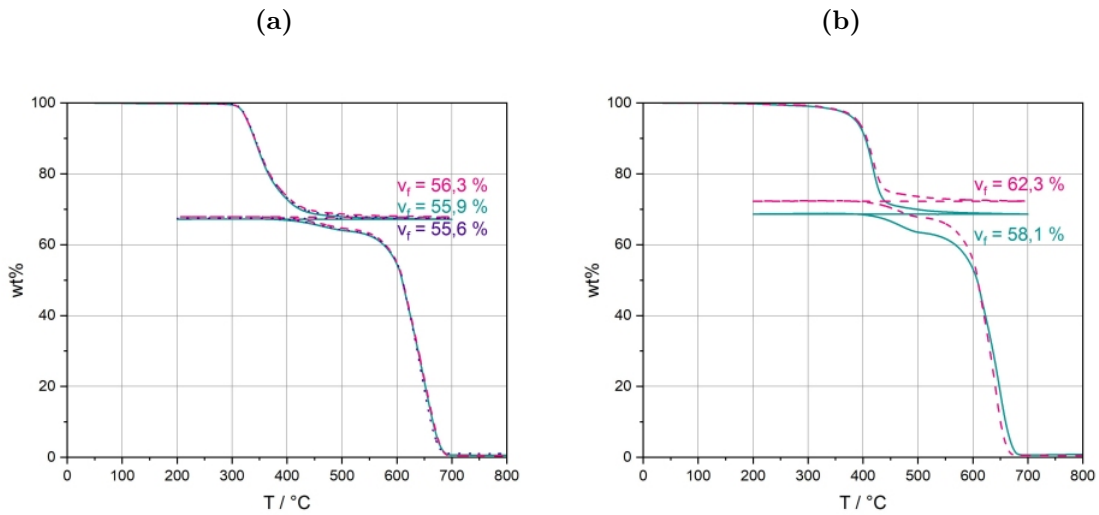


Figure 4.4: TGA-graphs with estimated v_f for two plates, (4.4a) a UD-ep2_con manufactured via wlu and (4.4b) a UD-ep2_FP manufactured via VARI.

produced via VARI (see figure 4.4b) on the contrary shows a significant difference of 4.2 %, in v_f according to different locations both in edge regions. This finding however matches the expectations, since the infusion process took quite a long time and therefore an uneven distribution was expected. Although such a big difference can be found between the single values, their average value and the calculated v_f differ just 0.2 %, which approves the validity of the method used for calculating v_f .

Concerning the void content, a direct correlation between v_v and $t_{av} : t_{ex}$ can be found. Although calculating v_v via image processing is more precise for a single surface, the ratio-method is faster and less sensitive to variations throughout a plate. Therefore, it was decided not to take micrographs of all plates to save time. A general trend, which

matches the expectations, is that $t_{av} : t_{ex}$ values of the plates produced via wlu are higher, which refers to a higher v_v , compared to the VARI-plates. For wlu the ratio covers a range of 1.02 to 1.21, with an average of 1.09. The VARI-plates show values between 0.96 and 1.04, with an average of 1.00. Values lower than 1 can be attributed to a high compaction of the fibres. In figure 4.3b, this high compaction can be seen, since the borders of the single layers cannot be recognised.

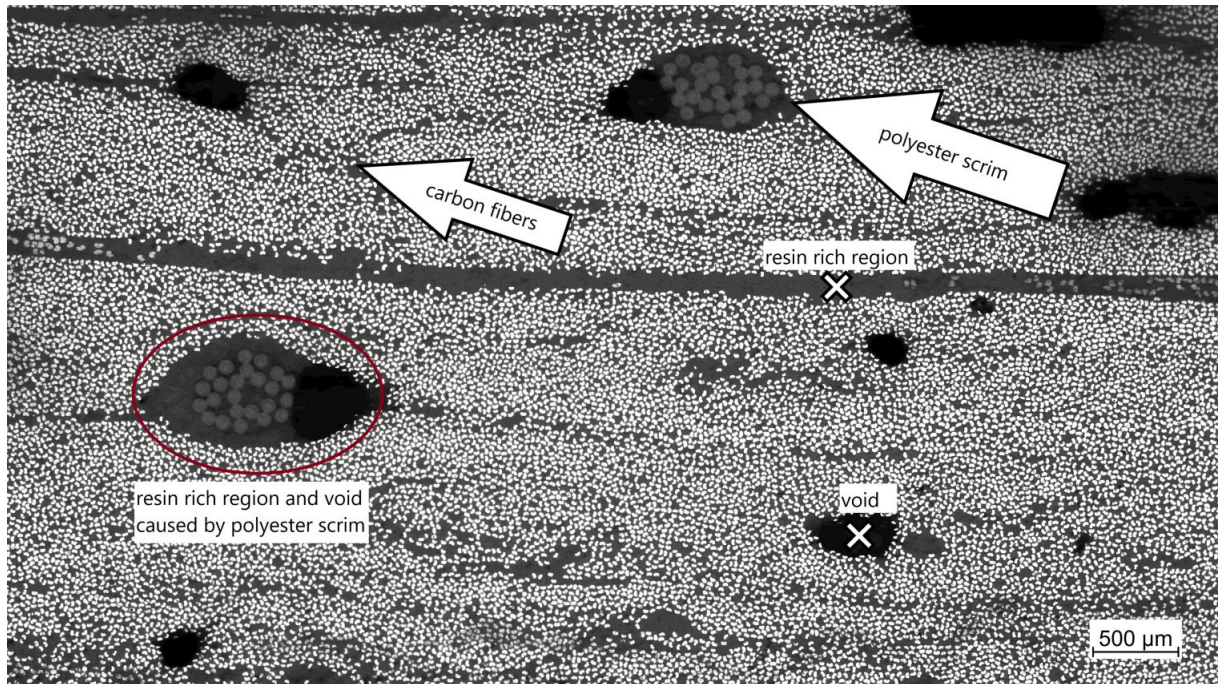


Figure 4.5: Micrograph of a wlu-UD sample with different morphological aspects.

It should be mentioned here, that the phenomenon of gathering resin around the polyester scrim can be observed for all manufacturing types. However, in wlu plates the polyester scrim additionally is part of bigger voids in some cases. In figure 4.5, the aforementioned effects of polyester scrims are shown in a micrograph of a wlu specimen, together with other morphological aspects.

Figure 4.3 shows four micrographs of composite plates manufactured for compression, DMA and ILSS. Figure 4.3a and figure 4.3b are cross-sectional areas of UD-ep1_con specimens produced in wlu and VARI, respectively. The higher void content is clearly visible for the wlu specimen. Figure 4.3c and figure 4.3d show specimens produced via VARI. They are both frontally cured and out of the same resin however with different reinforcement types. The lower v_f for the fabric specimen is clearly identifiable, by significantly bigger resin rich regions. Even if the VARI-UD specimens show a high v_f , there were no dry regions found in any specimen. Other micrographs can be found in the appendix (figure A.2).

4.3 Dynamic mechanical analysis

In the following section, the results from DMA shall be discussed. In the first step, the influence of different methods shall be outlined and afterwards, the results are interpreted with regard to material properties. A DMA was exclusively performed on UD specimens since no significant influence from the reinforcement type on the T_g is to be expected [4].

In figure 4.6, two graphs are depicted, both showing E' and $\tan(\delta)$ in dependence of temperature, with one specimen type each. However, for either specimen type the measurements were conducted with two different sets of testing parameters, method 1 (10 N offset force and 40 μm amplitude) and method 2 (400 % auto-offset and 10 μm amplitude). The most striking differences between the two methods concern the shape of the curves, but other deviations can be found as well.

Firstly, the E' -curve gained using method 1 exhibits a significant hump, which is located slightly after $T_{g\text{onset}}$, the temperature where E' starts to decrease. In literature, a similar hump sometimes is assigned to internal stresses or thermal extension [55]. However, since the hump does not appear when method 2 is used, this explanation cannot be valid here.

Secondly, noteworthy differences can be found between the shape of the $\tan(\delta)$ -curves. While method 2 leads to smooth curves, method 1 results in blurred graphs. However, no substantial impact on the T_g , calculated using the maximum of $\tan(\delta)$, could have been detected.

A third significant divergence, only detectable for the wlu-UD-ep1_con specimens, is the level of E' after the glasstransition. For method 1 E' decreases approximately 15 GPa less than for method 2. Moreover, the curve of E' for method 1 shows discontinuities on a slightly increasing level. For method 2, a significant rise in E' is detectable. It is assumed, that in both cases the effects are caused by post-curing.

The artefacts in the curves appeared systematically exclusively when method 1 was used. Therefore, it is assumed that they can be assigned to the method and were not caused by a bad specimen quality. Additionally, it can be mentioned here, that neither irregularities on the surface nor a distortion of the specimens were observed. Due to the high stiffness and modulus values of the specimens, high forces need to be applied in the course of measuring. Therefore, the existing issues may be assigned to the controlling or sensing element of the measuring apparatus.

Comparing the methods concerning T_g shows no significant variation, for neither of the two different ways of calculating. Just in one out of four cases a slightly lower T_g ,

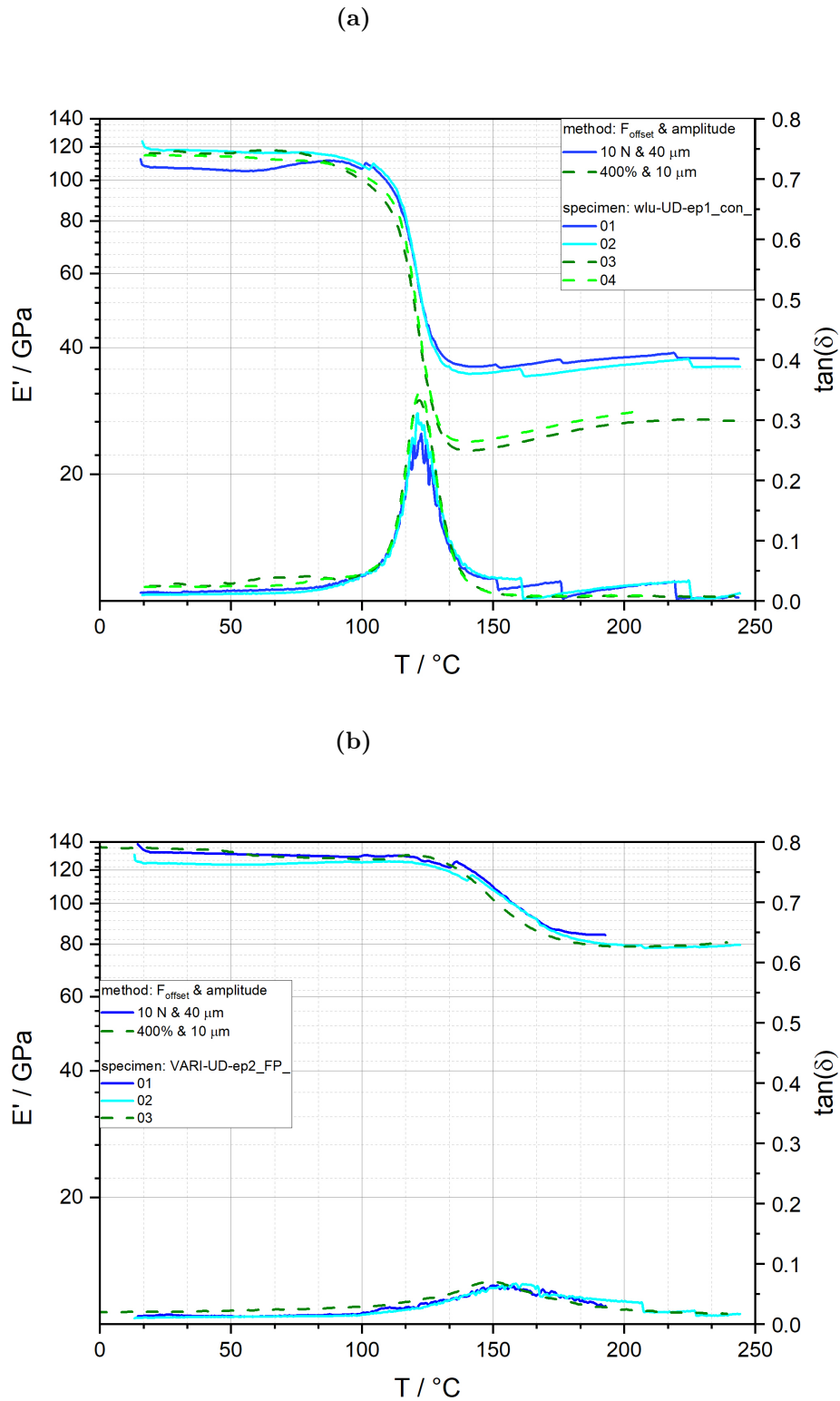


Figure 4.6: E' and $\tan(\delta)$ in dependence of temperature, derived from DMA, for: (4.6a) wlu-UD-ep1_con and (4.6b) VARI-UD-ep2_FP specimens, measured with different parameters, as indicated in the legend. Each measurement was performed with 1 Hz.

T_{gpeak} for method 2, was determined. Those results are viewed as confirmation of the validity of the T_g values for both measuring methods. Furthermore, no influence of the used methods on E' at 30 °C could have been detected.

As explained in section 3.3.3, the T_g was calculated via two methods. The average values for both methods are presented in table 4.3, with no standard deviations shown since just a small number of specimens per type were tested. The method of calculating T_g via the maximum of the loss factor, T_{gpeak} , led to values 8 to 15 % higher than T_{eig} , with higher deviations for the FP specimens. However, this deviation is not surprising, since it is well described in literature [55]. The difference between FP and con specimens is caused by their different shape of E' curves and shall be discussed later. Since the calculation of T_{gpeak} is more precise and explicit, further discussions on T_g will focus on this value.

Table 4.3: Average T_g values for all UD-specimens, derived from DMA, calculated via two different methods.

Curing method	con		FP	
	VARI	wlu	VARI	wlu
	ep1			
$T_{eig} / ^\circ\text{C}$	109.2	111.1	125.9	116.5
$T_{gpeak} / ^\circ\text{C}$	120.9	122.0	145.1	134.5
	ep2			
$T_{eig} / ^\circ\text{C}$	118.2	109.8	134.8	128.0
$T_{gpeak} / ^\circ\text{C}$	129.2	123.4	153.7	142.4

In figure 4.7, the average T_{gpeak} values for all resin and curing types are compared concerning the manufacturing processes. The ep1_con specimens show nearly identical results for either manufacturing methods. For the other resin and curing types, a rise in T_{gpeak} up to 11.3 °C was detected from wlu to VARI. Interestingly, the FP specimens showed higher deviations. To some extent this finding can be explained by the differences in void content. [61] While all VARI specimens show hardly any voids, it is significantly lower for the wlu-UD-ep1_con specimens than for the other wlu specimens. Therefore, it is suggested that the differences in T_{gpeak} can be attributed to specimen quality.

On average, the same effect of the curing method on T_{gpeak} can be detected. For either resin and manufacturing type, FP leads to higher T_g values than the con curing. For identical materials, a higher T_g implicates a higher crosslink density. Since additional information on the crosslink density is delivered by the curve progression, this topic shall be discussed later. As expected, the values of the T_g measured on neat resin samples with DSC are lower than the ones determined with DMA. This increase is

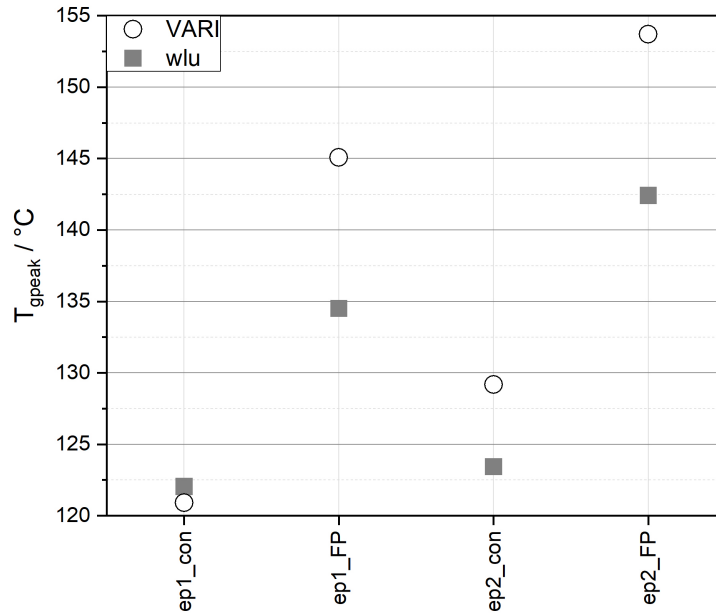


Figure 4.7: Average T_{gpeak} values for all UD specimens compared with regard to manufacturing type.

caused by the different measuring methods and the high fibre content. Both tests revealed higher T_g values for ep2.

The storage modulus was determined for all specimens at 30 °C and the average values, together with the average E_t values determined from tensile tests are listed in table 4.4. The relation of E_t and E' at 30 °C is depicted in figure 4.8. They show a strong correlation. Although, the specimens were not cut out of the same plates, since the standards require different thicknesses for tensile testing and DMA, respectively. In all cases, the DMA delivers results in/nearly in the region of the standard deviation from tensile tests. The correlation between the VARI and wlu is noteworthy, especially because different DMA methods has been used as well. For three specimen types, the E' delivered by DMA is lower, than the results from tensile tests. Just ep2_con shows higher modulus values in DMA, for both manufacturing types. Here, the different load application types for E_t and E' also needs to be considered. Taking into consideration the remarkably higher E_c for ep2_con the results from DMA are not surprising.

Due to the smoother shape of the curves gained using method 2, just wlu-specimens are shown in this section. The graphs of the VARI specimens can be found in the appendix (figure A.4). All characteristics discussed in the following section are valid for both manufacturing types. For all types at least two specimens were tested. The deviations between the single specimens of one type were small, therefore just one per type is

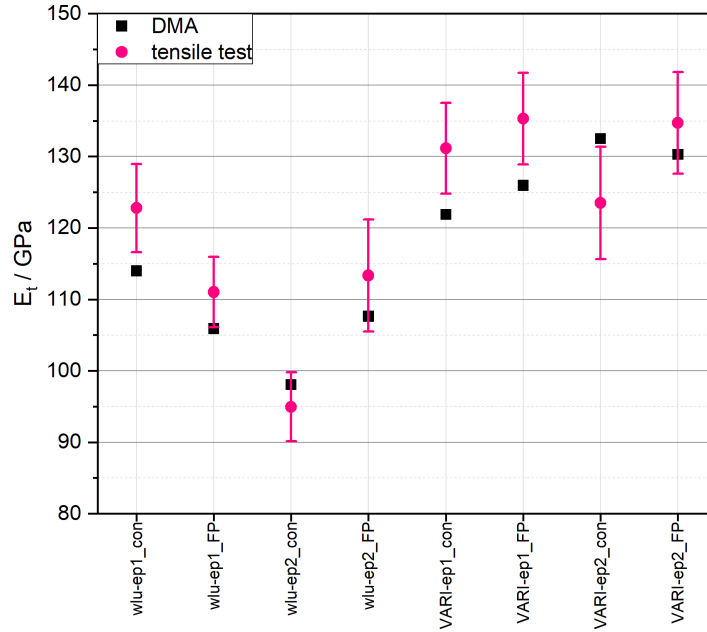


Figure 4.8: Average E' values derived from DMA for all UD specimens compared with average E_t values, with indicated standard deviation, from tensile testing.

Table 4.4: Average values for tensile moduli: E_t , derived from tensile tests and E' from DMA.

Curing method	con		FP	
	VARI	wlu	VARI	wlu
ep1				
E' at 30 °C / GPa	122	114	126	106
E_t / GPa	131 ± 6	123 ± 6	135 ± 6	111 ± 5
ep2				
E' at 30 °C / GPa	132	98	130	108
E_t / GPa	124 ± 8	95 ± 5	135 ± 7	113 ± 8

shown here. The graphs, delivered by DMA, showing E' and $\tan(\delta)$ in dependence of temperature, are presented in figure 4.9.

On average the plateau of E' before the transition region is stable for all specimens. Small instabilities can be attributed to load application issues, caused by distortions of the specimen. The decrease of E' is higher for the con specimens. The plateau of E' after the glass transition region, the rubbery plateau, is significantly higher for the FP specimens and resulting from this, the loss factor is lower. A higher loss factor indicates a higher non-elastic strain component. This finding is well reflected in the tensile tests, where the con specimens show significantly higher $\epsilon_{t_{Max}}$ values. All specimens show an increase of E' after the glass transition region. Remarkably, this increase is approximately two times higher for ep2_con than for all other specimens. Such an

increase indicates a post-curing effect and it may be caused by insufficient curing times. However, no second peak in $\tan(\delta)$ can be observed, which usually is associated with post-curing effects. Therefore, it is concluded that the effect is moderate. The more pronounced post-curing for ep2_con already has been detected in DSC tests.

The differences of the DMA curves comparing con curing to FP can be summarized as follows. The graphs derived from con cured specimens exhibit:

- Concerning E'
 - A higher decrease in the rubbery plateau
 - The transition region of E' covers a smaller temperature range
- Concerning $\tan(\delta)$
 - A higher maximum value
 - The maximum is located at lower temperatures
 - The peak is more defined/narrow

All these points indicate that a lower crosslinking density was achieved with con curing. However, two points need to be considered. Firstly, care must be taken comparing the two different curing types with regard to crosslinking density, which is closely related to the molecular weight between the crosslinks. In the course of con curing, a foreign molecular structure is integrated in the polymer network. Whereas FP is based on a ring opening mechanism of the epoxy prepolymers themselves. Resulting from this the molecular weight between the crosslinks and the crosslinking density can not be used accordingly. Secondly, ep2_con showed a higher post-curing effect than all other specimens. Consequently, the crosslinking density of ep2_con could be increased by higher curing times. However, as already discussed, the post-curing effect is small. Therefore, it is assumed, that even for complete curing the aforementioned aspects would be recognizable. Nevertheless, the assumption that FP leads to a higher crosslinking is supported by the results of other mechanical tests. Such as a low $\epsilon_{t_{Max}}$ or the different behaviours in ILSS tests.

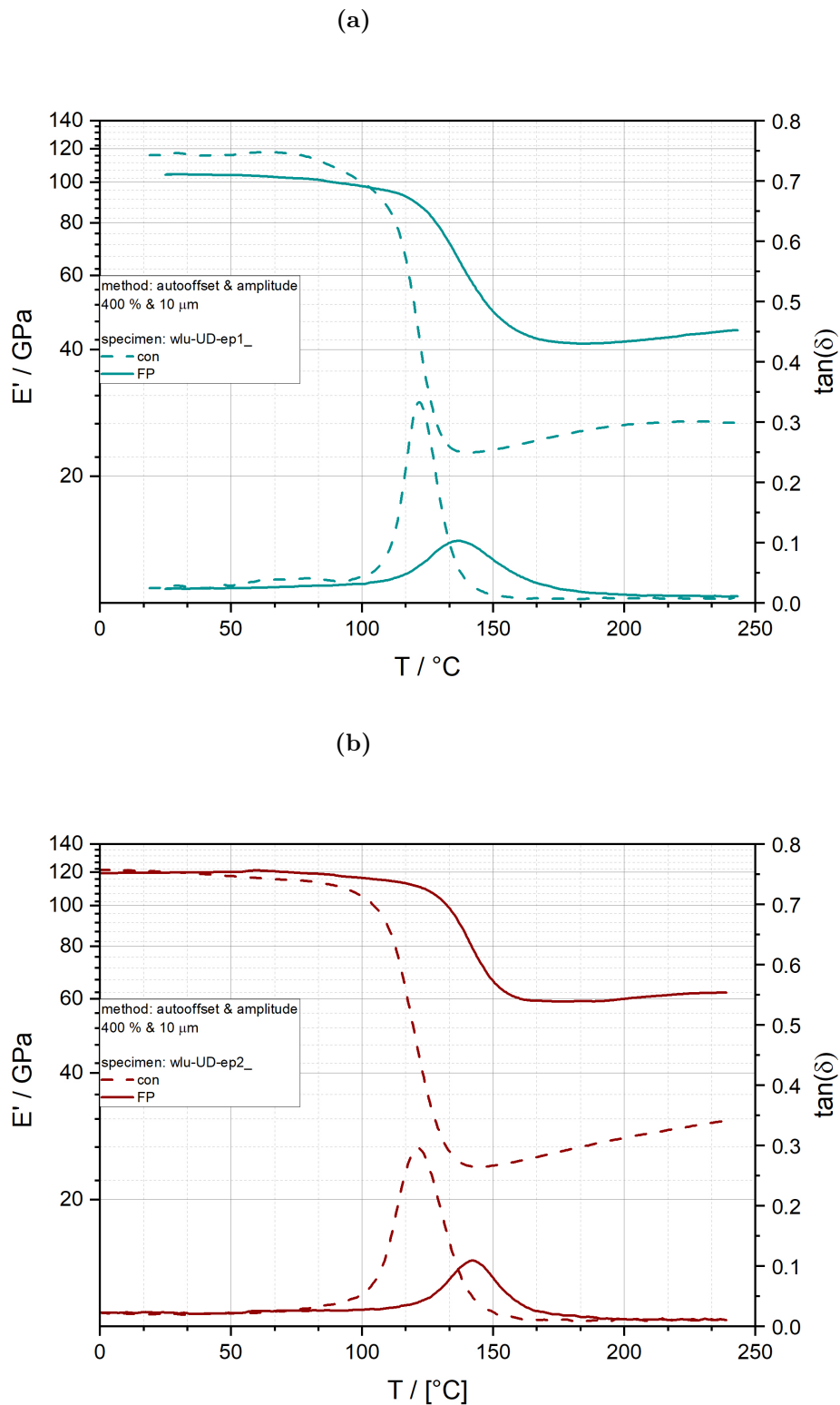


Figure 4.9: E' and $\tan(\delta)$ in dependence of temperature, derived from DMA, for wlu-UD specimens with (4.9a) ep1 and (4.9b) ep2 matrix, respectively. Each graph shows one con and one FP specimen. All measurements were performed with 1 Hz.

4.4 Tensile tests

In figure 4.10 example σ_t vs ϵ_t curves from tensile tests are shown. All of the depicted graphs belong to VARI specimens and show fb as well as UD reinforced specimens of all resin and curing types. The derived σ_t vs ϵ_t curves show the typical behaviour of CF-epoxy composites as described in literature: linear, with neither pronounced yield strength nor plastic deformation region [19]. Additionally, $\sigma_{t_{MAX}}$ and the stress at break are, in most cases, identical, which is another typical behaviour of CF-epoxy composites [19]. Example curves are shown in figure 4.10. Since there is no significant difference in the curves between wlu and VARI specimens, just one manufacturing method – VARI, is depicted here, the other graphs can be found in the appendix (figure A.6). E_t , $\epsilon_{t_{MAX}}$ and $\sigma_{t_{MAX}}$ shall be discussed in more detail in the following sections. Concerning the curve progression (see figure 4.10), it should be mentioned here that most of the FP specimens failed without non-linearities in the last section, most con specimens with. This could indicate that a better fibre-matrix adhesion was achieved with con curing.

In figure 4.11, the average values for $\sigma_{t_{MAX}}$ and their standard deviations are presented in a bar chart, grouped by reinforcement type, manufacturing method and resin type. The curing method is indicated by colour and pattern. (This type of diagram shall be used for presenting other average values in this thesis likewise.) The values can additionally be found in table 4.5. The $\sigma_{t_{MAX}}$ of the fabric specimens varies in a region of 523 MPa (wlu-fb-ep2_con) to 658 MPa (wlu-fb-ep1_con). For the UD specimens $\sigma_{t_{MAX}}$ covers a range from 1075 MPa (wlu-UD-ep1_FP) to 1816 MPa (VARI-UD-ep1_con).

The different reinforcement types for specimens with same manufacturing process, matrix material and curing method are compared and defined by a ratio known as UD:fb. The ratio for all tested specimen types lies between 2.9 and 2. This matches the expectations for a fibre dominated material property since a 2×2 twill fabric has half the amount of fibres aligned in loading direction in comparison to a UD composite. Additionally, the fibres used for the fb show, according to their data sheet, lower inherent $\sigma_{t_{MAX}}$ values.

A comparison of the $\sigma_{t_{MAX}}$ values with respect to manufacturing methods shows different behaviours for fb and UD specimens, respectively. The UD specimens show an increase in $\sigma_{t_{MAX}}$ from wlu to VARI. The increase varies from 9 % (UD-ep1_con) to 21 % (UD-ep1_FP). (Detailed information can be found in the appendix, table A.2). This difference between wlu and VARI specimens can be explained by the different specimen quality. For the specimens tested, two main quality aspects influencing the

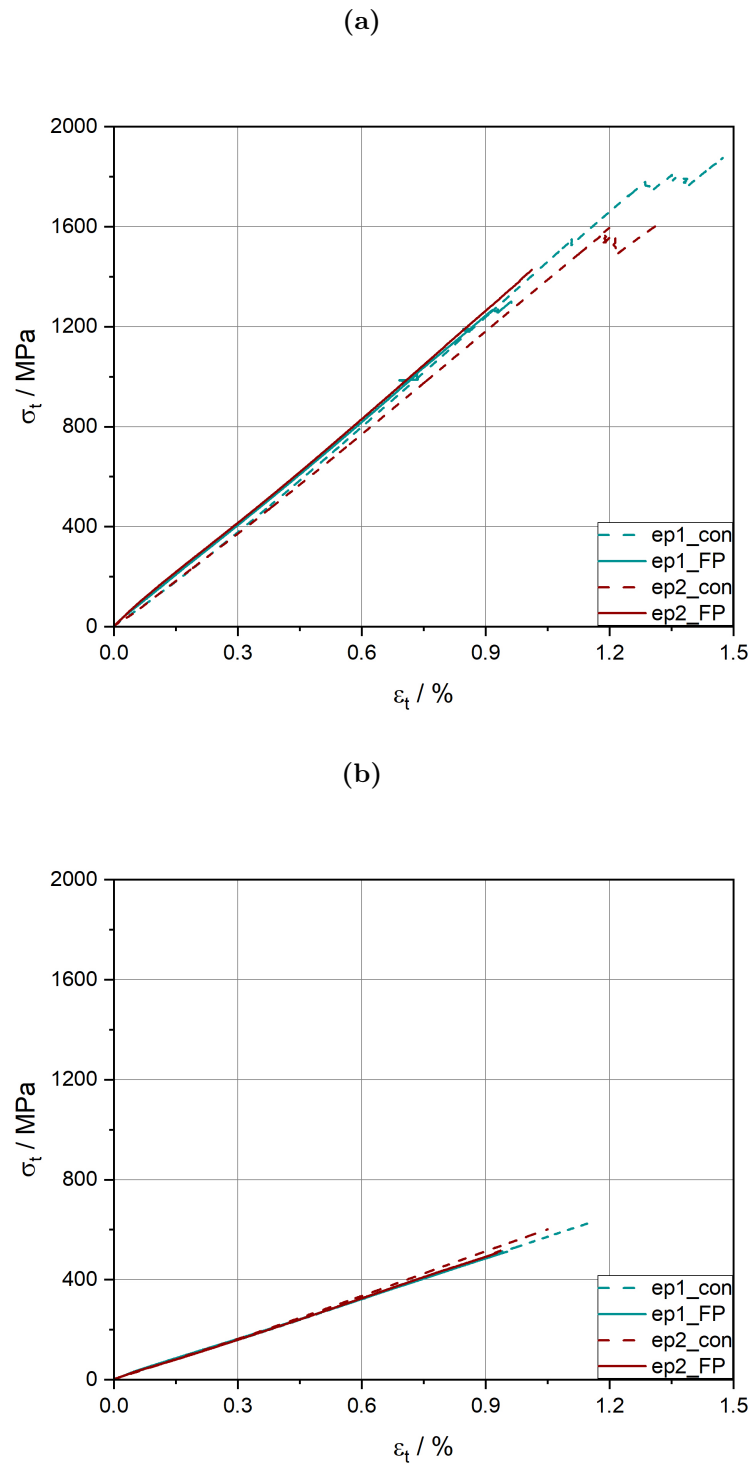


Figure 4.10: Example σ_t vs ϵ_t curves of tensile tests for (4.10a) UD and (4.10b) fb specimens produced via VARI.

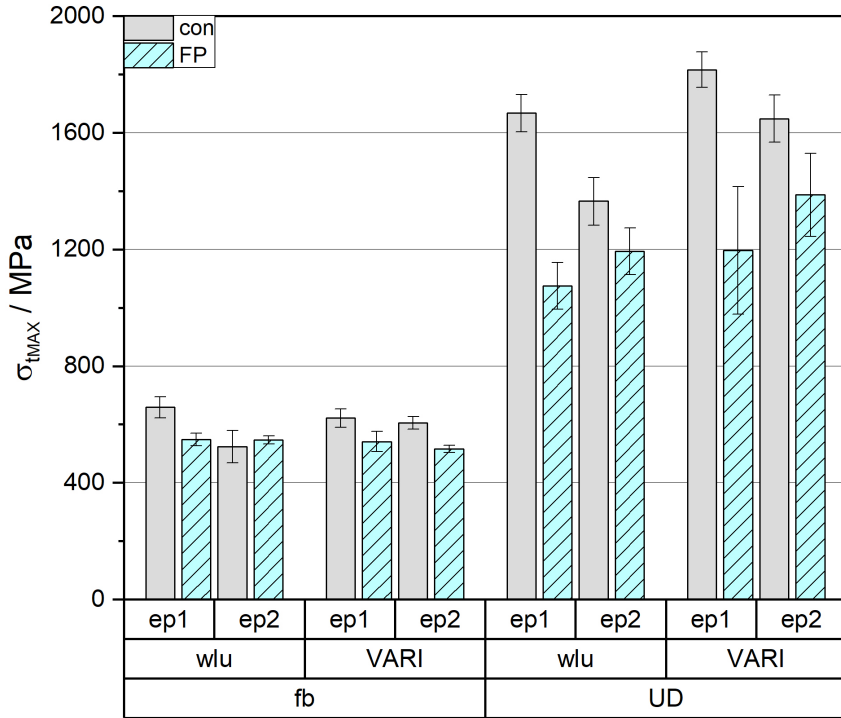


Figure 4.11: Comparison of the average σ_{tMAX} , including standard deviation.

tensile properties can be named. Firstly, the alignment of the fibres and second, the effect of voids. In a VARI process, the fibres can more precisely be stacked and additionally, the compaction gained through the applied vacuum prevents undulations in z-axis. The second factor of voids on the one hand, impose a negative impact on the material properties, as discussed in section 2.3.3. But on the other hand, voids lead to an apparent increase of the crosssections, which furthermore results in an apparent decrease of the σ_{tMAX} values. In the figure A.5 (appendix) the ratio of expected and real thickness as well as the ratio comparing σ_{tMAX} values in terms of manufacturing process are depicted. The different ratios show a good correlation for the UD specimens, which supports this theory. Concerning the fb specimens, no significant difference of the σ_{tMAX} values can be found comparing wlu and VARI specimens. However with microscopy, voids have also been detected for the wlu-fb specimens. This discrepancy may be caused by the fibre type. The high amount of fibres perpendicular to the loading direction in the fb specimens have a mitigating effect on the propagation of cracks. An additional explanation for this phenomenon may be delivered by the higher resin proportion used in the VARI process. Since this lead to bigger crosssections for the VARI-fb specimens, even if the number of plies, which is mainly responsible for tensile properties, was the same.

Interestingly, no evidence for a dependency of $\sigma_{t_{MAX}}$ on the resin types alone was found. Regarding exclusively the con-specimens, ep1_con can be found to show higher values than ep2_con. This is in good agreement with the expectations. Since for the pure resin ep1_con shows higher $\epsilon_{t_{MAX}}$ values, which positively impacts the $\sigma_{t_{MAX}}$ of the composite (This effect will be discussed in more detail in the next paragraph.). Such difference can not be detected for ep1_FP and ep2_FP, respectively. It can be summarized, that using different prepolymers (ep1 and ep2) leads to a significant gap in $\sigma_{t_{MAX}}$ when cured with different hardener types. However, FP results in similar $\sigma_{t_{MAX}}$ values when the same prepolymers are used. This significant high difference in $\sigma_{t_{MAX}}$ could also explain the extent of destruction of the specimens, since higher values equal a higher amount of energy, being released in the moment of failure.

Table 4.5: Average values and standard deviation of $\sigma_{t_{MAX}}$ in MPa.

Manufacturing method	wlu		VARI	
Curing method	con	FP	con	FP
Resin type	fb			
ep1	658 ± 36	548 ± 21	622 ± 32	541 ± 34
ep2	523 ± 56	547 ± 13	605 ± 22	516 ± 13
UD				
ep1	1667 ± 63	1075 ± 80	1816 ± 61	1196 ± 219
ep2	1365 ± 82	1193 ± 80	1648 ± 81	1387 ± 142

Within all sets of same manufacturing and reinforcement type, a strong correlation between $\sigma_{t_{MAX}}$ and $\epsilon_{t_{MAX}}$ can be found. The $\epsilon_{t_{MAX}}$ values for the fb specimens are located between 0.92 and 1.18 %, for the UD between 0.85 and 1.41 %. All mean values and standard deviations can be found in table 4.6. The bar chart in figure 4.12 represents the average values and the standard deviations of $\epsilon_{t_{MAX}}$. In contrary to $\sigma_{t_{MAX}}$ the difference between fb and UD is not as pronounced. However, this trend was expected, since the amount of fibres in loading direction has theoretically no impact on the maximum elongation. Additionally, no significant difference can be found comparing the two manufacturing processes. This trend strengthens the theory, that the differences in $\sigma_{t_{MAX}}$ result from higher crosssections caused by a high number of voids.

The most striking result to emerge from the data is that $\epsilon_{t_{MAX}}$ does not exceed 1 % for any FP specimen. This is a remarkable deviation from the expected results (see section 2.3.1) which can be summarized as follows. The maximum elongation of a composite is expected to equal the value of the fibre, given that the basic design rule, concerning the resin is fulfilled. This design rule demands the use of a resin with an $\epsilon_{t_{MAX}}$ twice the $\epsilon_{t_{MAX}}$ of the fibre. The used UD fibres have, according to the data sheet, a $\epsilon_{t_{MAX}}$ of 1.7 %, and the fb 1.6 %. Although this value is not reached by the con specimens, their $\epsilon_{t_{MAX}}$ is around 1.4 %, and is more close to it. This difference can

be caused by the specimen quality, since no equipment for aligning the fibres has been used and even small deviations from 0° direction lead to a weaker performance. The difference between the con and FP specimens can be explained regarding the $\epsilon_{t_{Max}}$ of the pure resin (table 3.2). Whereas the relevant design rule concerning the relations of

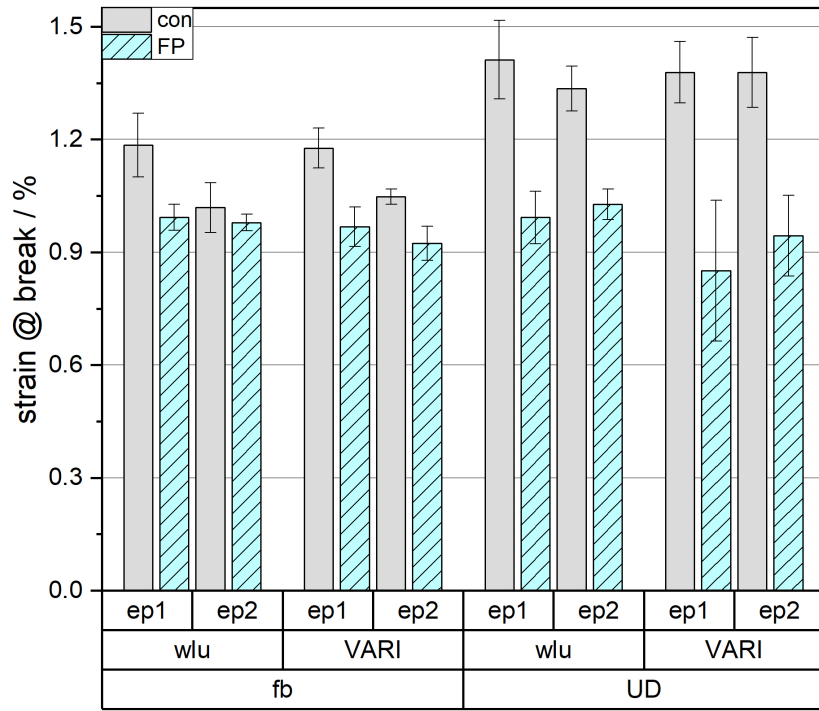


Figure 4.12: Comparison of the average $\epsilon_{t_{Max}}$, including standard deviation.

$\epsilon_{t_{Max}}$ is fulfilled for the con specimens. The $\epsilon_{t_{Max}}$ of the FP pure resin is more than one third too low. This leads to the conclusion that the fibres in the composites cured with FP cannot develop their full reinforcement potential, since they are more constrained by the matrix.

Table 4.6: Average values and standard deviation of ϵ_t values at $\sigma_{t_{MAX}}$ in %.

Manufacturing method curing method	wlu		VARI	
	con	FP	con	FP
resin type				
fb reinforcement				
ep1	1.18 ± 0.08	0.99 ± 0.03	1.18 ± 0.05	0.97 ± 0.05
ep2	1.02 ± 0.07	0.98 ± 0.02	1.05 ± 0.02	0.92 ± 0.05
UD reinforcement				
ep1	1.41 ± 0.10	0.99 ± 0.07	1.38 ± 0.08	0.85 ± 0.18
ep2	1.34 ± 0.06	1.03 ± 0.04	1.38 ± 0.09	0.94 ± 0.11

All values concerning E_t can be found in table 4.7 and figure 4.13. It can be concluded, that the estimated values are in good correlation with literature results [62], which

describes a E_t of 117 GPa for UD reinforced CF-epoxy composite ($v_f=50\%$), with fibres of a slightly lower E_t . The E_t of the UD specimens range between 95 GPa to 135 GPa whereas, for the fb specimens the values are located in a region between 49 GPa and 56 GPa.

As for the $\sigma_{t_{MAX}}$ values the E_t show a ratio between 1.9 and 2.7 comparing UD to fb values, caused by the already mentioned effect of a fibre dominated property. Addi-

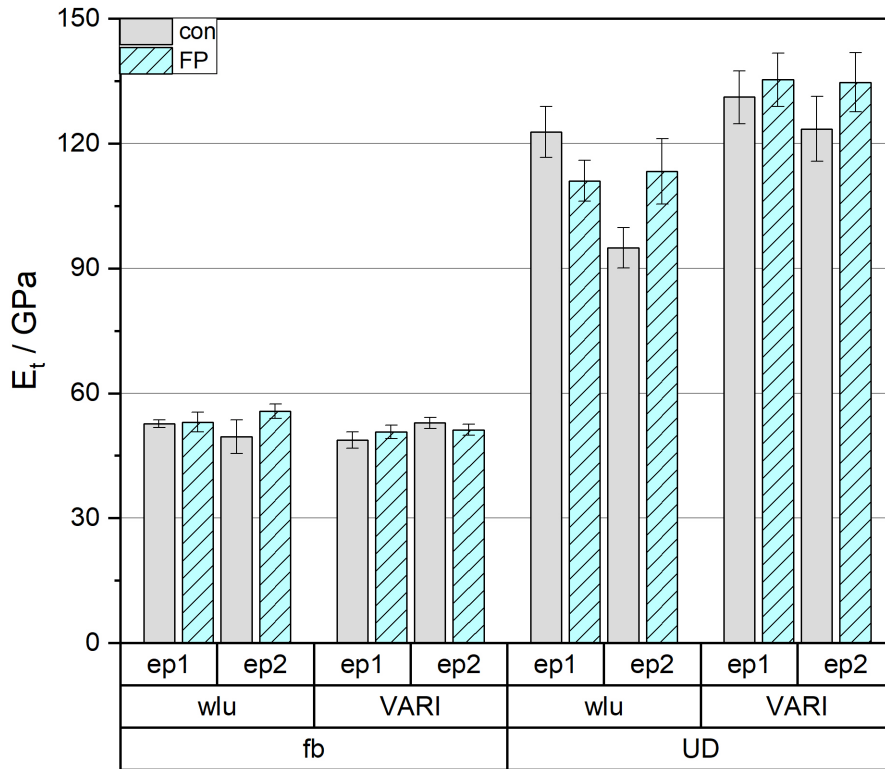


Figure 4.13: Comparison of the average E_t values, including standard deviation.

tionally, a decrease in value for UD specimens produced via wlu, reaching from 7 % (UD-ep1_con) to 30 % (UD-ep1_FP). The same explanations as for the $\sigma_{t_{MAX}}$ can be found valid, in particular specimen quality in terms of fibre alignment. No significant correlation concerning different resin and curing types was detected. This emphasizes that E_t is a fibre dominated property. Just a slight tendency towards smaller differences between the FP specimens, than the con specimens was found, as for the $\sigma_{t_{MAX}}$.

Table 4.7: Average values and standard deviation of E_t in GPa.

manufacturing method curing method	wlu		VARI	
	con	FP	con	FP
resin type	fb			
ep1	53 ± 1	53 ± 2	49 ± 2	51 ± 2
ep2	50 ± 4	56 ± 2	53 ± 1	51 ± 1
	UD			
ep1	123 ± 6	111 ± 5	131 ± 6	135 ± 6
ep2	95 ± 5	113 ± 8	124 ± 8	135 ± 7

During the tensile tests, loads up to 30 kN were applied. These high forces led to an explosive failure of the specimens, which was characterized through a loud bang and in case of UD specimens, a complete destruction. The fb specimens on the other side broke twice, which can be attributed to the high amount of energy released in one moment. However, there are no optical differences in fracture surfaces between the various specimen types with fb reinforcements. Moreover, all fb specimens broke within the tab region, which in general is regarded as not valid. As explained in section 3.3.4 for this thesis they were used nevertheless. Therefore, just one picture of them is depicted in figure 4.14. It is assumed that the main reason for this are the fibres perpendicular to loading direction, which keep the specimen in form. Consequently, no differences in extent and fineness of fragmentation can be described.

The UD reinforced specimens on the contrary showed defined trends in their fracture behaviour, and shall therefore be discussed in more detail. In figure 4.15 to 4.18 pictures of typically failed UD reinforced test specimens are shown.

As a general observation it can be stated, that there is an apparent difference between the curing types. The con specimens broke into more and finer fragments. Additionally, more of those fragments were lost, more precisely thrown away in the moment of failure. The manufacturing processes seem to have a small additional influence. The specimens manufactured via VARI tend to keep their shape more than the wlu - specimens. This is perhaps caused by a better fibre-matrix adhesion due to the applied vacuum. Consequently, it can be assumed that the matrix material itself has a higher influence on the failure behaviour than the quality, with respect to voids.

**Figure 4.14:** Picture of a typically failed fb specimen.

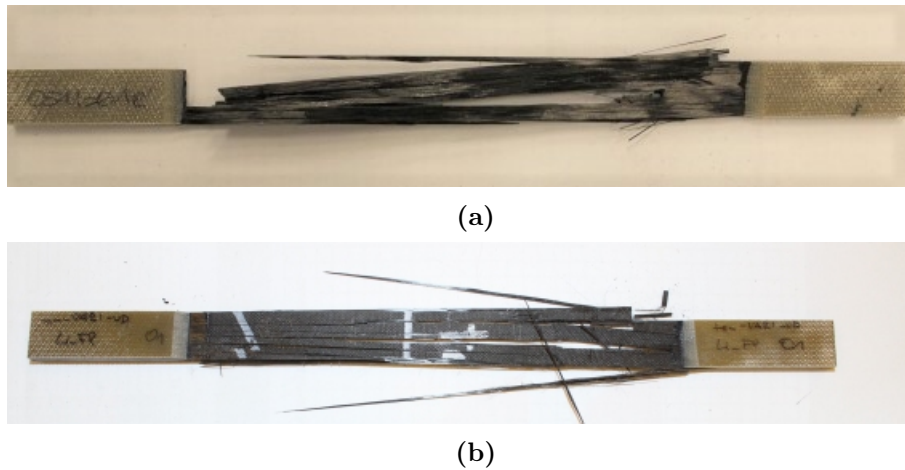


Figure 4.15: Typical fracture images of UD-ep1_FP specimens, manufactured in a (4.15a) wlu and (4.15b) VARI process, exhibiting rough fragmentation and little loss.

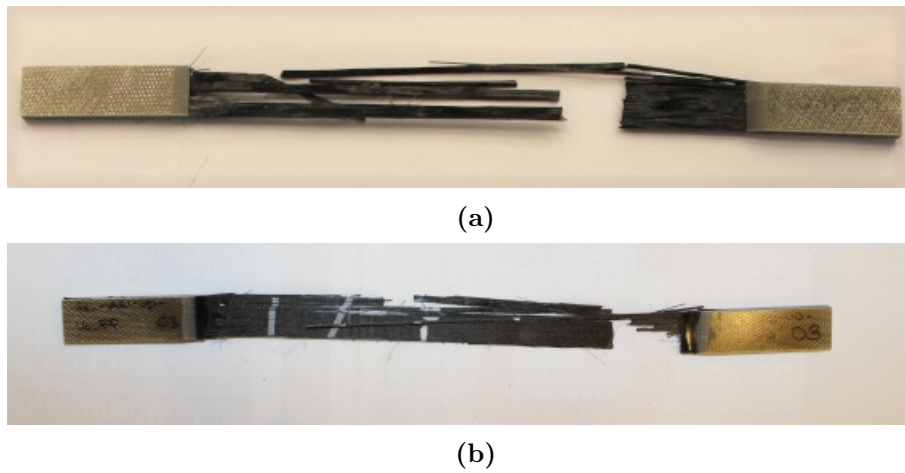


Figure 4.16: Typical fracture images of UD-ep2_FP specimens, manufactured in a (4.16a) wlu and (4.16b) VARI processes, exhibiting rough fragmentation and little loss.

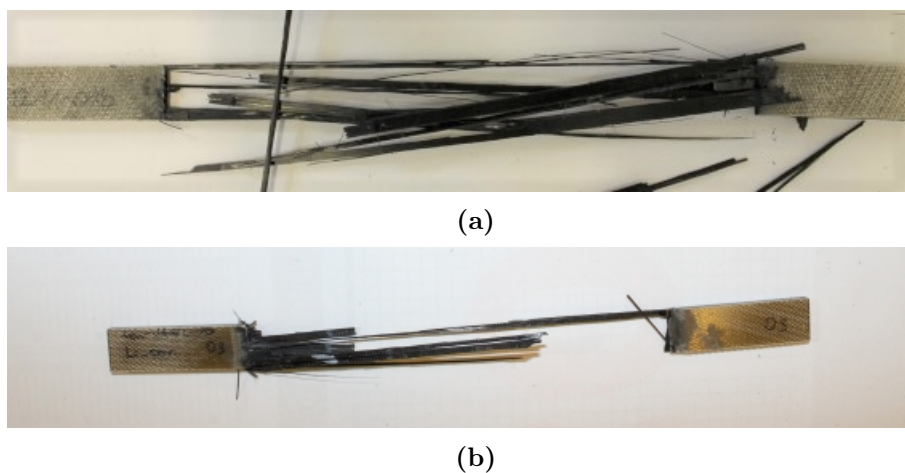


Figure 4.17: Typical fracture images of UD-ep1_con specimens, manufactured in a (4.17a) wlu and (4.17b) VARI processes, exhibiting fine fragmentation and much loss.

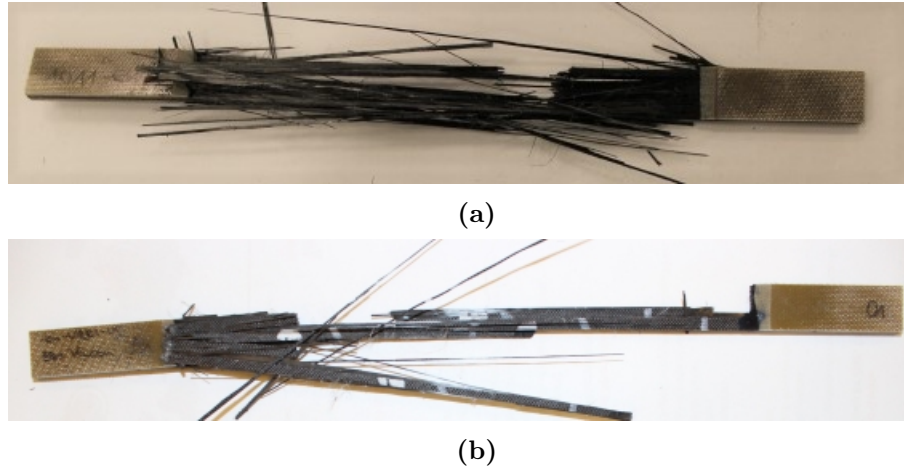


Figure 4.18: Typical fracture images of UD-ep2_con specimens, manufactured in a (4.18a) wlu and (4.18b) VARI processes, exhibiting finest fragmentation and much loss.

4.5 Compression tests

Compression tests were just performed on VARI specimens since it was assumed, that the high v_v of the wlu specimens would bias the results. In figure 4.19 typical σ_c vs ϵ_c curves are depicted, for UD (figure 4.19a) and fb (figure 4.19b) composite reinforcements, respectively. The linear curve progression is similar for all curves and slight deviations can be found for the value of σ_{cMAX} or, in case of the fb specimens, the slope. Noteworthy difference were found for the ep1_con specimens, both reinforcement types show significant lower σ_{cMAX} values and slopes, this trend also is reflected in the average values, which can be found in table 4.8. Fb-ep2_FP additionally shows lower σ_{cMAX} values, visible in the graphs as well as the average values. This unexpected deviation of the fb-ep2_FP can be explained by its specimen quality, in terms of voids. It was the only specimen type showing voids. [63] [64]

Figure 4.20 illustrates the average values of σ_{cMAX} and their standard deviation. Comparing the reinforcement types delivers similar results as in tensile testing. The values for the UD specimens were 2 to 2.6 times higher. In addition to the reasons already mentioned in section 4.4, the higher v_f for the VARI-UD specimens can be an explanation for the value of this ratio. [63]

No significant difference can be found for the UD specimens between ep1_FP and both ep2 types. The average σ_{cMAX} value of ep1_con is 200 MPa lower than an average of all other UD-specimens, which equals a reduction of approximately 20 %. This trend can also be observed within the fb specimens, however, not as pronounced (fb-ep2_FP is neglected here due to its bad specimen quality). Interestingly, this trend is contradictory to the findings in tensile testing. Where the highest strength values within one

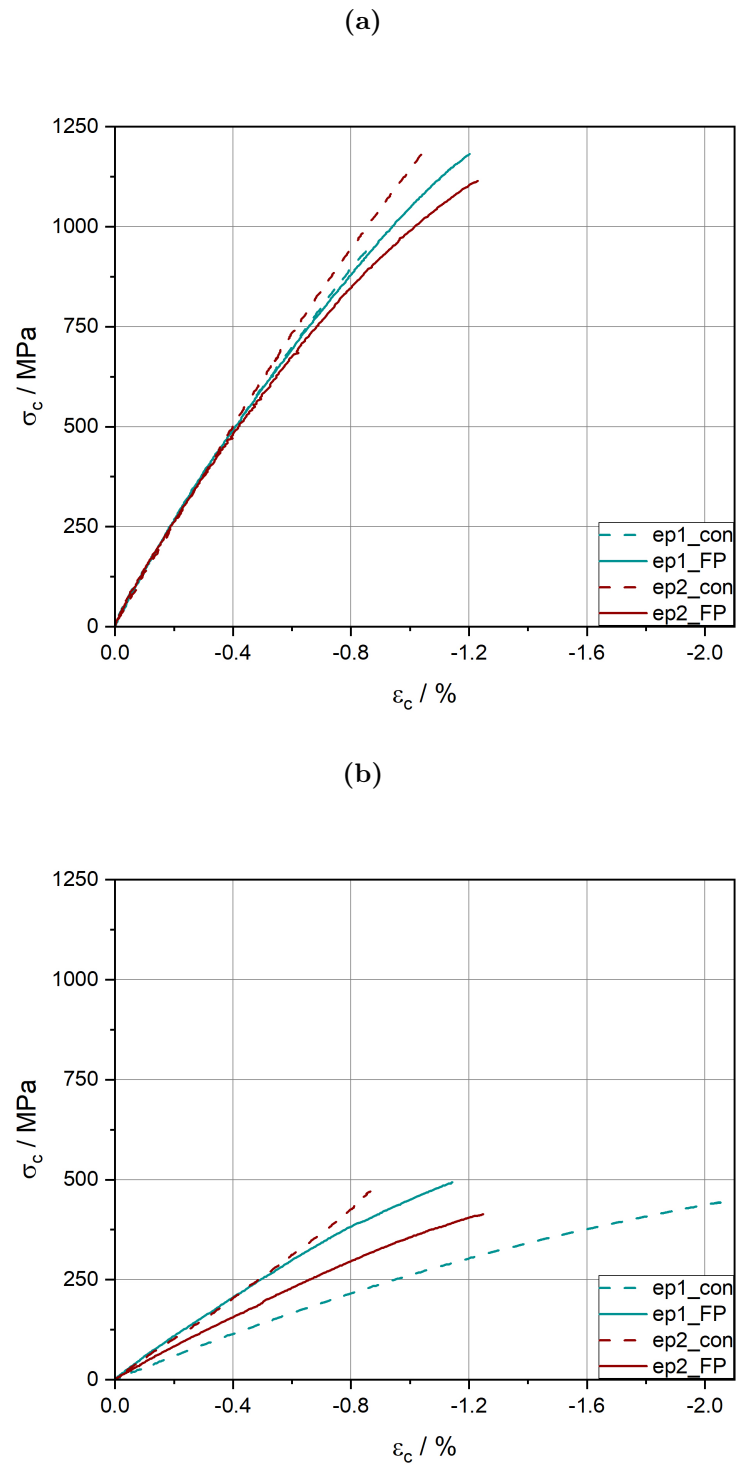


Figure 4.19: Typical σ_c vs ϵ_c curves from compression tests, for (4.19a) UD and fb (4.19b) specimens, respectively.

set were determined for the ep1_con specimens. As a consequence, it was assumed, that the differences in $\sigma_{t_{MAX}}$ are caused by differences in the ductility of the matrix, resulting from different crosslink densities (see also sector 4.3) and impacting the performance of the fibres. Therefore, a possible explanation, for different behaviours in

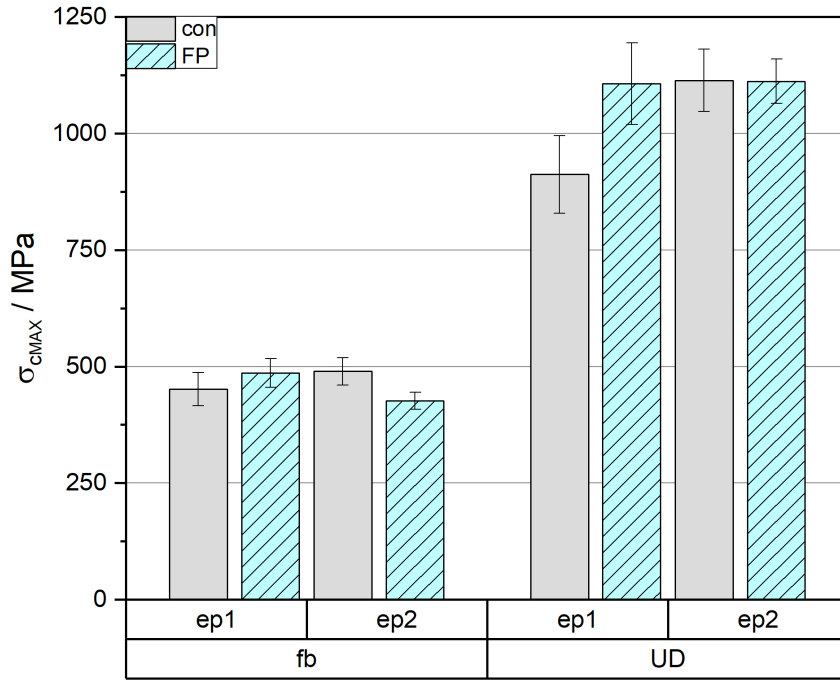


Figure 4.20: Comparison of the average $\sigma_{c_{MAX}}$, including standard deviation.

compression and tensile testing, respectively, may be delivered by the lower crosslink density of the ep1_con resin [62]. Which on the one hand, positively influences the tensile properties by enabling a better fibre performance, due to higher $\epsilon_{t_{Max}}$ values. But on the other hand, higher crosslink densities are favourable for compression properties, which are in general more dependent on the matrix properties than tensile properties.

Table 4.8: Average values and standard deviation of $\sigma_{c_{MAX}}$ in MPa.

manufacturing method curing method	VARI	
	con	FP
resin type	fb	
ep1	452 ± 36	486 ± 31
ep2	489 ± 29	427 ± 18
	UD	
ep1	912 ± 83	1107 ± 88
ep2	1114 ± 67	1112 ± 48

The moderate slope of the σ_c vs ϵ_c -curve of the fb-ep1_con specimens also is reflected in its, with 34 GPa, compared to the other specimens, low E_c (figure 4.21). The bad specimen quality of fb-ep2_FP as well is visible in the E_c values. The highest average E_c of the fb specimens can be found for the ep1_FP, ep2_con however, lies within the range of its standard deviation. Similar as for the E_t , the ratio UD to fb, for the same curing and resin type, is 1.9 to 2.3. For the UD specimens, with up to 7 GPa, slightly

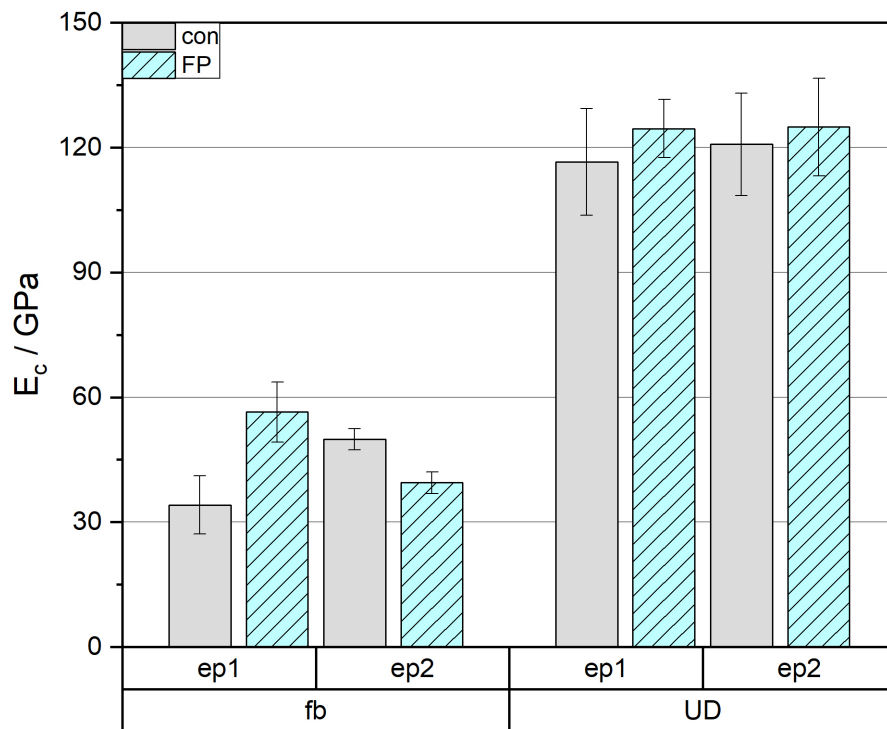


Figure 4.21: Comparison of the average E_c values, including standard deviation.

higher average values of E_c can be found for the FP specimens. However, regarding the standard deviations (up to 13 GPa) this difference is not significant. All average values and standard deviations can be found in table 4.9. The σ_{cMAX} values show an overall correlation with the E_c values.

Table 4.9: Average values and standard deviation of E_c in GPa.

manufacturing method curing method	VARI	
	con	FP
resin type	fb	
ep1	34 ± 7	56 ± 7
ep2	50 ± 3	39 ± 3
	UD	
ep1	117 ± 13	125 ± 7
ep2	121 ± 12	125 ± 12

The nomenclature of the fracture types for compression tests is not consistent in literature. For this thesis, the compression tests were performed in accordance to ISO 14126 and therefore its nomenclature was adopted.

In figure 4.22 micrographs of typical fracture surfaces in side view are depicted. The most common failure types for the fb specimens were complex failure (in figure 4.22a) and through thickness shear (in figure 4.22b). Complex failure can be described as a combination of shear within single layers, splitting, axial fractures and kinking, whereas those components vary in degree. Furthermore it resembles what in literature sometimes is called brooming [65] [66], also referred to as wedge splitting [64]. This type of failure was more common for the FP specimens. The fb-ep1_con samples on the contrary failed mainly in through thickness shear, the fb-ep2_con samples showed both failure types. A connection between the failure type and the shape of the curves can be observed most clearly for the fb-ep1_con specimens. They mainly failed under shear and show the flattest σ_c -vs-compressive strain (ϵ_c)-curve, due to higher elongation values. According to Odom et al. [67], through thickness shear can be a consequence of specimen buckling. Yet, here this can be excluded, since the values of the deformation in the horizontal plane is in an acceptable range and does not differ from the other specimen types.

For the UD specimens, no significant difference between the fracture types can be documented. An example is depicted in figure 4.22c. Nearly 50 % of the UD specimens failed in the tab region. Due to this high share and no significant differences in the σ_c -vs-compressive strain (ϵ_c)-curves they also were used for the evaluations.

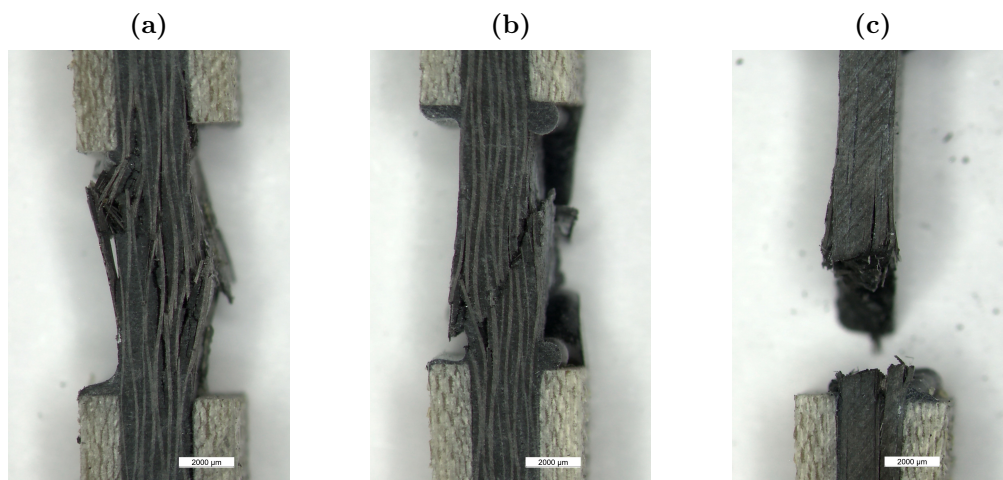


Figure 4.22: Example pictures of different failure types appeared during compression tests: (4.22a) showing complex failure in fabric specimen, (4.22a) showing through thickness shear in fabric specimen and (4.22c) showing a typically failed UD specimen.

4.6 Inter laminar shear strength tests

An apparent ILSS estimated in the course of this kind of tests is no real material property, since the geometry has a significant influence. However, if the same geometry and composition of specimens is used it can be an informative value. Therefore, ILSS tests are popular in quality assurance and for comparison purposes.

In ILSS tests the failure mode of the specimen is essential. According to ISO 14130 it can be distinguished between four failure types:

- single or multiple interlaminar shear (valid)
- combined failure, shear and tension or compression (not valid)
- non-shear failure, tension or compression (not valid)
- plastic deformation (not valid)

Just one of the mentioned failure types is valid for the calculation of an apparent ILSS. However, for comparison purposes an apparent ILSS can be calculated for other failure types as well. The failure mode usually is determined by optical evaluation of the specimen itself. However, also the shape of the force- time or deformation curve can provide information on it. For these reasons one curve for each type of specimens is depicted in figure 4.23. Additionally example images of specimens after testing are shown from figure 4.25 to figure 4.28. In each case, one bottom side and one side view image is depicted.

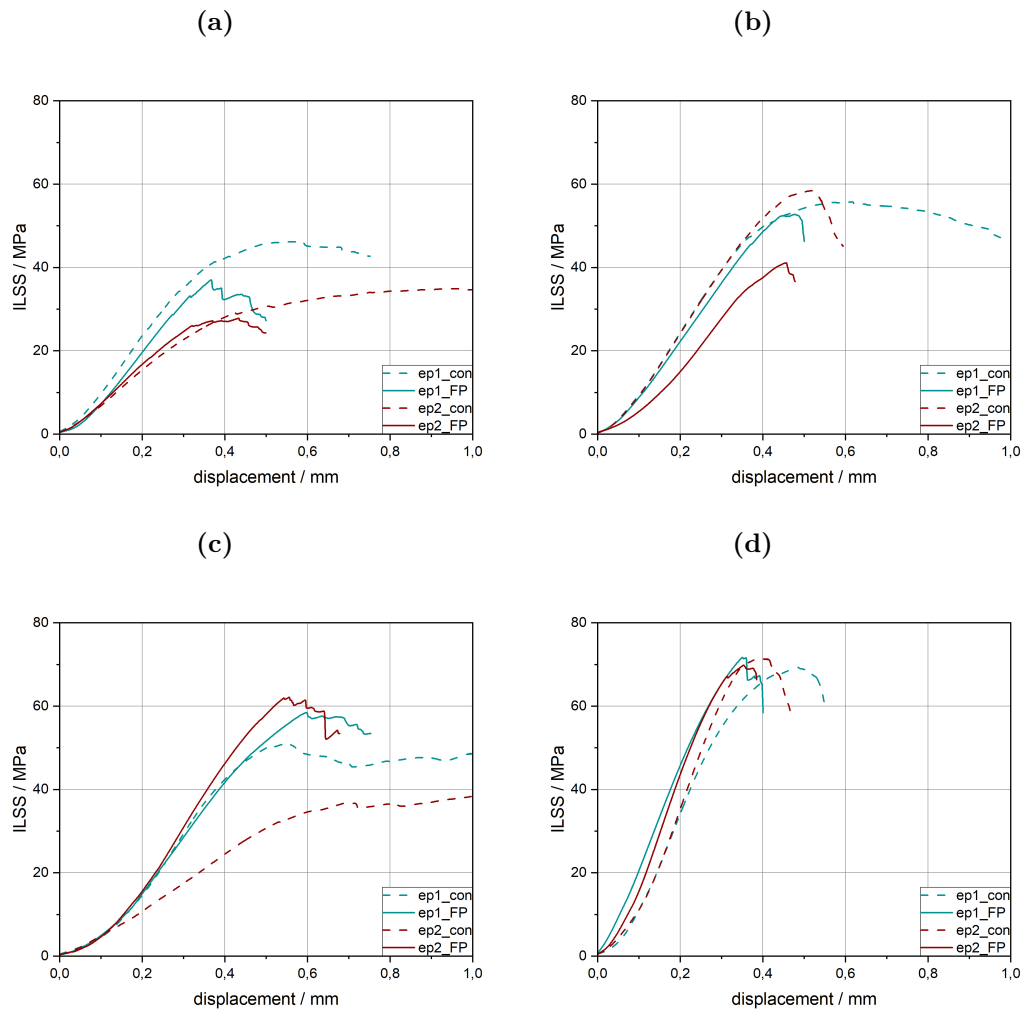


Figure 4.23: Typical stress vs displacement curves for ILSS tests, of all types of specimens: (4.23a) showing curves for wlu-fb, (4.23b) VARI-fb, (4.23c) wlu-UD and (4.23d) VARI-UD specimens.

For all types of resin, manufacturing process and reinforcement, especially for the fb specimens, the con cured specimens show smoother curves, with broad maxima. This indicates a plastic deformation [68]. An additional indicator for constant plastic deformation is the absence of a peak, indicating abrupt failure. Evidence for this also is given by the testing machine, which was set to an automated stop when reaching a defined decrease in force. However, the automated stop did not react for most con specimens. By contrast, FP specimens generally show a more defined maximum and in most cases the tests were stopped automatically. Additionally, a crack was audible in most cases just before the machine was stopped. According to the standard, this behaviour of the FP specimens excludes a failure due to plastic deformation and indicates shear failure. This stands in contrast to the findings of Tran et al. [17], who observed a more plastic behaviour for the FP specimens. However, they added reactive

diluents to the frontally cured composites, which resulted, according to them in a “more flexible matrix”. Tran et. al. [17], used fb reinforcement ($v_f = 53\%$) and a vacuum assisted manufacturing process and gained ILSS values between 40 and 50 MPa, which stands in good correlation to the findings of this thesis, respecting the higher v_f .

All average and standard deviation values of the ILSS can be found in table 4.10 and are illustrated in figure 4.24. The ratio UD:fb, comparing same resin and curing type, lies between 1.2 to 1.9, detailed information can be found in the appendix (table A.3). Therefore, the ILSS shows a lower dependency from the fibre type than the tensile or compression properties. This was expected, since the ILSS is known as a matrix dominated property, consequently more influenced by changes in matrix or curing type.

The specimens produced via VARI show a higher ILSS than specimens produced via wlu, approximately 10 MPa for either reinforcement type. It has to be considered, that the ILSS is very sensitive to voids, as described in section 2.3.3. This effect can clearly be seen in this series of tests. Most obvious by the differences in value and the divergences in ranking between the different test series. An overall trend shows lower ILSS values for the specimens produced via wlu, where the number of voids is higher, proved by a higher $t_{av} : t_{ex}$ and v_v . Regarding exclusively the specimens produced via VARI the influence of voids gets even more pronounced. The thickness ratio value for all different types of VARI specimens except one, lies between 0.97 and 1.01. The exceptions are the VARI-fb-ep2_FP specimens, which additionally were the only ones with visible voids. They have a thickness ratio of 1.03 and an even higher v_v of 5.5 %, where all other v_v values in this set are lower than 2.5 %. Therefore, it can be assumed, that the ILSS values of these specimens, on the contrary to them of other VARI specimens are strongly influenced by its void content. The average ILSS values support this theory, for the VARI-fb-ep2_FP, where it is considerably lower than for the other specimens in this set. In fact, it makes up 78 % of the ILSS of the VARI-fb-ep1_FP specimen, while usually FP specimens of one set show a quite similar ILSS.

Although it is clearly visible that voids have a severe impact on the level of the ILSS, as described in the previous paragraph, it is hard to quantify. Primarily because voids themselves are hard to quantify since they are not evenly distributed. Secondly, they are hard to qualitatively analyse, yet, as mentioned in literature ([69] [70] [46]), their size and shape do have an effect. However, the scope of this thesis is to show the effect of different curing methods on mechanical properties. For the epoxy and curing types no significantly pronounced difference in ILSS and no general trend can be described. Additionally, the failure types are different for con and FP specimens. Therefore, it is hard to tell whether voids have an equal influence on the ILSS for both curing types. Circumventing the influence of voids, by regarding exclusively the VARI-UD specimens,

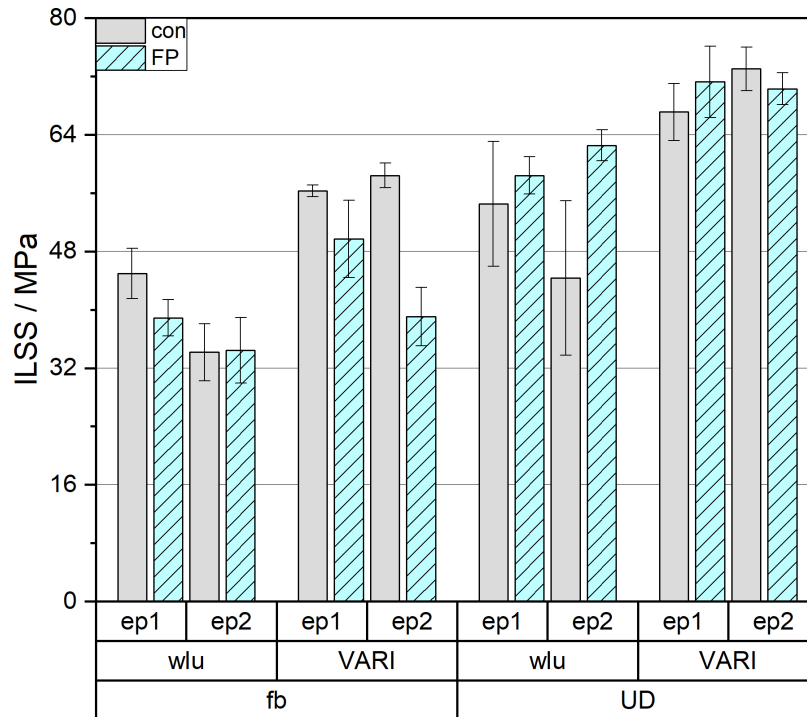


Figure 4.24: Comparison of the average ILSS values, including standard deviation.

it can be concluded, that there is no significant difference in value for neither resin, nor curing type.

Table 4.10: Average values and standard deviation of ILSS in MPa.

manufacturing method	wlu		VARI	
	con	FP	con	FP
resin type				
fb				
ep1	45 ± 3.5	39 ± 2.5	56 ± 0.8	50 ± 5.3
ep2	34 ± 3.9	34 ± 4.5	58 ± 1.7	39 ± 4.0
UD				
ep1	54 ± 8.6	58 ± 2.5	67 ± 3.9	71 ± 4.9
ep2	44 ± 10.6	63 ± 2.1	73 ± 3	70 ± 2.2

An optical analysis leads to clear results, supporting the assumed failure types. At the UD (figure 4.25) as well as fb (figure 4.26) con specimens, the plastic deformation can clearly be seen. Firstly, by the deformation itself, visible in side view, which well replicates the curvature of the loading nose and secondly, by the pronounced marks of the bearing devices on the bottom side.

Some FP specimens also showed these marks however, they were not as pronounced. A curvature visible in side view, was not found in any FP specimen. At some FP

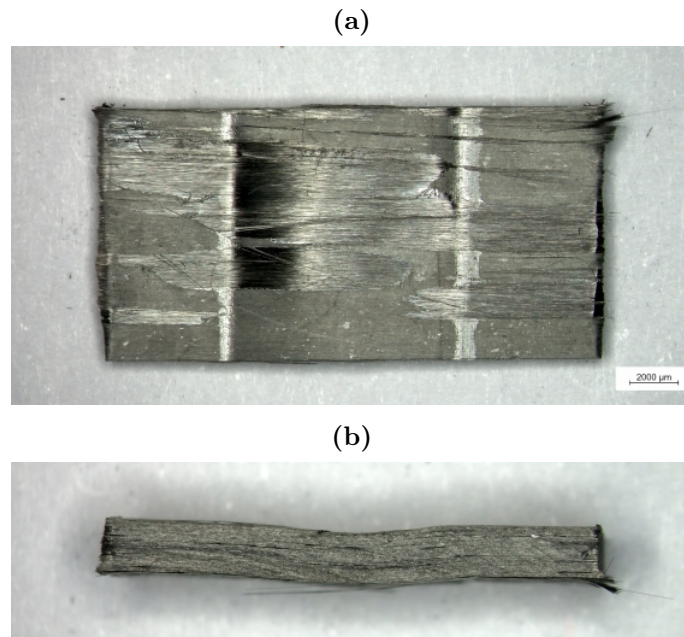


Figure 4.25: Image of the (4.25a) bottom side and (4.25b) side view of a wlu-UD-ep1_con specimen after testing, showing plastic deformation.

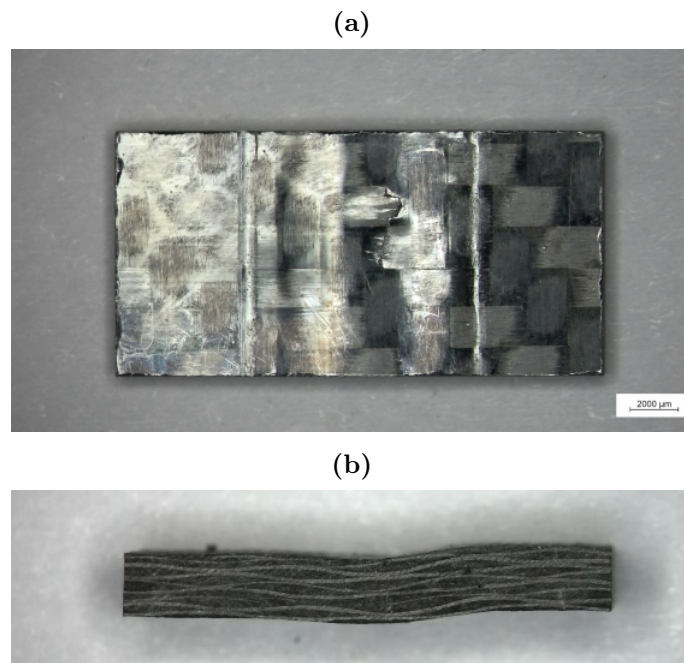


Figure 4.26: Image of the (4.26a) bottom side and (4.26b) side view of a wlu-fb-ep1_con specimen after testing, showing plastic deformation.

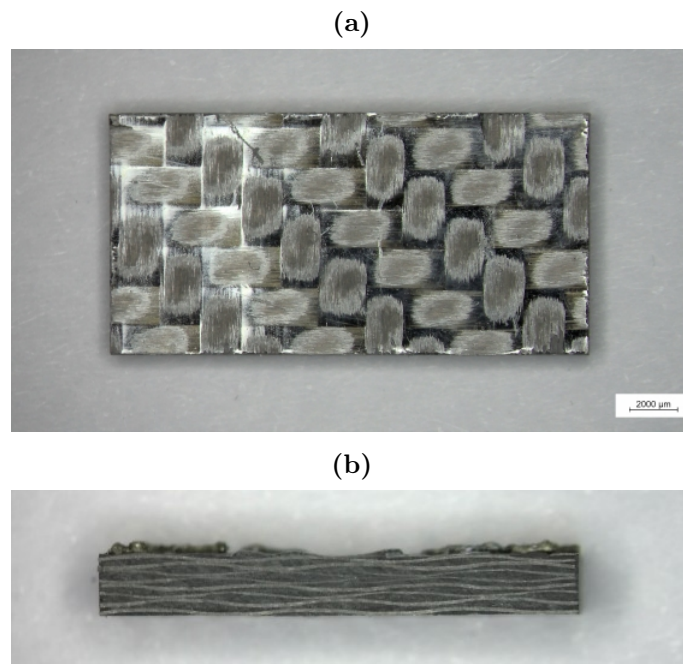


Figure 4.27: Image of the (4.27a) bottom side and (4.27b) side view of a wlu-fb-ep1_FP specimen after testing, showing shear failure.

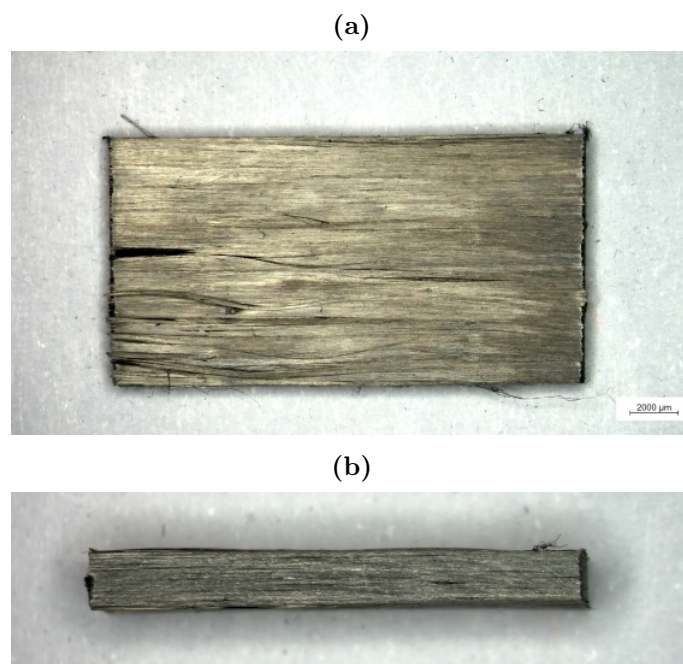


Figure 4.28: Image of the (4.28a) bottom side and (4.28b) side view of a wlu-UD-ep2_FP specimen after testing, showing shear failure.

specimens, especially the ones produced via VARI (e.g. figure 4.27), no defect is visible at all. However, the majority shows shear failure in the edge regions. Both, single and multiple shear failure was observed and randomly distributed, no dependence could be observed.

4.7 Joint discussion

It can be summarized that the most important finding gained, is the difference in failure types for the different curing techniques. All con specimens failed due to plastic deformation, clearly distinguishable by the shape of the ILSS - deformation curve and the specimen itself. Whereas the FP specimens mostly failed by shear. One of the main outcomes of tensile testing was that FP leads to lower $\epsilon_{t_{Max}}$ values than con curing, which is also reflected in the ILSS tests. Considering this fact and taking into account that the manufacturing, fibre and epoxy types were the same it is assumed, that the polymer network of the matrix is responsible for those divergences. A high degree of crosslinking is reflected in a less flexible matrix. The differences in crosslinking have already been explained in section 4.3. It can be summarized that for con curing longer polymer chains exist between the crosslinks. Therefore, the molecules are more flexible to be arranged in loading direction. Two possible explanations can be mentioned for this result, whereas it is expected, that a combination of both is valid. A first explanation is the difference in polymerization route. For con curing crosslinking inhibits the incorporation of an amine/anhydride hardener between the prepolymers, whereas in FP the prepolymers undergo the network formation by a ring opening reaction. The second explanation is the not complete curing, especially for the ep2_con specimens, which results in a lower crosslink density.

This remarkable difference in the network structure and/or the crosslinking density was also reflected by the findings of FTIR. It can furthermore be assumed that con curing results in a better fibre-matrix adhesion, which was also found by the optical investigation of tensile specimens.

5 SUMMARY AND OUTLOOK

The goal of the present thesis was to investigate the feasibility of frontal polymerization (FP) as curing technique of carbon fibre (CF) reinforced epoxy composites with a fibre volume content (v_f) of 50 % or higher. This investigation was done via common thermomechanical test methods for composite materials on specimens out of different reinforcement and resin types. Dynamic mechanical analysis (DMA), tensile and compression tests as well as inter laminar shear strength (ILSS) analysis were conducted, for comparison reasons also on specimens out of the same resin and reinforcement materials. However, cured with commercially available hardeners. Furthermore, two different manufacturing processes i.e, wet lay-up (wlu) and vacuum assisted resin infusion (VARI), were chosen for the fabrication of composites.

Generally, it can be stated that FP is a promising curing method for composites with an epoxy resin matrix. The amount of energy needed, in terms of heating time, was lower for FP. A slight difference in processing behaviour was observed, for the VARI process. At room temperature, the FP resin formulations showed slightly higher viscosities, which led to impregnation problems of the unidirectional (UD) plates. This problem was also observed for the con resin formulations however, not as pronounced. It was solved by heating all formulations up to 40 °C. Furthermore, FP led to a bad surface quality in every manufacturing process.

For all types of specimens, except the fb specimens produced via VARI, a v_f of 50 % or higher could have been reached. The v_f of the VARI-fb specimens lies between 41 and 46 % and this difference was caused by the infusion behaviour. The calculation of v_f was done via masses of the components and additionally proved, for some specimens, via thermogravimetric analysis (TGA).

The first approach of producing specimens via wlu led to an unsatisfactory specimen quality, in terms of voids. This was described by a rise in the actual thickness of about 10 % and later on had a lowering effect on the thermomechanical properties, especially the ILSS.

The DMA showed that FP leads to higher glass transition temperature (T_g) values compared to con curing. However, for all specimens and especially the ep2_con specimens, a moderate post-curing effect was observed, by a rise in storage modulus (E') after the transition region. Since this rise was not pronounced, the highest rise detected was 6 GPa, it was concluded not to have a significant effect on the specimen properties. This theory is supported by the E_t values, which did not show any significant trend to higher values for neither curing nor resin type. However, for future investigations the curing time of the con specimens should be increased. The value of E' at 30 °C showed a good correlation with the tensile modulus (E_t).

The tensile tests showed on the one hand comparable E_t values for all resin and curing types within one set of same manufacturing and curing method, with a modest trend to higher values for the FP specimens. On the contrary, comparing the strength values, a slight difference for the con cured specimens and a pronounced divergence for the FP specimens were detected. It could have been shown, that FP leads to a reduction in strength and corresponding maximum strain values, of approximately 33 %. This was attributed to the low inherent ductility of the matrix resins cured via FP and the resulting disregard of a vital design rule; which demands a matrix with maximum strain twice the maximum strain of fibres, in order to ensure maximum performance of a composite.

In compression tests, no significant differences between FP and con curing in general was observed. Just one specimen type i.e, ep1_con, showed different compressive strength and modulus values than the others. This implies that the severe impact of the curing type on the material properties in some cases exceeds disparities between the resins. This theory was additionally supported by the findings in FTIR analysis and rheological measurements on neat resin and tensile testing.

The ILSS analysis showed no significant difference in values between con curing and FP. However, different failure types were detected. FP specimens showed shear failure, whereas con curing led to plastic deformation. Moreover, the severe impact of voids on the ILSS could have been observed.

Generally, it can be summarized that FP leads to very similar values of the studied material properties for both resins tested. Whereas significant differences between ep1_con and ep2_con could have been found for tensile and compression properties, ep1_con showing higher values in tensile, yet lower in compression tests. Moreover, in all tests, except tensile testing FP is competitive to con curing. However, FP leads to higher T_g values.

Further research should be done concerning two aspects. Firstly, a deeper investigation of the material behaviour and properties is needed. The influences of temperature and environmental aspects have been neglected in this thesis, however should be investigated. For this purpose, mechanical tests, as the ones performed and additional, such as tensile and compression tests perpendicular to fibre direction, should be conducted at elevated and sub-zero temperatures and after wet conditioning. Additionally, the behaviour under high strain rates, like impact tests, should be investigated. Furthermore, the fracture mechanical behaviour of FP composites should be investigated. Moreover, the fibre-matrix adhesion should be studied via scanning electron microscopy, in order to see whether the assumption that it is negatively affected by FP can be confirmed.

In order to save time and money molecular modelling and simulation, as described in [71] [72] [73], could be taken into account.

Secondly, it has to be considered, whether an adaption of the monomer formulation would be beneficial. For example to ameliorate the ductility, strain at break ($\epsilon_{t_{Max}}$), and for ensuring best performance of the fibres, since the crosslinking itself cannot be influenced once the reaction is started. Therefore the addition of diluents, or oligomers with a higher molecular weight, could be an option worth studying. The developed resin formulations should at first be tested as pure resins, with regard to their ductility e.g. in tensile or ILSS tests. Once a certain formulation shows a higher ductility, it should be used for manufacturing composites and subsequently, their tensile properties should be tested to prove a positive effect on tensile strength and maximum elongation. Additionally, it could be a promising path to change from bisphenol A diglycidyl ether (BADGE) based monomers to cycloaliphatic, since they produce more heat during the curing reaction and can therefore improve the front stability, even for highly filled composites. This would simplify the manufacturing process and insure full cure.

BIBLIOGRAPHY

- [1] Grand View Research, “Market analysis report: Epoxy resin market size, share and trends analysis report,” 2016.
- [2] R. M. Jones, ed., *Mechanics of Composite Materials*. Boca Raton: Chapman and Hall/CRC, 2nd ed. ed., 2014.
- [3] Helmut Fahrenholz, “Prüfen von langfaserverstärkten verbundwerkstoffen: intelligent testing,” 2018.
- [4] J. D. Menczel and R. B. Prime, *Thermal analysis of polymers: Fundamentals and applications*. Hoboken N.J.: John Wiley, 2009.
- [5] Zwick//Roell, “Produktinformation hydraulische druckvorrichtung für verbundwerkstoffe hccf.”
- [6] B. Klein, *Leichtbau-Konstruktion*. Wiesbaden: Springer Fachmedien Wiesbaden, 2013.
- [7] Dr. Elmar Witten (AVK) & Alfons Schuster, “Composites-marktbericht 2018: Marktentwicklungen, trends, ausblicke und herausforderungen.”
- [8] D. Abliz, Y. Duan, L. Steuernagel, L. Xie, D. Li, and G. Ziegmann, “Curing methods for advanced polymer composites - a review,” *Polymers and Polymer Composites*, vol. 21, no. 6, pp. 341–348, 2013.
- [9] P. Knaack, N. Klikovits, A. D. Tran, D. Bomze, and R. Liska, “Radical induced cationic frontal polymerization in thin layers,” *Journal of Polymer Science Part A: Polymer Chemistry*, vol. 57, no. 11, pp. 1155–1159, 2019.
- [10] D. Bomze, P. Knaack, and R. Liska, “Successful radical induced cationic frontal polymerization of epoxy-based monomers by c-c labile compounds,” *Polymer Chemistry*, vol. 6, no. 47, pp. 8161–8167, 2015.
- [11] M. Atif, R. Bongiovanni, and J. Yang, “Cationically uv-cured epoxy composites,” *Polymer Reviews*, vol. 55, no. 1, pp. 90–106, 2015.
- [12] A. Mariani, S. Bidali, G. Caria, O. Monticelli, S. Russo, and J. M. Kenny, “Synthesis and characterization of epoxy resin-montmorillonite nanocomposites obtained by frontal polymerization,” *Journal of Polymer Science Part A: Polymer Chemistry*, vol. 45, no. 11, pp. 2204–2211, 2007.
- [13] M. Sangermano, I. Roppolo, and A. Chiappone, “New horizons in cationic photopolymerization,” *Polymers*, vol. 10, no. 2, 2018.

- [14] J. A. Pojman, "Frontal polymerization," in *Polymer Science: A Comprehensive Reference*, pp. 957–980, Elsevier, 2012.
- [15] A. Mariani, S. Bidali, S. Fiori, M. Sangermano, G. Malucelli, R. Bongiovanni, and A. Priola, "Uv-ignited frontal polymerization of an epoxy resin," *Journal of Polymer Science Part A: Polymer Chemistry*, vol. 42, no. 9, pp. 2066–2072, 2004.
- [16] N. Klikovits, R. Liska, A. D'Anna, and M. Sangermano, "Successful uv-induced ricfp of epoxy-composites," *Macromolecular Chemistry and Physics*, vol. 218, no. 18, p. 1700313, 2017.
- [17] A. D. Tran, T. Koch, P. Knaack, and R. Liska, "Radical induced cationic frontal polymerization for preparation of epoxy composites," *Composites Part A: Applied Science and Manufacturing*, vol. 132, p. 105855, 2020.
- [18] M. Sangermano, I. Antonazzo, L. Sisca, and M. Carello, "Photoinduced cationic frontal polymerization of epoxy-carbon fibre composites," *Polymer International*, vol. 68, no. 10, pp. 1662–1665, 2019.
- [19] G. W. Ehrenstein, *Faserverbund-Kunststoffe: Werkstoffe - Verarbeitung - Eigenschaften*. München: Carl Hanser Verlag GmbH & Co. KG, 2. völlig überarbeitete auflage ed., 2006.
- [20] H. Jahn, *Epoxidharze*. Leipzig: VEB Deutscher Verlag für Grundstoffindustrie, 1969.
- [21] H. Domininghaus, P. Elsner, P. Eyerer, and T. Hirth, *Kunststoffe*. Berlin, Heidelberg: Springer Berlin Heidelberg, 2012.
- [22] M. G. González, J. C. Cabanelas, and J. Baselga, "Applications of ftir on epoxy resins - identification, monitoring the curing process, phase separation and water uptake," in *Infrared Spectroscopy - Materials Science, Engineering and Technology* (T. Theophanides, ed.), InTech, 2012.
- [23] F.-L. Jin, X. Li, and S.-J. Park, "Synthesis and application of epoxy resins: A review," *Journal of Industrial and Engineering Chemistry*, vol. 29, pp. 1–11, 2015.
- [24] B. Ellis, *Chemistry and Technology of Epoxy Resins*. Dordrecht: Springer Netherlands, 1993.
- [25] S. L. Agius, M. Joosten, B. Trippit, C. H. Wang, and T. Hilditch, "Rapidly cured epoxy/anhydride composites: Effect of residual stress on laminate shear strength," *Composites Part A: Applied Science and Manufacturing*, vol. 90, no. 3, pp. 125–136, 2016.

- [26] N. M. Chechilo, R. J. Khvilivitskii, and N. S. Enikolopyan, "On the phenomenon of polymerization reaction spreading," *Dokl. Akad. Nauk SSSR*, vol. 204, pp. 1180–1181, 1972.
- [27] C. Nason, T. Roper, C. Hoyle, and J. A. Pojman, "Uv-induced frontal polymerization of multifunctional (meth)acrylates," *Macromolecules*, vol. 38, no. 13, pp. 5506–5512, 2005.
- [28] J. A. Pojman, V. M. Ilyashenko, and A. M. Khan, "Free-radical frontal polymerization: self-propagating thermal reaction waves," *Journal of the Chemical Society, Faraday Transactions*, vol. 92, no. 16, p. 2825, 1996.
- [29] J. V. Crivello, "Hybrid free radical/cationic frontal photopolymerizations," *Journal of Polymer Science Part A: Polymer Chemistry*, vol. 45, no. 18, pp. 4331–4340, 2007.
- [30] D. Bomze, P. Knaack, T. Koch, H. Jin, and R. Liska, "Radical induced cationic frontal polymerization as a versatile tool for epoxy curing and composite production," *Journal of Polymer Science Part A: Polymer Chemistry*, vol. 54, no. 23, pp. 3751–3759, 2016.
- [31] S. Scognamillo, C. Bounds, M. Luger, A. Mariani, and J. A. Pojman, "Frontal cationic curing of epoxy resins," *Journal of Polymer Science Part A: Polymer Chemistry*, vol. 48, no. 9, pp. 2000–2005, 2010.
- [32] M. Kaur and A. K. Srivastava, "Photopolymerization: A review," *Journal of Macromolecular Science, Part C: Polymer Reviews*, vol. 42, no. 4, pp. 481–512, 2002.
- [33] J. V. Crivello, "Photopolymerization," in *Polymer Science: A Comprehensive Reference*, pp. 919–955, Elsevier, 2012.
- [34] A. B. Scranton, C. N. Bowman, and R. W. Peiffer, eds., *Photopolymerization: Fundamentals and applications / Alec B. Scranton, editor, Christopher N. Bowman, editor, Robert W. Peiffer, editor*, vol. 673 of *ACS symposium series, 0097-6156*. Washington, DC: American Chemical Society, 1997.
- [35] R. W. Peiffer, "Applications of photopolymer technology," in *Photopolymerization* (A. B. Scranton, C. N. Bowman, and R. W. Peiffer, eds.), vol. 673 of *ACS symposium series, 0097-6156*, pp. 1–14, Washington, DC: American Chemical Society, 1997.

- [36] P. Lin, B. Falk, M. Jang, and J. V. Crivello, "Study of laser-induced photopolymerizations by optical pyrometry," *Macromolecular Chemistry and Physics*, vol. 205, no. 15, pp. 2040–2047, 2004.
- [37] Malik Muhammad Salman, Schlögl Sandra, Wolfahrt Markus, and M. Sangermano, "Review on uv-induced cationic frontal polymerization of epoxy monomers,"
- [38] J. V. Crivello, B. Falk, and M. R. Zonca, "Photoinduced cationic ring-opening frontal polymerizations of oxetanes and oxiranes," *Journal of Polymer Science Part A: Polymer Chemistry*, vol. 42, no. 7, pp. 1630–1646, 2004.
- [39] M. J. Hinton, P. D. Soden, and A. S. Kaddour, "Strength of composite laminates under biaxial loads," *Applied Composite Materials*, vol. 3, no. 3, pp. 151–162, 1996.
- [40] A. Puck and H. Schürmann, "Failure analysis of frp laminates by means of physically based phenomenological models," *Composites Science and Technology*, vol. 62, no. 12-13, pp. 1633–1662, 2002.
- [41] A. Puck, "Failure analysis of frp laminates by means of physically based phenomenological models," *Composites Science and Technology*, vol. 58, no. 7, pp. 1045–1067, 1998.
- [42] S. W. Tsai and E. M. Wu, "A general theory of strength for anisotropic materials," *Journal of Composite Materials*, vol. 5, no. 1, pp. 58–80, 1971.
- [43] B. F. Sørensen and H. Lilholt, "Fiber pull-out test and single fiber fragmentation test - analysis and modelling," *IOP Conference Series: Materials Science and Engineering*, vol. 139, p. 012009, 2016.
- [44] S. Seidler, V. Alstädt, and W. Grellmann, eds., *Polymer testing*. Munich: Hanser Publishers, 2nd edition ed., 2013.
- [45] Gottfried W. Ehrenstein, Gabriela Riedel, and Pia Trawiel, "Thermal analysis of plastics,"
- [46] M. Mehdikhani, L. Gorbatikh, I. Verpoest, and S. V. Lomov, "Voids in fiber-reinforced polymer composites: A review on their formation, characteristics, and effects on mechanical performance," *Journal of Composite Materials*, vol. 53, no. 12, pp. 1579–1669, 2019.
- [47] W. J. Cantwell and J. Morton, "The significance of damage and defects and their detection in composite materials: A review," *The Journal of Strain Analysis for Engineering Design*, vol. 27, no. 1, pp. 29–42, 1992.

- [48] V. Chandrasekaran, S. G. Advani, and M. H. Santare, “Role of processing on interlaminar shear strength enhancement of epoxy/glass fiber/multi-walled carbon nanotube hybrid composites,” *Carbon*, vol. 48, no. 13, pp. 3692–3699, 2010.
- [49] A. Maier, N. Schramm, and L. Kroll, “Temperature-dependent interlaminar shear strength of unidirectional continuous fiber-reinforced thermoplastic profiles,” *Composite Structures*, vol. 255, no. 4, p. 112959, 2021.
- [50] M. L. Costa, S. F. M. Almeida, and M. C. Rezende, “The influence of porosity on the interlaminar shear strength of carbon/epoxy and carbon/bismaleimide fabric laminates,” *Composites Science and Technology*, vol. 61, no. 14, pp. 2101–2108, 2001.
- [51] J. Michels, J. Sena Cruz, R. Christen, C. Czaderski, and M. Motavalli, “Mechanical performance of cold-curing epoxy adhesives after different mixing and curing procedures,” *Composites Part B: Engineering*, vol. 98, no. 5, pp. 434–443, 2016.
- [52] Y. Li, Q. Li, and H. Ma, “The voids formation mechanisms and their effects on the mechanical properties of flax fiber reinforced epoxy composites,” *Composites Part A: Applied Science and Manufacturing*, vol. 72, no. 3, pp. 40–48, 2015.
- [53] Deutsches Institut für Normung e.V., “Kunststoffe_- bestimmung dynamisch-mechanischer eigenschaften_- teil_1: Allgemeine grundlagen (iso_6721-1:2011); deutsche fassung en_iso_6721-1:2011,” 2002-01.
- [54] METTLER TOLEDO, “Tips on method development for dma measurements in 3-point bending,” 2010.
- [55] G. W. Ehrenstein, G. Riedel, and P. Trawiel, *Thermal analysis of plastics: Theory and practice*. Munich: Hanser, 2004.
- [56] Deutsches Institut für Normung e.V., “Kunststoffe_- bestimmung der zugeigenschaften_- teil_4: Prüfbedingungen für isotrop und anisotrop faserverstärkte kunststoffverbundwerkstoffe (iso_527-4:1997); deutsche fassung en_iso_527-4:1997,” 2009-05.
- [57] Deutsches Institut für Normung e.V., “Kunststoffe_- bestimmung der zugeigenschaften_- teil_5: Prüfbedingungen für unidirektional faserverstärkte kunststoffverbundwerkstoffe (iso_527-5:2009); deutsche fassung en_iso_527-5:2009,” 2009-05.
- [58] Deutsches Institut für Normung e.V., “Faserverstärkte kunststoffe_- bestimmung der druckeigenschaften in der laminatebene,” 2000-12.

- [59] Deutsches Institut für Normung e.V., “Bestimmung der scheinbaren interlaminaren scherfestigkeit nach dem dreipunktverfahren mit kurzem balken,” 1998-02.
- [60] D. Kim, H. J. Park, and K. Y. Lee, “Study on curing behaviors of epoxy acrylates by uv with and without aromatic component,” *Macromolecular Research*, vol. 23, no. 10, pp. 944–951, 2015.
- [61] P. Rodriguez, *Dynamic Mechanical Analysis for quality evaluation of additively manufactured continuous fiber reinforced thermoplastic matrix composites subject to manufacturing defects*. PhD thesis, Colorado State University, Fort Collins, 2019.
- [62] H. Schürmann, *Konstruieren mit Faser-Kunststoff-Verbunden*. VDI-Buch, Berlin, Heidelberg: Springer-Verlag Berlin Heidelberg, 2., bearbeitete und erweiterte auflage ed., 2007.
- [63] J. M. F. d. Paiva, S. Mayer, and M. C. Rezende, “Evaluation of mechanical properties of four different carbon/epoxy composites used in aeronautical field,” *Materials Research*, vol. 8, no. 1, pp. 91–97, 2005.
- [64] C. V. Opelt, G. M. Cândido, and M. C. Rezende, “Compressive failure of fiber reinforced polymer composites – a fractographic study of the compression failure modes,” *Materials Today Communications*, vol. 15, pp. 218–227, 2018.
- [65] D30 Committee, “Test method for compressive properties of polymer matrix composite materials with unsupported gage section by shear loading.”
- [66] S. J. Kim and S. H. Chang, “The relation between compressive strength of carbon/epoxy fabrics and micro-tow geometry with various bias angles,” *Composite Structures*, vol. 75, no. 1-4, pp. 400–407, 2006.
- [67] E. M. Odom and D. F. Adams, “Failure modes of unidirectional carbon/epoxy composite compression specimens,” *Composites*, vol. 21, no. 4, pp. 289–296, 1990.
- [68] Deutsches Institut für Normung e.V., “Faserverstärkte kunststoffe_ - bestimmung der scheinbaren interlaminaren scherfestigkeit nach dem dreipunktverfahren mit kurzem balken (iso_14130:1997); deutsche fassung en_iso_14130:1997,” 1998-02.
- [69] Hong-yan ZHU, Di-hong LI, Dong-xing ZHANG, Bao-chang WU, and Yu-yong CHEN, “Influence of voids on interlaminar shear strength of carbon/epoxy fabric laminates,”

- [70] H. Huang and R. Talreja, “Effects of void geometry on elastic properties of unidirectional fiber reinforced composites,” *Composites Science and Technology*, vol. 65, no. 13, pp. 1964–1981, 2005.
- [71] A. Bandyopadhyay, P. K. Valavala, T. C. Clancy, K. E. Wise, and G. M. Odegard, “Molecular modeling of crosslinked epoxy polymers: The effect of crosslink density on thermomechanical properties,” *Polymer*, vol. 52, no. 11, pp. 2445–2452, 2011.
- [72] A. Shokuhfar and B. Arab, “The effect of cross linking density on the mechanical properties and structure of the epoxy polymers: molecular dynamics simulation,” *Journal of molecular modeling*, vol. 19, no. 9, pp. 3719–3731, 2013.
- [73] A. Vashisth, C. Ashraf, C. E. Bakis, and A. C. van Duin, “Effect of chemical structure on thermo-mechanical properties of epoxy polymers: Comparison of accelerated reaxff simulations and experiments,” *Polymer*, vol. 158, pp. 354–363, 2018.

A APPENDIX

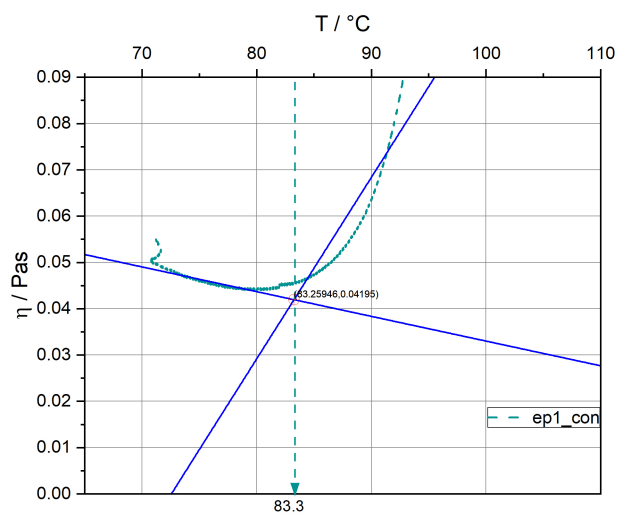


Figure A.1: Visualisation of the method for calculating T_{gel}^{onset} in viscosity measurements.

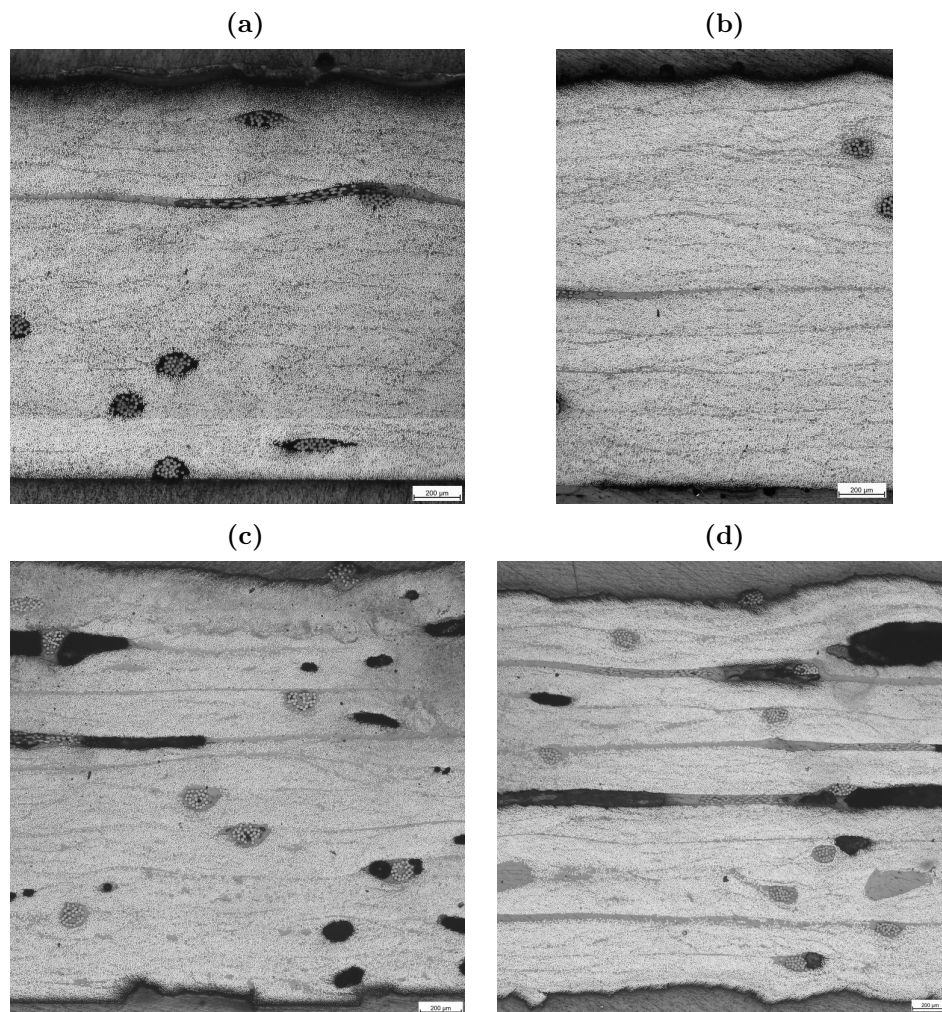


Figure A.2: Micrographs of 2 mm plates for compression, DMA and ILSS tests: A.2a showing VARI-UD-ep2_con, A.2b showing VARI-UD-ep2_FP, A.2c showing wlu-UD-ep1_FP and A.2d showing VARI-UD-ep2_FP.

Table A.1: Calculated v_f , v_v and thickness ratio.

specimen type	v_f %	v_v %	$t_{av} : t_{ex}$
UD and fb plates for compression, DMA and ILSS tests			
VARI-UD-ep1_con	57,3	0,3	0,97
VARI-UD-ep1_FP	57,2	0,3	1,01
VARI-UD-ep2_con	58,5	1,3	0,98
VARI-UD-ep2_FP	56,8	0,8	0,98
VARI-fb-ep1_con	41,6	0,4	0,96
VARI-fb-ep1_FP	43,8	2,5	0,97
VARI-fb-ep2_con	44,2	0,3	1,01
VARI-fb-ep2_FP	46,4	5,5	1,03
wlu-UD-ep1_con	56,2	3,4	1,02
wlu-UD-ep1_FP	55,1	6,1	1,10
wlu-UD-ep2_con	52,8		1,06
wlu-UD-ep2_FP	53,8	8,7	1,06
wlu-fb-ep1_con	50,5		1,07
wlu-fb-ep1_FP	50,9		1,06
wlu-fb-ep2_con	51,4		1,15
wlu-fb-ep2_FP	52,7		1,12
UD plates for tensile tests			
VARI-UD-ep1_con	53,1		1,04
VARI-UD-ep1_FP	51,2		1,00
VARI-UD-ep2_con	50		1,04
VARI-UD-ep2_FP	55,4		1,03
wlu-UD-ep1_con	52,7		1,02
wlu-UD-ep1_FP	51,5		1,14
wlu-UD-ep2_con	49,5		1,21
wlu-UD-ep2_FP	52,8		1,16

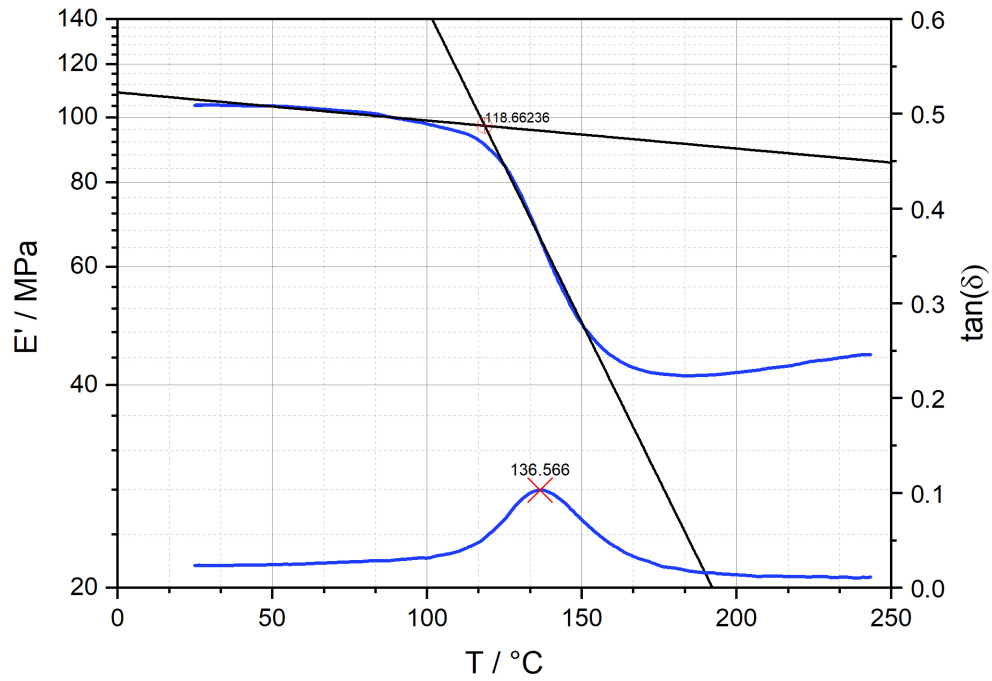


Figure A.3: Visualisation of the two methods used for calculating T_g .

Table A.2: Comparison of tensile properties.

Manufacturing method	wlu		VARI	
Curing method	con	FP	con	FP
Resin type	Ratio of $\sigma_{t_{MAX}}$ UD:fb			
ep1	2.5	2.0	2.9	2.2
ep2	2.6	2.2	2.7	2.7
	$\sigma_{t_{MAX}}$ divided by Li_con of according set fb			
ep1	1	0.83	1	0.87
ep2	0.79	0.83	0.97	0.83
	UD			
ep1	1	0.64	1	0.66
ep2	0.82	0.72	0.91	0.76
Resin type	Ratio of E_t UD:fb			
	UD reinforcement			
ep1	2.3	2.1	2.7	2.6
ep2	1.9	2.0	2.	2.6
	E_t divided by Li_con of according set fb			
ep1	1	1.00	1	1.04
ep1	0.94	1.06	1.08	1.04
	UD			
ep1	1	0.9	1	1.03
ep2	0.77	0.92	0.95	1.03

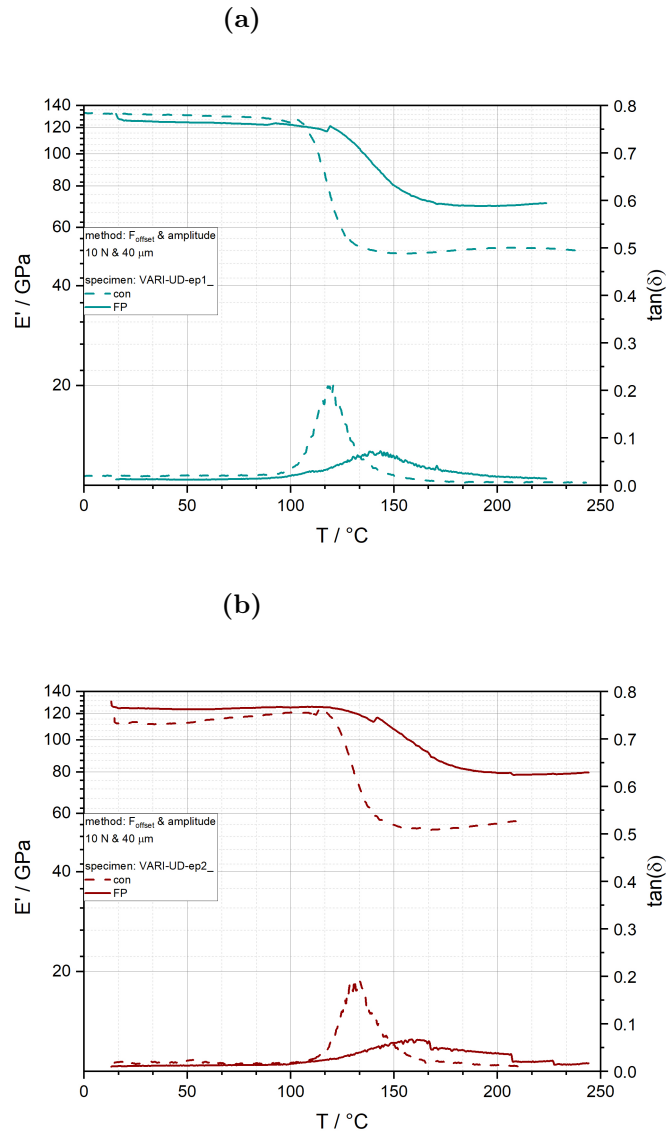


Figure A.4: E' and $\tan(\delta)$ in dependence of temperature, derived from DMA, for: (A.4a) VARI-UD-ep1 and (A.4b) VARI-UD-ep2 specimens, in each case con and FP cured as indicated in the legend. Each measurement was performed with 1 Hz and method 1.

Table A.3: Comparison of ILSS.

Manufacturing method	wlu		VARI	
	con	FP	con	FP
Resin type	Ratio of ILSS UD:fb			
ep1	1.2	1.5	1.2	1.4
ep2	1.3	1.9	1.3	1.8

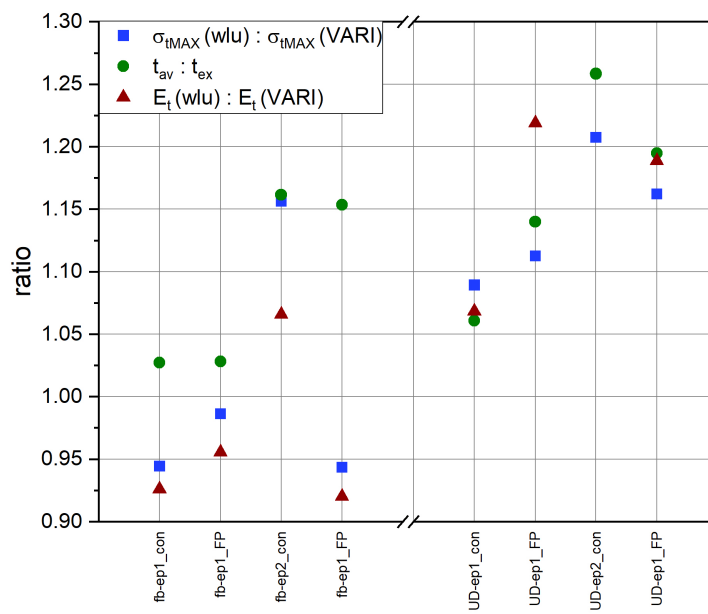


Figure A.5: Visualisation of the ratios expected to real thickness and wlu to VARI for $\sigma_{t_{MAX}}$ and E_t .

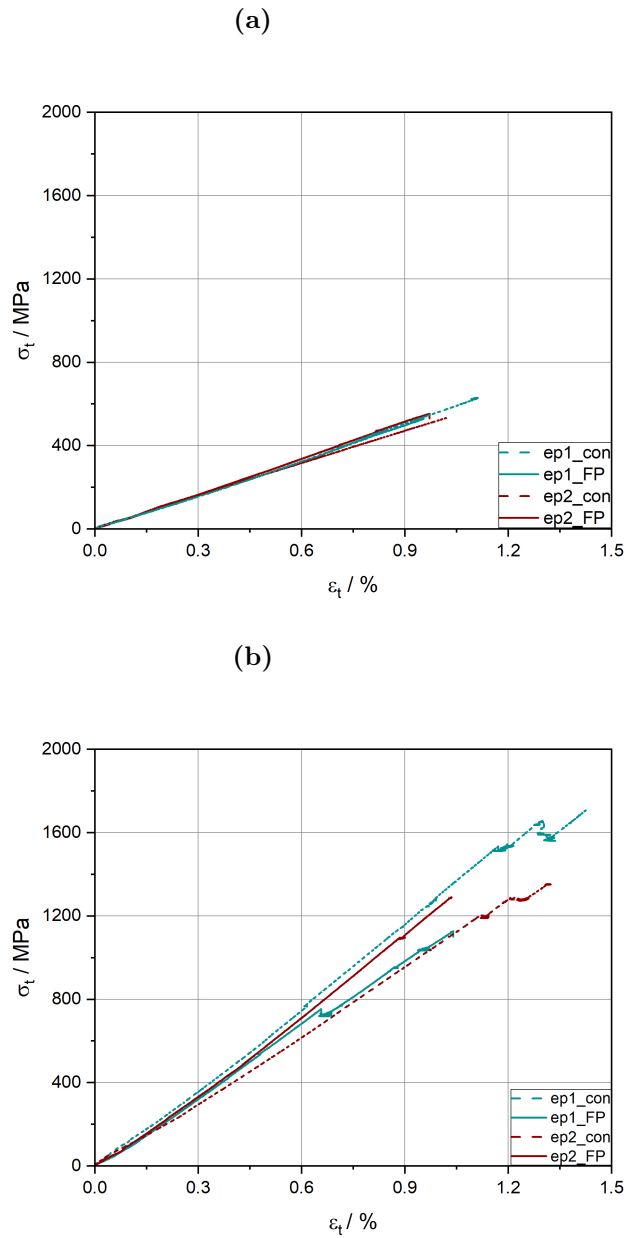


Figure A.6: Example σ_t vs ϵ_t curves of tensile tests for A.6a fb and A.6b UD specimens produced via wlu.